NOTE TO USERS

Page(s) not included in the original manuscript and are unavailable from the author or university. The manuscript was scanned as received.

xi

This reproduction is the best copy available.

UMI®

Phase Behaviour of Poly(*l*-lactic acid) (PLLA) and its Blends with Poly(ethylene oxide) (PEO)

by

Xiaocan Zhang

A Thesis Submitted to
the Faculty of Graduate Studies and Research
in Partial Fulfillment of the Requirements for the Degree of

Master of Science in Applied Science

Saint Mary's University
Halifax, Nova Scotia

April, 2006

Approved: Dr. Kathy Singfield
Senior Supervisor

Approved: Dr. Amyl Ghanem
External Examiner

Approved: Dr. Adam Piorko
Supervisory Committee Member

Approved: Dr. Adam J. Sarty
Supervisory Committee Member

Approved: Dr. David. Richardson, Dean of Science
Program Coordinator

Approved: Dr. J. Kevin Vessey
Dean of Graduate Studies

Date: April 27, 2006

Your file Votre référence
ISBN: 978-0-494-17656-6
Our file Notre référence
ISBN: 978-0-494-17656-6

ABSTRACT

Phase Behaviour of Poly(*l*-lactic acid) (PLLA) and its Blends with Poly(ethylene oxide) (PEO)

by Xiaocan Zhang

A combination of polarized light optical microscopy (PLOM), scanning electron microscopy (SEM), and total depolarized light intensity (DLI) investigations were performed to understand the phase behaviour and micro-level morphology of melt-crystallized poly(*l*-lactic acid) (PLLA) and its blend with poly(ethylene oxide) (PEO) before and after enzymatic degradation. Three distinct blend groups with respect to the blend composition have been identified: (i) 10 – 20 wt% PEO in which the PEO is not able to form any ordered structure in the binary blend; (ii) 30 – 50 wt% PEO in which the PEO is able to form some order but not enough to develop spherulitic crystals; (iii) 60 – 90 wt% PEO in which the PEO forms a network of spherulites throughout the pre-crystallized PLLA.The predominant lamellar structure of the PLLA component is concluded to be edge-on and flat-on in group (ii) and (iii), respectively.

April 7, 2006

ACKNOWLEDGEMENTS

I would like to express my gratitude to all those whose direct and indirect support helped me with the completion of my thesis.

First of all, I am deeply indebted to my supervisor Dr. Kathy Singfield, whose guidance, stimulating suggestions and encouragement helped me all the time of research and thesis writing, and of every possible aspect in my life. Her overly enthusiasm and integral view on research deeply impressed me. She could not even realize how much I have learned from her, and I am really glad that I have come to her lab and got to know her in my life.

I am grateful for all my lab mates, both past and present, who provided me a wonderful working environment and for all those great discussions and fun we had together.

I would like to thank Dr. Adam Piorko, for his help on enzymatic degradation, and for him has always been willing to answer my questions.

I acknowledge Dr. Xiang Yang, for his expertise and guidance concerning the electron microscope, and some discussion of the acquired SEM pictures.

I wish to express my sincere thanks to Darlene Gaucher and Elizabeth McLeod, for the equipment and technical support. It was a pleasure to work with them.

I extend my appreciation to both the Program of Applied Science and Chemistry Department of Saint Mary's University, for their two years' assistance.

I acknowledge NSERC for financial support.

Finally, I believe I owe the deepest thanks to my family who has supported me since I was born, and my friends for always being there for me. Particularly, I would like to give my special thanks to Long Sheng, whose patient love enabled me to complete this work.

Thank you all.

Table of Contents

Chapter Three

Microstructure of PLLA and its Blends with PEO

Chapter Four

A Critique of Non-Isothermal Crystallization Method

Chapter Five

General Conclusions & Future Directions

LIST OF SYMBOLS

PE	polyethylene
PP	polypropylene
PS	polystyrene
PVC	poly(vinyl chloride)
LDPE	low density polyethylene
PCL	polycaprolactone
PHB	poly(β-hydroxybutyrate)
PLA	poly(lactic acid)
PLLA	poly(*l*-lactic acid)
PDLA	poly(*d*-lactic acid)
PVA	poly(vinyl alcohol)
T_g	glass transition temperature
M_n	number average molecular weight
M_w	weight average molecular weight
M_w/M_n	polydispersity
T_c	isothermal crystallization temperature
DSC	differential scanning calorimetry
TEM	transmission electron microscopy
AFM	atomic force microscopy
G	spherulite radial growth rate
GPC	gel permeation chromatography

PET	poly(ethylene terephthalate)
PEG	poly(ethylene glycol)
DTC	2,2-dimethyltrimethylene carbonate
PVPh	poly(*p*-vinylphenol)
T_m	melting temperature
H-L model	Hoffman-Lauritzen crystallization model
cm	centimeter
μm	micrometer (10^{-6} m)
m	meter
g	gram
mg	milligram
s	second
kJ	kilojoule
°C	degrees Celsius
K	Kelvin
G_0	pre-exponential term
$\triangle T$	degree of undercooling
T_m^0	equilibrium melting temperature
U^*	activation energy of transport of polymer chains through the melt to the site of crystallization
R	universal gas constant
T_∞	hypothetical temperature at which all the molecular motions related to viscous flow are ceased

K_g	nucleation constant
f	unitless factor to account for the variation of the heat of fusion away from the melting point
b_0	crystallizing stem thickness
σ	lateral surface interfacial free energy
σ_e	fold surface interfacial free energy
k	Boltzmann constant
$\triangle h_f$	heat of fusion per volume of monomer units
DLI	depolarized light intensity
TRISMA	tris(hydroxymethyl) aminomethane
HCl	hydrochloric acid
PLOM	polarized light optical microscopy
WAXS	wide-angle x-ray scattering
SEC	size-exclusion chromatography
NMR	nuclear magnetic resonance
SEM	scanning electron microscopy
DIH	digital inline holography
DIHM	digital inline holography microscopy
r	radius of the spherulite
t	time
dT/dt	heating or cooling rate
PEEK	poly(ether ether ketone)
min	minute

LIST OF FIGURES

LIST OF TABLE

Chapter One: *General Introduction*

1.1 Situation Statement

The invention and widespread use of plastics is one of the most significant innovations of the 20th century. Today's plastics are ubiquitous due to their versatility, and light weight, as well as low cost and relative ease of processing. The world production of total polymeric materials is about 200 million tons annually.[1] This amount of material can take between 100 and 400 years to breakdown in a landfill.[2]

The principle fates of post-consumer plastic material items are their reuse, recycling, incineration, and their discarding in landfills.[3] The incineration and the landfill discarding of plastics can have damaging effects on the environment, and the reuse option is only applicable to a limited number of plastic products. Recycling is broadly accepted as an adequate approach in reducing pollution problems associated with waste polymer materials. However, the cleaning and sorting steps, in addition to the transport, add considerable cost to the overall polymer recycling process. The successful recycling of polymer materials requires a homogenous and clean supply of the post-consumer product material, free from contamination from both other types of materials as well as from other polymers. Furthermore, recycling involves reprocessing the material at elevated temperatures. Organic polymers are typically very susceptible to thermal degradation at these reprocessing temperatures, producing

an inferior second generation product with limited value as a functional material. Polymer materials can not be reprocessed indefinitely, unlike metals, and ultimately they are destined to be incinerated or to be placed in a landfill. Plastics left in a landfill remain relatively inert. In fact, any material which may be susceptible to microbial breakdown is unlikely to degrade under the typical landfill conditions of no light and no moisture.

Plastics persist in the environment for a long time after being used and discarded. It is increasingly being realized that it is not wise to use the traditional long-lasting polymer plastics for short-lived applications, particularly since environmentally responsible, sustainable development is now a major concern. This realization has also been an issue in dealing with the problem of unsightly plastic litter, a problem which has been repeatedly demonstrated as being detrimental to wildlife.

The use of biodegradable materials is a clever approach to address this outstanding problem. Some of these materials can be made from renewable resources to avoid a net depletion of resources in a practical time span, and are able to degrade under normal conditions on an appropriate time scale after the completion of their service life. When applied to soil as compost, biodegradable materials can improve the fertility and tilth, and the recycling of carbon in this manner contributes to the natural carbon cycle. Plants fix carbon dioxide emitted from the compost facilities, thereby extending the recycling loop. Under the right conditions, some biodegradable plastics can follow a complete life cycle of production, consumption, disposal and reuse.

In a changing world where producers and manufacturers are beginning to take more responsibility for the post-consumer treatment of their products, both traditional and new biodegradable plastics are receiving a lot of attention.

1.2 Plastics: A Fundamental Description

Plastics are essentially the solid state of organic molecules called polymers. Polymers are long-chain molecules that are composed of a large number of small repeat units, called monomers, covalently linked in a linear fashion. Some polymers are crystallizable and can form ordered structures. These polymers form materials that are more accurately described as thermoplastics. A thermoplastic polymer will soften on heating and harden on cooling, so that it can be melted and subsequently reshaped before cooling.

In the molten state, the polymer chains are totally disordered and intertwined. Upon lowering the temperature, the free volume available to the polymer chains is reduced, and therefore the chains must assume a lower energy conformation, triggering the crystallization process. The first step in crystallization is the formation of primary nuclei and is called primary nucleation. There are two types of primary nucleation: homogeneous and heterogeneous. Homogeneous nucleation results from a density fluctuation in the undercooled melt; whereas heterogeneous nucleation is the more probable event in most undercooled systems in which a foreign surface gives rise to the formation of a primary nuclei. The purposeful addition of foreign particles, or, nucleating agents, increases the rate of primary nucleation and also encourages the event to occur at smaller undercoolings. After the nucleus reaches a

critical size, crystallization continues with polymer chains attaching to the growth surface; this step is referred to as secondary nucleation. Because of their sheer length, polymer chains need to fold back and forth as they are incorporated into what is called a lamella. This basic building block of the ultimate polymer solid is sketched in Figure 1.1(a). The chain axis is roughly perpendicular to the lamellar fold-surface plane. Crystallization is spontaneous because the large, negative change in entropy is offset by the large, favorable change in enthalpy which is in turn mostly due to the strong intra-chain forces. The fold surfaces of the lamellae are rough with loops and loose chain ends as well as with those chains which do not end up inside the lamellae. Neighboring crystalline lamellae are separated by relatively disordered amorphous regions, as illustrated in the sketch in (b). The sketch in (c) demonstrates how aggregates of lamellae can form what are called fibrils. Lamellae grow radially outward in all directions and undergo continuous branching and volume-filling to form what are called spherulites. The sketch in (d) illustrates the spherulite as the higher level of order in the series of sketches showing the structural hierarchy of the solid crystallizable polymer material. Spherulites can range in diameter from a few microns to hundreds of microns, depending mostly on the number of crystals initially nucleated and also on the crystallization temperature. Spherulite radial growth ceases when neighboring spherulites impinge upon each other, as shown in the sketch in (e). Impingement lines are straight when the radial growth of the two spherulites is the same, as expected under isothermal conditions. Consequently, the solid plastic material is filled with spherulites. There are other possible crystalline morphologies

encountered on solidification from the melt, such as hedrites and dendrites[4], yet the spherulite is most common.

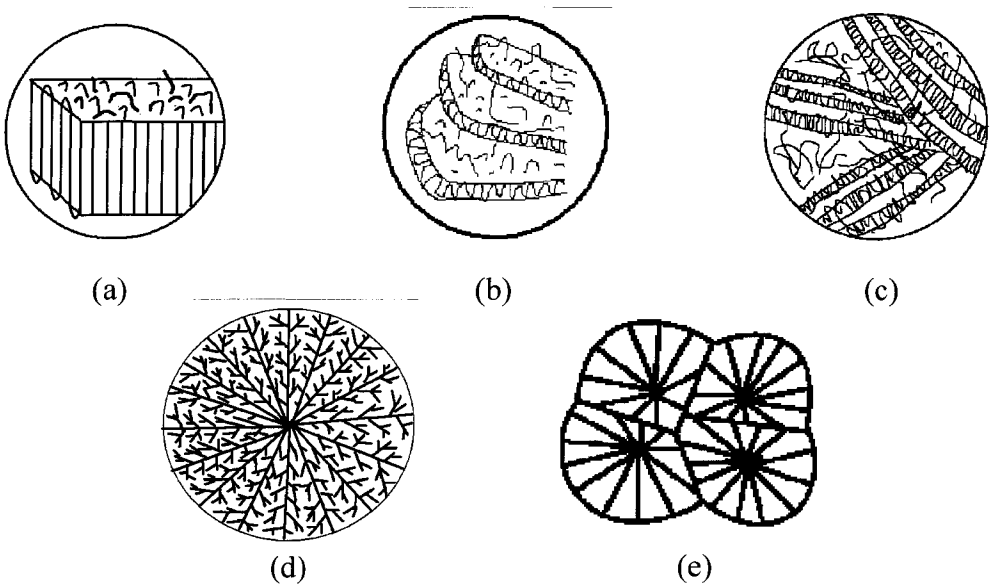

Figure 1.1: A series of sketches illustrating the structural hierarchy of the crystalline solid phase of a thermoplastic material from the level of (a) folded polymer chains forming one lamella; to (b) neighbouring lamellae growing radially with relatively amorphous inter-lamellar regions; to (c) the concerted growth of multiple lamellae to form bundles, or fibrils; to (d) a polymer spherulite, showing the radially growing and branching lamellar building blocks of its interior; to (e) finally the level of the crystalline thermoplastic material showing impingement of the polymer spherulites.

The microstructures of polymer materials strongly affect their macroscopic properties. Accordingly, it is important to examine these structures and to understand the factors which govern their formation in order to predict and/or optimize the properties of the final product material. The physical properties of the final material (which determine its useful function) can be tailored for specific applications by controlling the structure of the material. The structure and consequently the material properties are influenced and/or determined by a number of

factors, including crystallization temperature, polymer chain molecular weight, and by the addition of particles to the melt such as nucleation agents. The modification of the crystalline structure and material properties can also be achieved by the addition of a second component polymer with select properties. Polymer blending, as the name implies, is the physical mixing of two or more polymers together to form a blend that possesses the desired combination of physical properties of its component polymers.

Polymer blends can be initially mixed by dry blending, mixed in a common solvent and then cast, or mixed in the melt and then further processed. For a binary polymer blend, each polymer component can be crystalline or amorphous. Binary polymer blends are popular as the system can remain manageable while providing a desired mix of physical properties. In general, the ultimate solid state microstructures of a binary blend can be homogeneous, possess an 'island structure' two-phase morphology, or possess a multilayer phase-separated morphology, as illustrated by in Figure 1.2 by the sketches (a) through (c).

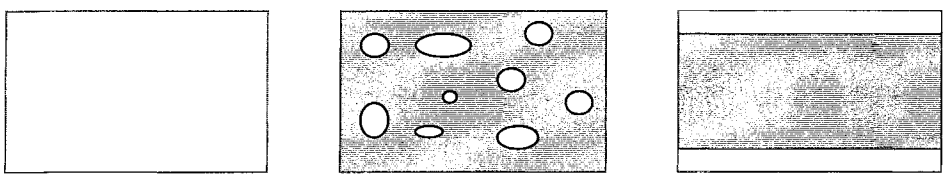

(a) (b) (c)

Figure1.2: Sketches of possible final microstructures in binary polymer blends showing (a) homogeneous blend; (b) binary blend with 'island structure' and; (c) a phase-separated multilayer blend.

The individual phases in each of these descriptions can contain either amorphous or crystallized polymer, depending on the nature of the two polymers blended. The type of final microstructure in the blend material depends on the nature of the two

polymers involved, their respective melting temperatures and crystallization temperature regions, as well as their potential for phase separation, and the specific blend composition.

A multilayered structure results from the complete phase separation of the two polymers. This type of structure usually requires processes of (co)extrusion, injection moulding and compression moulding,[5] and is extensively used in optical devices. The morphologies in (a) and (b) can arise from intimate mixing or phase separation respectively, of amorphous or crystalline polymers, such as the amorphous/amorphous blend of poly(methylmethacrylate)/polycarbonate and amorhous/crystalline blend of poly(phenylene ether)/polyamide.

The morphologies in Figure 1.2 (a) and (b) can also result from a binary blend of two crystallizable polymers which are melt-miscible. The sketches in Figure 1.3 demonstrate how the spherulite morphology might look of two crystallizable polymers in a binary blend that manifests the morphologies in Figure 1.2 (a) and (b), respectively.

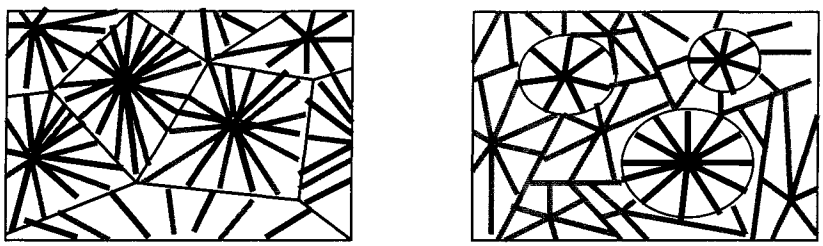

(a) (b)

Figure 1.3: Sketches showing the spherulitic morphology of co-crystallized (a) and partially phase-separated (b) which can result from undercooling a melt-miscible binary blend of two crystallizable polymers.

The melt-miscible polymers may continue to be 'miscible' in the solid and completely co-crystallize as shown in (a). Co-crystallization can occur at the different levels of structural hierarchy in the crystalline solid material, i.e., within the same unit cell, lamella, or spherulite. On the contrary, the polymers may not be completely 'miscible' in the solid state and partially phase separate (b). Such a separation of the blend into a continuous phase and a discontinuous phase can result from the interruption of the thermodynamically-favoured complete phase-separation in the solid by the kinetically-controlled crystallization event of one or both crystallizable polymers. In this way, it is interesting to consider the many possible morphologies which might be designed by controlling the events associated with undercooling the polymer blend. A wide range of morphologies between these two extremes can be achieved by varying the composition, crystallization temperature, and the rate of cooling.

1.3 Biodegradable Plastics: General

Polymers commonly used to make such commodity products as grocery bags, plastic containers, foams and tubing include polyethylene (PE), polypropylene (PP), polystyrene (PS) and poly(vinyl chloride) (PVC). These synthetic polymers are normally made from petrochemical sources and are not biodegradable. The chemical structure of the repeat unit is rather inert, so that there is little to no opportunity for chemical breakdown of the molecules. Even if the chains were susceptible to microbial attack, it would be difficult for decomposer organisms to assimilate these essentially crystalline solid constituents of the thermoplastic materials and

consequently breakdown these molecules. Conversely, thermoplastics made from polymers with a functional group in their repeat unit that can chemically respond to the elements of the environment are therefore potentially biodegradable. Biodegradable polymers can be naturally-occurring or be synthetically made. Chemicals used to synthesize biodegradable polymers may be derived from either renewable resources, or non-renewable resources but the desire to synthesize them from renewable sources is in keeping with the environmentally responsible desire to make biodegradable polymers in the first place.

It is both appropriate and helpful at this point to clarify some definitions that exist surrounding the popular use of the terms *biodegradable* and *compostable.* According to the ASTM standard D-5488-94d, the term biodegradable implies "capable of undergoing decomposition into carbon dioxide, methane, water, inorganic compounds, or biomass in which the predominant mechanism is the enzymatic action of microorganisms that can be measured by standard tests, over a specific period of time, reflecting available disposal conditions."[5] There are many different specifications of biodegradability, and they vary from country to country. However, it is generally accepted that 60% to 90% of a biodegradable material can be decomposed within 60 to 180 days in a standard composting environment.[6] A compostable material is defined as "capable of undergoing biological decomposition in a compost site as part of an available program, such that the material is not visually distinguishable and breaks down to carbon dioxide, water, inorganic materials and biomass, at a rate consistent with known compostable materials."[7]

Biodegradable polymers can be considered to comprise two main families: agro-polymers (e.g., starch) and biodegradable polyesters. The latter group can be considered to further comprise three categories which include (i) microbially-produced polymers (e.g., poly(beta-hydroxybutyrate)); (ii) synthesized polymers from monomers that are obtained from agro-resources (e.g., poly(lactic acid)); and (iii) synthesized polymers from chemically-synthesized monomers (e.g., polycaprolactone).[5] Table 1.1 is a current list of both biodegradable and physically degradable polymer materials along with their industry trademarks and industrial developers.

Table 1.1: A list of degradable* polymer materials and their developers, trademarks and polymer key components, taken from reference [1].

Polymer Developer	Trade Mark Name(s)	Key Components
Bayer	BAK 1095	Polyester amide
Bioplastics	Envar	Starch and polycaprolactone
Cargill Dow	EcoPLA®	Polylactic acid
Chronopol	Heplon ™	Polylactide
DuPont	Biomax®	Polyester, copolymer
Eastman	Eastar Bio ™ Copolyester 14766	Polyester made of conventional diacids and diols
EPI	DCP ™	Polyethylene + additives (not a Masterbatch)
Indaco	Bio-Solo ™	Recycled PE + activators

Monsanto	Biopol™	Polyhydroxyalkanoate
Novamont	Mater-Bi™	Corn starch + polycaprolactone
Novon Intl.	DegraNovon®	Polyolefine + additives
Planet Polymer Technologies	EnviroPlastic® C	Polycaprolactone-based resins (no starch or polyethylene)
Showa Highpolymer	Bionolle®	Aliphatic polyester
Technicoat	Tech-No-Bag®	Polyethylene + additives
Union Cambridge	TONE® P-787	Polycaprolactone
Willow Ridge	Polystarch®	Polyethylene + starch

** The term degradation is used here to include both the physically breakdown of polymer chains and subsequent chemical breakdown by microorganisms.*

1.3.1 Starch

Until recently, starch remained the most investigated naturally-occurring polymer for balancing both biodegradation issues and production cost issues.[9] It had continued to show considerable promise as a biodegradable plastic on its own or in blends. Starch is generally a mixture of linear and branched molecules called amylose and amylopectin, respectively (shown in Figure 1.4). A unique ratio of these two components gives rise to alternating amorphous and crystalline zones in the overall material which in turn generates various characteristic physical properties.

Native starch is used as filler to make reinforced plastics,[5,10] but must be modified for useful application.[5] The chemical modification of starch has been performed since the first half of the twentieth century. In 1942[11] and 1943[12], Mullen and Pacsu,

together, published a critical analysis of starch-ester-preparation methodologies, and on the industrial use of modified starch, respectively.

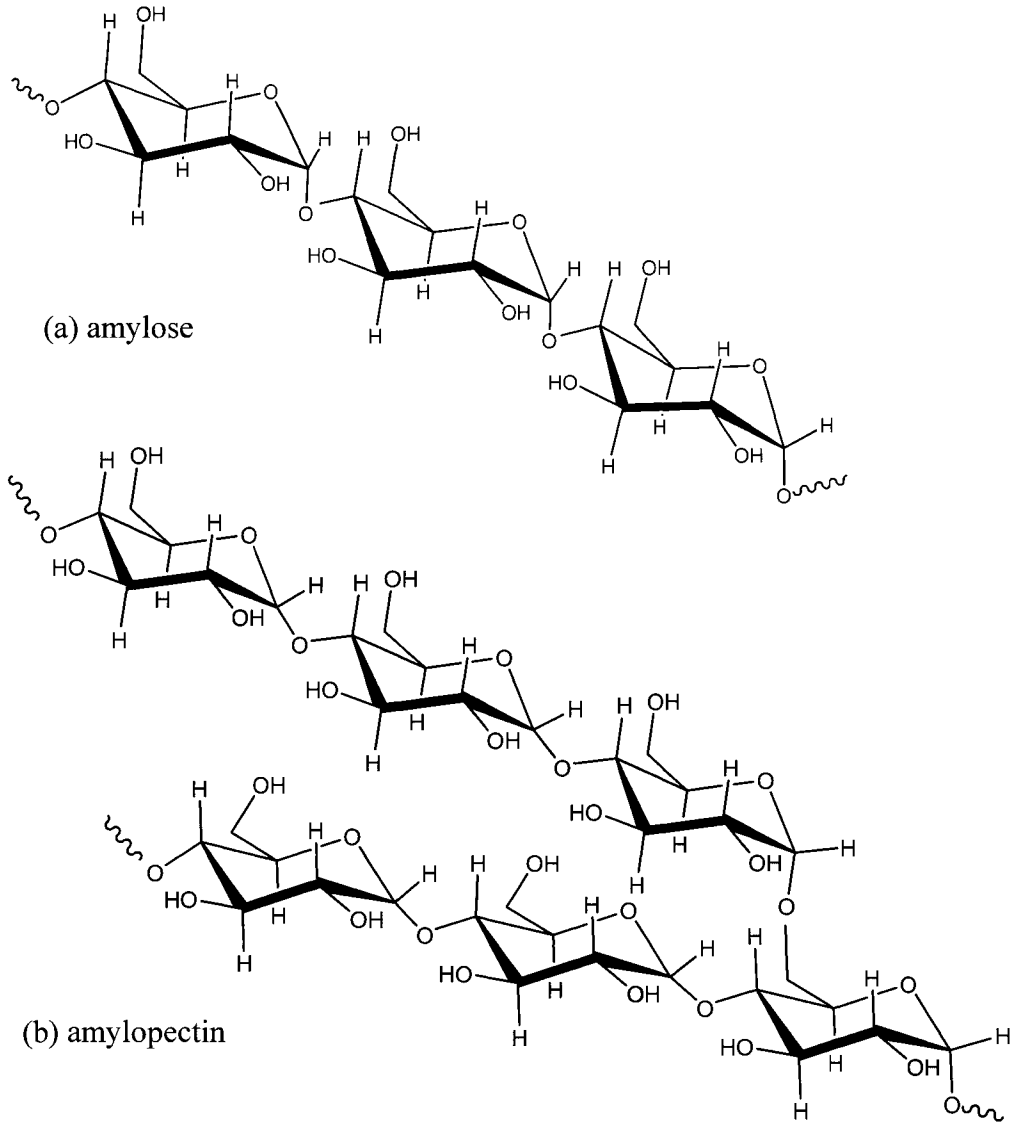

Figure 1.4: Representative partial structures of amylase (a) and amylopectin (b)

Plasticized starch (or, *modified starch*) can also be blended with other polymers. These binary blends possess the desired combination of properties of biodegradability, as well as flexibility and ease of processing derived from the synthetic polymer component. There are a number of categories of biodegradable starch-based polymer

blends reported in the literature, which include as the second synthetic component low density polyethylene (LDPE),[13] polycaprolactone (PCL),[14] poly(β-hydroxybutyrate) (PHB),[15] poly(lactic acid) (PLA),[10] and poly(vinyl alcohol) (PVA).[16]

The large number of research published work on starch based materials has lead to the identification of some processing challenges associated with blending starch with other polymers. In contrast to the synthetic polyolefin polymers which are hydrophobic, starch is a *hydrophilic* polymer and this fundamental physical difference can lead to physical difficulties in the preparation of blends. Treatment of starch granules with surfactants (i.e., the graft copolymerization of starch with hydrophobic monomers) has been used to improve their compatibility.[17] These surface-treated starch-based polymers have been successfully blended with high-performance polymers such as aliphatic polyesters and polyvinyl alcohols, to attain desirable functional properties that fit diverse applications.

1.3.2 Poly(β-hydroxybutyrate)

Poly(β-hydroxybutyrate) (PHB) is a bacterial polyester and was first isolated from a *Bacillus magaterium* bacteria cell by Lemoigne in 1926.[18,19] The basic repeat unit is shown in Figure 1.5. It has attracted much attention as a biodegradable thermoplastic polyester which can be produced without the depletion of non-renewable resources.

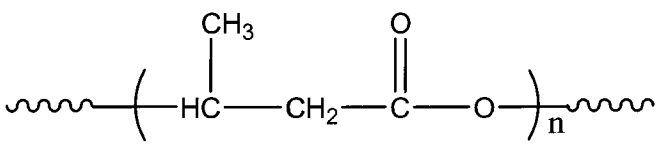

Figure 1.5: Structure of the repeat unit of PHB.

In addition to being entirely biodegradable, PHB is a biocompatible thermoplastic possessing similar physical properties to conventional thermoplastics. However, PHB is a highly crystalline polymer which can render materials made from this homopolymer very brittle and with unfavorable mechanical performance. Its limited utilization as a commodity plastic is associated with both its brittleness as well as with its relatively high cost of production. These shortcomings of the homopolymer have in part promoted research into using PHB in polymer blends. Blending could address both the brittleness issue as well as the cost issue. Therefore, blending with a natural and inexpensive polymer, such as starch,[15] is one potential way to improve its properties and achieve lower cost of production.

1.3.3 Poly(lactic acid)

Poly(lactic acid) (PLA) is a linear aliphatic thermoplastic polyester, and its repeat unit is represented in Figure 1.6. This is an interesting polymer as it is can be produced not only from non-renewable sources but also from renewable ones. Lactic acid can be obtained from the fermentation of renewable agricultural sources such as corn, sugar cane, and sugar beet.

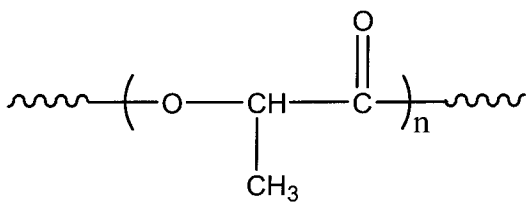

Figure 1.6: Structure of the repeat unit of PLA.

As a biocompatible polymer, PLA has been used successfully primarily in medical applications for many years[20-22] and less so in commodity-type applications

due to the relatively high cost of processing. Currently, new processing technologies have permitted PLA to take a competitive place in the plastic materials industry. Details of these improved processes are described in the following section of this chapter. Widely accepted because of its biodegradability, this polymer can be processed to replace less environmentally friendly hydrocarbon-based polymers, such as polyethylene or polystyrene. PLA is a potential polymer for diverse end-use application due to its fine mechanical properties, thermal plasticity, biocompatibility, and degradability.[23] Moreover, it does not release nitrogen oxide and only produces one third of the combustible heat compare with other polyolefins while burned, which provides enormous energy savings. The combination of these properties allows PLA to emerge as a wide-spread material in a rather broad range of applications.

1.3.4 Poly(ε-caprolactone)

Poly(ε-caprolactone) (PCL) is another linear aliphatic thermoplastic polyester. The structure of the repeat unit is shown in Figure 1.7.

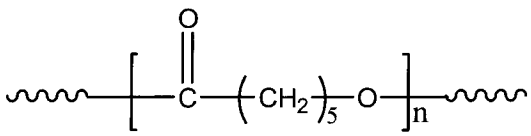

Figure 1.7: Structure of the repeat unit of PCL.

PCL is generally prepared by the ring-opening polymerization of ε-caprolactone[24] and its synthesis was first reported in 1934.[25] Material from PCL demonstrates good mechanical properties, and PCL is widely used as a plasticizer in poly (vinyl chloride) and in polyurethane applications.[5] In 1973, this synthetic PCL was first identified as a biodegradable polymer.[26,27] Since then it has been discovered that it exhibits great

biodegradability in different biotic environments, such as fresh water systems, sewage sludge, farm soil, and a variety of sediments.[28,29] In addition, it is biocompatible, non-toxic and shows high permeability, and thus has been widely studied as a controlled drug-release carrier and as degradation substrate.[30,31]

The application of PCL in a wide variety of potential uses is limited by processing difficulties that arise due to its very low T_g (*ca* -61 °C) and relatively low melting temperature (*ca* 65 °C). Therefore, PCL is usually modified (e.g, crosslinked[32] or copolymeriz[33] with other monomers) or blended with other polymers (e.g., starch[5,14,34,35]) for commercial applications.

In all of the above-mentioned polymers, their biodegradation is attributable to the action of specific microorganisms that secrete enzymes to break them down for consumption. Very generally, the mechanism of this biodegradation starts with the enzyme attack at weak polymer linkages, which leads to chain scission, or a decrease in polymer length. The resultant smaller pieces can be readily utilized in biochemical pathways.

Research on the development of polyesters as biodegradable materials represents the most active area of research and manufacture response to the current polymer waste situation. This research includes the areas of compostable polymers and polymer blends. Biodegradable polyesters from renewable sources offer great potential as commodity plastics that can meet the big picture objective by providing functionality as well as biodegradability on an appropriate time scale without the depletion of natural resources.

1.4 Poly(lactic acid)

Lactic acid, as the repeat unit or building block of poly(lactic acid) (PLA) polymer chain, was first isolated in 1780 from sour milk, and was first produced commercially in 1881.[36] Carothers[37] pioneered the manufacture of PLA in 1932, but this was on a low molecular weight polymer. An improved polymerization technique was developed by DuPont in 1954 to obtain a higher molecular weight product.[38] However, the elevated cost of the product polymer restricted the use of PLA until the late 1980s, when the price was lowered by the production of lactic acid from corn fermentation.[39] Subsequently, this technology was modified by different research groups[40-42] bringing PLA to the point of commercial production.[8]

There are different synthesis routes to convert lactic acid into high molecular weight PLA, as shown in Figure 1.8. In route [1], PLA can be prepared through the condensation of lactic acid to form low molecular weight prepolymers followed by a second step that uses external coupling agents to produce high molecular weight PLA. Direct condensation using azeotropic distillation is a second route [2]. In the third route [3], depolymerizaiton of low molecular weight prepolymer produces lactide, which is in turn used to create PLA via ring-opening polymerization.

In industry (e.g., Cargill Dow), the ring-opening polymerization path has routinely been used in synthesis of pure, high molecular weight PLA. Mitsui Toatsu[43] has recently commercialized the azeotropic process [2] in the production of PLA. Cargill Dow LLC is one the first companies that has first produced PLA from annually renewable resources such as fermentable sugar.[44] Corn is used as it is one of

the cheapest and most abundant sugar sources. In the Cargill Dow process, the raw sugar is milled to separate out the starch, from which unrefined dextrose can be processed. Lactic acid can then be derived through fermentation. Subsequently, lactide is formed through condensation and depolymerization as in route [3] above. The lactide monomer is further purified by vacuum distillation. The final step is the ring-opening polymerization of the lactide in a solvent-free melt process.

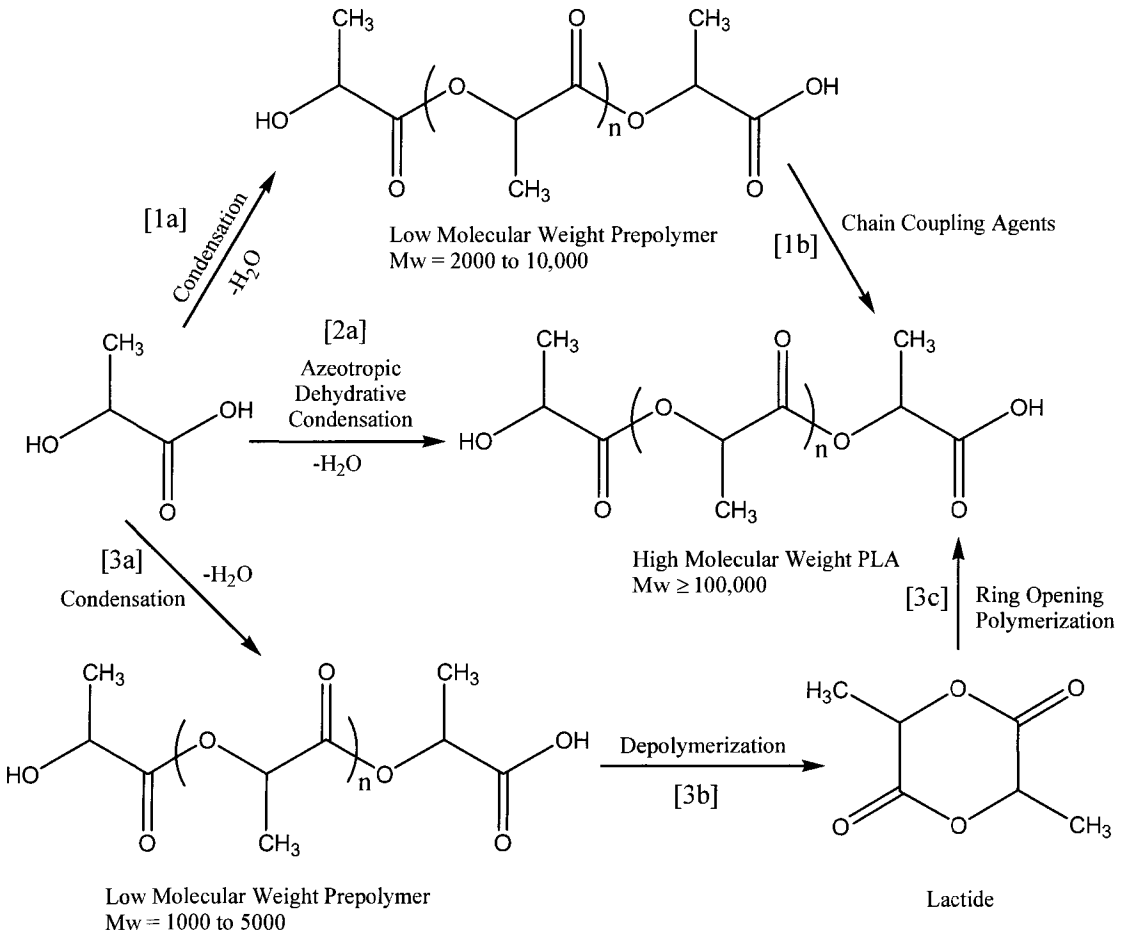

Figure 1.8: Synthesis of high molecular weight PLA[39,45]

The degradation of polymers can be induced by ultra-violet rays, ionizing radiation, heat, chemical oxidation and hydrolysis, and the latter two are the major

ways of degradation. Synthetic hetero-chain polymers (e.g. polyesters) normally degrade by a hydrolytic process, which goes along with microbial bioassimilation of the hydrolytic products. Carbon-chain polymers, on the other hand, undergo degradation by peroxidation. Microorganisms, such as bacteria and fungi, then attack the low molar mass carboxylic acids that are produced previously.[46] According to Eggins *et al.*[47]synthetic hydrocarbons can be degraded by a variety of thermophilic microorganisms following transition metal-catalysed thermal peroxidation.

PLA is a polyester which is susceptible to moisture, and this grants the primary driving force in the degradation pathway. As depicted in Figure 1.9, the water molecule diffuses into contact with hydrolytically labile bonds, resulting in the cleavage of the ester linkage and reduces the molecular weight via chain scission.[45,48] The degradation rate via hydrolysis primarily depends on temperature and relative humidity.

Once breakdown of the chain has resulted in a reduction in average molecular weight to about 10 000, PLA is ready to be metabolized by various microorganisms in natural environments, such as through fungi assimilation,[49] from which the low molecular weight lactic acid oligomers are converted to carbon dioxide and water.[45] Composting is a preferred disposal route to biodegradation, and PLA degrades rapidly with this relatively high temperature (55-70 °C) and high relative humidity.[45]

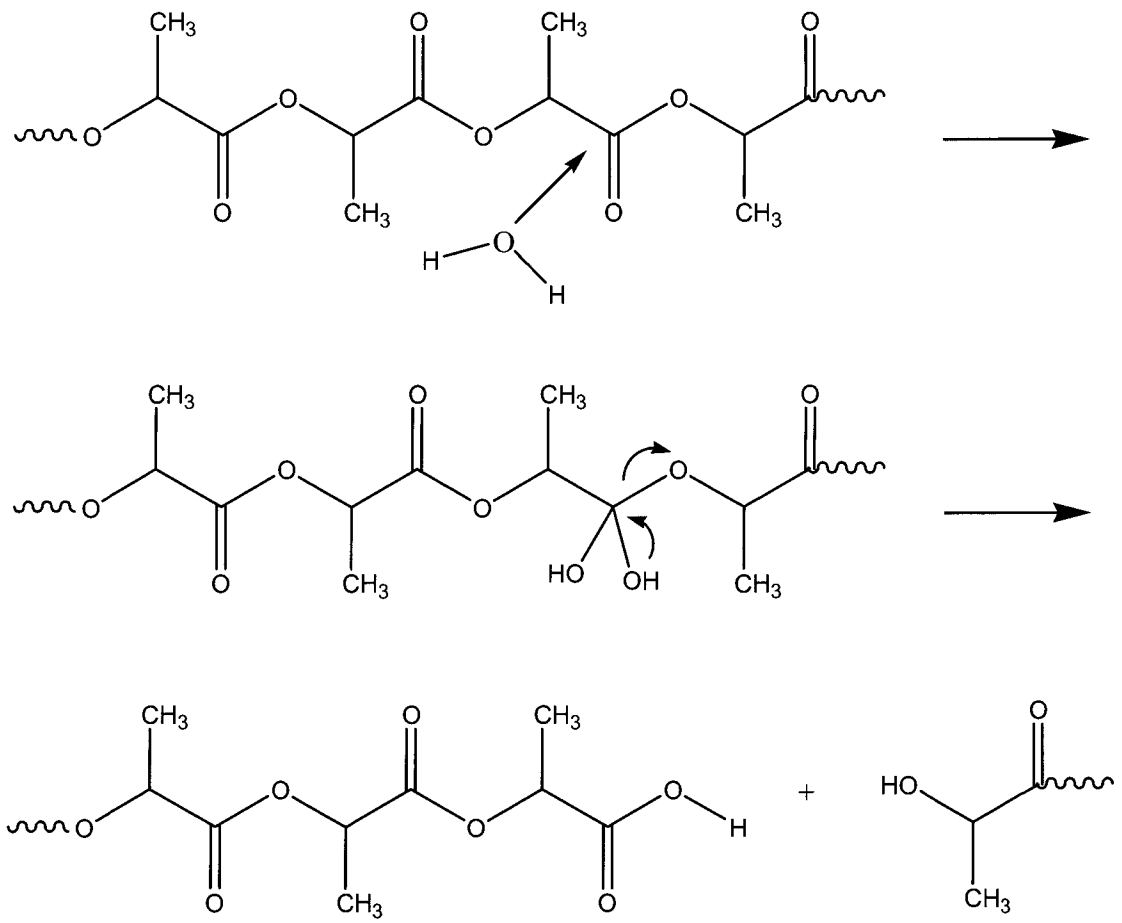

Figure 1.9: Hydrolysis of PLA[45,48]

1.4.1 Poly(*l*-lactic acid): A Literature Review

Lactic acid possesses a chiral center and therefore exists in two enantiomeric forms. The two enantiomers are *d*(+) and the naturally occurring *l*(-) forms, which can rotate polarized light in the clockwise and counter-clockwise direction, respectively. Figure 1.10 illustrates the two stereoisomers in their *R* and *S* configurations. The *R* and *S* assignments are based on the rank of priority of the substituent atom that bonded to the asymmetric carbon. Commercially available PLA is generally a copolymer of both enantiomeric monomers. Properties such as melting temperature and degree of crystallinity are greatly influenced by the relative

optical purity of the polymer repeat units. Optically pure PLA homopolymer (either all *d*- or all *l*- form) is isotactic and highly crystalline. However, if the repeat units in the polymer are a mixture of *d*- and *l*-monomers then the stereoregularity and crystallinity of that copolymer decreases with decreasing optical purity. If a poly(*l*-lactic acid) backbone contains more than 15% *d*-enantiomer component, it is actually characterized as an amorphous polymer.[50]

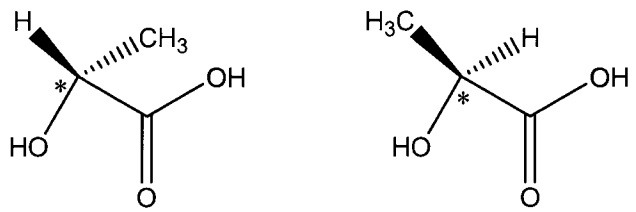

R *S*

Figure 1.10: The *R* and *S* stereoisomers of lactic acid showing the chiral centers.

The lactic acid monomers can be produced either by the petrochemical route or by the fermentation route. The former produces a 50/50 racemic optically inactive mixture of the two enantiomeric forms, while the latter technique yields the *l*-lactic acid in high purity.[45]

1.4.1.1 Crystal Structure

It is reported evidence that PLLA can form three different crystal types, resulting from particular thermal and mechanical conditions (e.g., spinning and drawing). The three crystal types (reported as modifications) are distinguished on the basis of helix conformations and unit cell symmetries. From solution-spun fibers, De Santis and Kovacs[51] first determined the crystal structure of the α-modification. This α-form has a pseudo-orthorhombic unit cell through which passed two chains that were

assumed to form a left-handed 10_3 helix. The unit cell was determined as having the parameters of a = 1.07 nm, b = 0.645 nm, and c (fiber axis) = 2.78 nm. A number of more recent papers reported slightly different parameter values of the α-phase unit cell.[52-54] In one particular study, the results indicated some deviation from a "pure" 10_3 helix.[54] The second structure modification of PLLA, known as the β-modification, was first observed by Eling *et al.* in 1982 from mechanically stretched PLLA fibers.[55] Although no solved crystal structure has been reported, there are a few investigations which show that this modification is based on a three-fold helical chain conformation, with parameter c = 0.88 nm[56] or 0.9 nm.[54] Furthermore, Hoogsteen *et al.*[54] proposed an orthorhombic unit cell (a = 1.031 nm, b = 0.821 nm, c = 0.900 nm), which included six helical chains, to form a left-handed 3_1 helix. However, Brizzolara *et al.*[57] suggested this β-form orthorhombic unit cell has two parallel chains, based on the data of Hoogsteen *et al.* More recently, the β-modification was considered as a *frustrated structure*[58], and the proposed trigonal unit cell (a = b = 1.052 nm, c = 0.88 nm) was reported to have three chains (not six or two). The γ-form is the third modification that has been reported, which was found by epitaxial crystallization from hexamethylbenzene substrate. It is very close to Brizzolara *et al.*'s β-model, and has a reported orthorhombic unit cell with parameters a = 0.995 nm, b = 0.625 nm, c = 0.88 nm[52] with two *antiparallel* helices passing through.

1.4.1.2 Morphology and Crystallization Kinetics

In general, the properties of a polymer material which make it useful are a consequence of the structure. As PLLA is a crystalline polymer, many of its

properties arise from its crystalline structure. The crystalline structure in turn depends on the crystallization conditions (e.g., sample thickness, isothermal crystallization temperature or cooling rate). Other polymer properties such as the number and weight average molecular weights (M_n and M_w) of the constituent chains and the polydispersity (M_w/M_n) also play an important role in influencing the crystallization process and therefore determining the physical properties in the crystalline material.

Investigations on morphology and crystallization events are essential to the understanding of polymers and their processing. Temperature control promotes the development of a certain morphology which in turn regulates the ultimate properties of the material made from it. Consequently, both T_c and the cooling rate used to approach the T_c are critical since they provide a kinetic control of crystallinity and the crystal morphology. Since T_c governs thermodynamics and kinetics of structure formation, morphology and kinetics information at different T_c from isothermal crystallization is able to be gathered and used together to model non-isothermal events.[59-64]

A significant number of studies on morphologies and crystallization behaviour of PLLA have been reported, and extensive progress has been made in elucidating its crystalline structure and describing its crystallization kinetics.[65-71] Using optical microscopy, Vasanthakumari and Pennings varied undercooling conditions (e.g., T_c) and molecular weight, and reported the effects on both growth and morphology of the PLLA spherulites.[66] In succession, Kishor and Vasanthakumari[67] used

differential scanning calorimetry (DSC) to investigate the PLLA crystallization parameters. Subsequently, Miyata and Masuko examined the morphology and structural characteristics of PLLA solution-grown crystals, using transmission electron microscopy (TEM), X-ray diffraction and atomic force microscopy (AFM).[69] They also studied the crystallinity and spherulite morphology of PLLA in bulk films as a function of thermal conditions.[70] Doi *et al* published extensively on structure and properties of PLLA crystals in thin-films crystallized from the melt state under controlled conditions.[72] Using electron microscopy and AFM, they found the crystal structures of the dendritic and hexagonal growth habits to be identical. They also found that the lateral growth rates of the two structures are the same, suggesting that crystalline morphology depends on film thickness to a greater degree than previously understood.

PLLA has also been reported to crystallize according to different so-called regimes, depending on the crystallization temperature range and undergoing a regime change at a specified 'regime transition temperature'. Studies of the dependence of this regime transition temperature of PLLA on molecular weight and molecular weight distributions have also been carried out. Based on electron diffraction examinations, Abe *et al.* found that the average individual lamellar growth direction is parallel to the crystallographic b-axis. Observed morphology changes in the crystalline aggregates were found to correspond to a change in the crystallization regime, a so-called regime I-to-II transitions. No noticeable morphological changes were detected, however, to correspond with the change in crystallization regime

II-to-III transition. The authors suggested that the changes associated with regime I-to-II transition may be associated with the secondary nucleation rate on the {100} plane growth surface.[73]

There are two unique characteristics of PLLA, regarding its morphology and kinetics, respectively. PLLA lacks an extremely common morphological feature among most polymer spherulites: the appearance of regular, periodic extinction birefringence rings, or bands, when viewed under polarized light. All morphological indications show non-banded PLLA spherulites, while most other polymers possess concentric extinction bands, due to twisting of the radially-extending lamellar crystals, or at least to their periodic orientation with radius.[74] Nevertheless, quite a few research articles[75-79] reported the appearance of banded spherulites in PLLA blends when crystallized from the melt. The banding phenomenon in polymers has been extensively investigated and discussed for decades and still no accordant conclusion has been achieved.[74,80-93]

A distinctive kinetic characteristic of PLLA is its surprising *non*-bell-shaped spherulite growth rate curve, specifically, the plot of spherulite radial growth rate versus isothermal crystallization temperature. Isothermal bulk crystallization rates (G) have been measured in the range of 70 °C to 165 °C with a proposed maximum G occurring at around 130 °C.[94,95] However, in the temperature span of 110 °C to 120 °C, G increases again, forming a second, even higher peak on the growth rate curve.[53,54] Two explanations have been suggested for this observed anomaly. The second, lower temperature maximum growth rate is proposed to be related to a regime

II – III transition[73,95], or to the possibility of β-modifications developed upon the already formed α-phases.[53,96]

1.4.1.3 Single Crystals

The crystallization of PLLA has been explored from the melt,[59-64] in dilute solution,[65,69,97-100] and by solvent casting.[73,93,101,102] Single crystals, mainly developed from dilute solution, have the most well-defined structures due to the clean and smooth surfaces that result from such slow, close-to-equilibrium growth conditions, and therefore have been widely used as an ideal substrate to illustrate degradation of crystals.[97]

Several research groups have been developing solution-grown PLLA lamellar single crystals, to study their crystal morphology and structural properties.[65,69,98,99] Fischer *et al.* [98] was the first to grow PLLA single crystals, but with 15% *d*-enantiomer. Kalb and Pennings[65] acquired two types of PLLA single crystals from toluene and *p*-xylene dilute solution. By means of electron diffraction, they found a smaller dimension hexagonal molecular structure than previously reported. From acetonitrile, Miyata and Masuko[69] prepared lozenge-shaped PLLA single crystals by isothermal crystallization. They then determined the orthorhombic unit cell parameters, from electron diffraction patterns and X-ray diagrams. Iwata and Doi[99] obtained both hexagonal and lozenge shaped PLLA single crystals from *p*-xylene, and these crystals were reported to have the same orthogonal unit cell parameters. Hence, it was concluded that the hexagonal crystals are actually pseudo-hexagonal with orthorhombic packing of PLLA chains.

In addition to the aforementioned studies, the effects of annealing[69,97,103,104] and its consequences on degradation of PLLA single crystals has also been investigated. Miyata *et al.*[69] reported that annealing increases the lamellar thickness after examinations using TEM, X-ray diffraction and AFM (*ex situ*). More recently, Fujita *et al.*[97] equipped an AFM with a heating stage to record the direct visualization of the PLLA single crystal growth manner during annealing *in situ*. The edges of the crystal were found to thicken during annealing, indicating that the edges were initially less stable and less ordered than central regions of the lamellae. Melting of the un-thickened part started at a higher annealing temperature, and this began from the boundary between thickened section and growth front rather than the folding surfaces. Combined with what has been reported, the authors deduced that crystal chains in the edges and defected area are more mobile than those in the well-ordered region, and that processes of melting and degradation initiate in edges of lamellae and at their sites of defects.

1.4.1.4 Stereocomplexes

Polymers of opposite stereoisomer monomers may have the same or different chain configurations. When the interaction between different configuration polymer chains is stronger than that between two of the same, stereocomplex formation (i.e., stereocomplexation) can take place.[105] As the lactic acid monomer can exist in either of its two stereoisomers, PLA is one of the few polymers in which the stereochemical structure can be controlled by varying the composition of these two chiral monomers during its synthesis.

In 1987, Ikada *et al.*[106] first reported on the stereocomplexation between enantiomeric poly(*l*-lactic acid) and poly(*d*-lactic acid). Since then, intensive studies have been carried out and a sufficient amount of information has been obtained and accumulated.[50,102,107-118] Tsuji and Ikada found that, in comparison with optically pure PLA enantiomers, the overall completion of stereocomplex crystallization takes shorter time.[107] They suggested this phenomenon results from the smaller sizes of the final stereocomplex crystallites and therefore they give rise to higher spherulite density.[50,107] Brochu *et al.*[108] then discovered that stereocomplex crystallites are able to form epitaxially on the PLLA homocrystallites. Urayama *et al.*[109] also reported that talc enhances the spherulite nucleation of stereocomplex crystallites. In addition, PDLA can be served as nuclei and add to PLLA materials to form stereocomplex crystallites on PLLA spherulites, as published by Tsuji and Ikada.[107] Most notably, Tsuji and Ikada[111] reported a high enthalpy of melting for stereocomplex crystallites in equimolar blending of PLLA and PDLA with M_w less than 200 000. In this 1:1 blend sterecomplex sample, it was also found that the spherulite formation was suppressed. Very recently, Tsuji and Tezuka[110] investigated the mechanism of the rapid crystallization completion of the overall stereocomplex PLA crystallites, and they concluded that this results from the combination of the short induction period, the high growth rate, and the high density of those spherulites. Regarding the merits of stereocomplex crystallization, it has been discovered to improve the mechanical properties, thermal stability and hydrolysis resistance of PLLA materials.[111-114]

1.4.1.5 Degradation

Research on the degradation of PLA has focused on the *chemical* hydrolysis of ester bonds in the main chains.[100,119-122] Recently, there are an increasing number of studies on the *enzymatic* hydrolysis of PLA.[39,99,101,115-118, 122-126] PLLA is able to degrade by simple hydrolysis in a moist environment without the enzyme to catalyse.[39] In the laboratory environment, enzymes are typically used to accelerate this process in the studies of the degradation mechanism. The enzyme proteinase K is generally the enzyme of choice for PLLA work since Williams first used it in 1981.[127] Proteinase K is considered to be a very effective catalyst to accelerate the degradation process.

Subsequently, this enzyme has been used extensively to study the mechanism of degradation of PLLA.[99,117,123] It has been found that this enzyme hydrolyzes *l*-lactyl units preferentially to *d*-lactyl units in the polymer chain, making the stereochemical structure of the chain an important factor in the degradation of the polymer. It has also been shown that enzymatic degradation occurs predominantly in the amorphous regions of the polymer solid as compared to the more crystalline regions.[115-118]

There is a general agreement among groups studying PLLA degradation, that the property of biodegradability is not independent of other properties. In fact, biodegradability depends on a lot of different factors, such as polymer chemical structure, molecular weight, molecular weight distribution, degree of crystallinity, distribution of amorphous regions inside its crystal, and overall morphology of the sample.[39,100] These are in turn controlled by crystallization temperature and method of preparation (i.e., from thin film melts or from dilute solution). Moreover, the

water diffusion rate into polymer affects the accessibility of enzyme reaction, and therefore is another controlling issue for the degradation rate.[124] While PLLA manufactured for commercial use is not single crystal form, fundamental studies on the degradation of these controlled morphologies are essential contributions to the understanding of the overall process.

As a group, studies of the enzymatic degradation of solution-grown PLLA single crystals are typically performed using different types of microscopy to actually view the changes in the morphology with degradation. These include TEM and AFM. TEM gives sample overall morphology and its pattern provides angles between growth faces. AFM offers the advantages of *in situ* observation of the process at high resolution, while the sample, in theory, remains unperturbed in its enzyme solution environment. For a more quantitative look at the process, gel permeation chromatography (GPC) is used to determine changes in chain length and polydispersity as the degradation process chews the material.[123,125,126] It is generally accepted that proteinase K enzyme preferentially attacks disordered chain packing regions of a given morphology rather than more ordered chain folding surfaces. In extraordinary cases, a hole is observed after a longer degradation period, perhaps due to hydrolysis of polymer chains chopped out of crystalline regions.[99]

PLLA thin films can be prepared from the melt without free amorphous region at controlled temperatures and thicknesses which permit the controlled variation of morphology.[123] Again, it is generally found that enzymatic hydrolysis rates strongly

depend on crystallinity and thickness, and that enzymatic degradation primarily occurs in restricted amorphous regions rather than in lamellar folding surfaces.

These studies demonstrate that the degradation process, while chemical in nature, is very dependent on the physical nature of the sample, relying on the physical permeation of the material and diffusion of the enzyme into the sample.

Advances in the study of PLLA degradation characterization have included a characterization of the amorphous regions of thin-film morphologies into free and restricted regions.[125] These correspond to inter-crystalline and intra-lamellar regions, respectively. AFM, TEM and X-ray diffraction were used to define these characterizations.

A novel gravimetric approach was employed to test the rate of weight loss using GPC during enzymatic hydrolysis with the various morphologies.[125] This rate was found to decrease rapidly in a sample with a degree of crystallinity below 33%, and decreased slowly in samples above 33%. The amorphous material in the former sample was considered "free" and in the latter samples, it was considered to be 'restricted'. Results of this work have been able to further the understanding of the degradation process by demonstrating that restricted amorphous regions are more hydrolysis resistant than free amorphous regions. In addition, by using GPC, they uncovered that an increase of crystallinity during degradation process was ascribed to the hydrolysis and removal of the amorphous state, rather than to crystallize of it.

On another enzymatic degradation study of PLLA thin film of specific thickness, the surface morphology was examined before and after degradation using AFM.[101]

Two types of amorphous regions were found, around the crystals and between the crystal and glass substrate, respectively. The degradation rate of the former was found to be faster than that of the latter. Temperature-controlled AFM was also used to examine the crystals during melting, to correlate chain folding process and crystal stability. The unstable {100} plane melted to a comb-like state while no changes of {110} plane demonstrated that the thermal behaviour was affected by the stability of chain folding, chain packing state and crystal growth direction.

1.4.1.6 Physical Properties

PLA is a high-strength, high-modulus thermoplastic, and it is versatile in replacing traditional plastics in a more environmentally benign manner. It exhibits many properties that are equivalent to or even better than a lot of petroleum-based plastics. PLA presents a medium permeability level for water and oxygen.[5] It is clear and naturally glossy as conventionally-used polystyrene, and it thus can be used as common packaging materials. PLA can also make blister-like bags for fragile products.[128] PLA is more grease/oil and moisture resistant and provides a better flavor and odor barrier than popularly-used poly(ethylene terephthalate) (PET). Its tensile strength and modulus of elasticity is also comparable to PET, and therefore, it is appropriate for food packaging and beverage containers.[129,130] PLA is suitable for substitution of fiber in some aspects. Clothes made from PLA are not only soft and light, but easily absorb away moisture from skin. According to its biodegradable and biocompatible nature, PLLA can be applied in medical applications, such as sutures, implants and controlled drug release carriers.[20-22]

1.4.1.7 PLLA-based Materials

To date, PLLA has been mainly used in biomedical areas, as its applications in the packaging industry are limited by its low strain at break and high modulus. Hence, endeavors have been taken to improve its mechanical properties. Generally, three approaches have been taken for this purpose, such as copolymerization with other monomers, modification with plasticizers, and blending with a second polymer.

Poly(ethylene glycol) (PEG) and PLLA di- and multiblock polymers have been intensively reported[131-138] as copolymers to vary physical and biological properties of PLLA. Other monomers such as ε–caprolactone[139-141], 2,2-dimethyltrimethylene carbonate (DTC)[142] , d-xylofuranose[143] have also been used to copolymerize. It has been investigated that a wide spectra of mechanical properties are able to be achieved by this copolymerization approach, yet none is economically applicable and thus none has been produced on industrial scale for packaging applications.

Plasticization is another option to modify PLLA. Examined candidates include lactic acid monomer,[144,145] PEG,[145,146] glucose monoesters,[146] partial fatty acid esters,[146] thermoplastic starch,[10,145] citrate ester,[145,147,148] PCL,[77,149,150] poly(3-hydroxy butyrate) (PHB),[79,151,152] and glycerol.[145] Sometimes more than one additive has been used as plasticizer, such as lactic acid /ethylene oxide blend[136] and PEO and PPO copolymer.[153] The resulting plasticized PLLA materials gained flexibility and impact resistance. However, there are still potential problems. Low molecular weight materials are normally the best for plasticizing agents,[154] but leaching (e.g, weight loss) tends to occur owing to their small molecule mobility.[147,155] The lactic acid monomer itself has disadvantages of fast migration and therefore causes a

stiffened polymer with a slushy surface.[146] Polymeric plasticizing agents solve the leaching problem with their high molecular weight, nevertheless, the long-chain polymers typically generate macrophase separation due to the unfavorable thermodynamics of mixing, which in turn leads to unstable morphology and the development of weak interfacial adhesion and poor mechanical properties.[156,157] As a result, the ideal plasticizing agent for PLLA modifiers is quite limited by the requirement of application. It has to be miscible with PLLA, possess a considerably lower T_g, be non-toxic, and maintain biodegradable properties for final materials, while being unleachable, not too volatile, nor be able to migrate very easily.

Polymer blends have attracted much interest as a method to improve polymer properties by simple physical blending.[153] Quite a few polymers have been used to blend with PLLA in order to control the overall physical and mechanical properties. If an added plasticizer is a polymer, then the plasticized PLLA could also be called a blend. Therefore, besides polymer plasticizers listed above, other polymers including PEO,[158] poly(ethylene/butylene succinate),[159] poly(β-hydroxy butyrate),[79,160] poly(*p*-vinylphenol) (PVPh),[161] and poly(vinyl alcohol) (PVA)[162,163] have been investigated as second components in blends with PLLA. In particular, blending of PLLA with PEO exhibits exceptional promise because of the outstanding miscibility and marvelous improvement of mechanical properties,[136,158] due to the good combination of hydrophobic, stiff and hydrolytically degradable PLLA chains and hydrophilic, flexible and non-degradable PEO segments.

1.5 Scope of the Thesis

The understanding of the relationship between the molecular structures and the macroscopic properties of a material is a major part of polymer characterization. In order to control the desired final properties of a crystalline polymer or crystalline polymer blend system material, the mechanism of the formation and destruction of its order, as well as the factors that govern these phase transitions need to be comprehensively understood. It is therefore the aim of this thesis to contribute to the overall understanding of the phase behaviour (i.e., both crystallization and melting) and micro-level morphology of a specific crystallizable polymer and its blend with a second component. The selected polymer system is a biodegradable and biocompatible polyester, poly(l-lactic acid) and the chosen second crystallizable blend component is a polyether, poly(ethylene oxide). The chosen system is ideally suited for fundamental phase behaviour study with its rich morphology and measurable kinetics. The results of such a fundamental study can be readily applied to the production of this currently industrially important homopolymer and blend system. The aim is realized using a combination of controlled hotstage microscopy and image analysis to evaluate the effects of temperature and composition on the rate of condensation of the melted system to form ordered structures possessing an internal hierarchical structure. The same methods are also used to monitor the thermal behaviour of these ordered structures during the melting process. A combination of optical and electron microscopy is employed to examine the different morphologies that arise under the different conditions of crystallization temperature, as well as

composition in the blend studies. The combination of all of these results is used to elucidate the internal structure of these solids, and to help explain the observed physical properties of the materials including the biodegradablility of the material.

The thesis is divided into five chapters:

Chapter One is a general introduction. The biodegradability of PLLA is highlighted and a thorough literature review on this polymer is included to present the current state of the study of PLLA. Each subsequent chapter begins with an introduction to the topics specifically addressed in that chapter.

Chapter Two presents the investigation of phase behaviour of PLLA and its blends with PEO. Using polarized light optical microscopy and depolarized light intensity, the changes of the crystallization behaviour of PEO in PEO/PLLA blends with different blend compositions are identified. These findings are critically discussed and a mechanism for the lamellar growth conformation of PLLA is proposed.

In Chapter Three, techniques for polymer structure characterization are briefly reviewed. Scanning electron microscopy is employed to examine the morphology of the PLLA spherulites and those of its blends with PEO. These visual evidences are used to support claims made in Chapter Two.

Chapter Four has a rather distinct topic from the other chapters. After a brief introduction of a non-isothermal crystallization method and a review of published statements, a series of experiments has been designed to investigate the feasibility of this novel method on PLLA and its blend with PEO. The results of non-isothermal

spherulite radial growth rate are critically discussed, and some general concerns are presented.

Chapter Five contains a summary of the main results from this thesis. The major original findings are noted and several ideas for potential further investigations are also included.

1.6 References

[1] Avella, M.; Bonadies, E.; Martuscelli, E.; Rimedio, R. *Polymer Testing* **2001,** 20, 517.

[2] Waste reduction facts clean Nova Scotia information on the internet: http://www.clean.ns.ca/15/ publications/wrfacts.html (accessed Feb., 2004)

[3] Azapagic, A.; Emsley, A.; Hamerton, I. *Polymer: The Environment and Sustainable Development*; John Wiley: England, 2003.

[4] Wunderlich, B. *Macromolecular Physics*; Academic Press: New York, 1973; Vol.1.

[5] Averous, L. *J. Macromol. Sci., Part C* **2004**, C44(3), 231.

[6] Australian academy of science webpage: http://science.org.au/nova/061/ 061key.htm (accessed Nov., 2005)

[7] Farrell, M.; Goldstein, N. BioCycle, **1995,** 36(11), 74.

[8] Riggle, D. *BioCycle.* **1998,** 39 (3), 64.

[9] Pavlath, A. E.; Robertson, G. H. *Criti. Rev. Anal. Chem.* **1999,** 29 (3), 231.

[10] Jacobsen, S.; Fritz, G. *Polym. Eng. Sci.* **1996,** 36(22),2799.

[11] Mullen, J. W.; Pacsu, E. *Ind. Eng. Chem.* **1942,** 1209.

[12] Mullen, J. W.; Pacsu,E. *Ind. Eng. Chem.* **1943,** 381.

[13] Raj, B.; Sankar, U.; Siddaramaiah, K. *Adv. Polym. Technol.* **2004,** 23(1),32.

[14] Myllymaki, O.; Myllarinen, P.; Forssell, P.; Suortti, T.; Lahteenkorva, K.; Ahvenainen, R.; Poutanen, K. *Packa. Technol. Sci.* **1998,** 11, 265.

[15] Godbole, S.; Gote, S.; Latkar, M.; Chakrabarti, T. *Bioresour. Technol.* **2003,** 86(1), 33.

[16] Chen, L.; Imam, S. H.; Gordon, S. H.; Greene, R.V. *J. Environ. Polym. Degrad.* **1997,** 5(2), 111.

[17] Nolan-ITU Pty Ltd and Excelplas webpage: http://www.deh.gov.au/industry/ waste/biodegradable/chapter2.html (accessed Mar., 2004)

[18] Lemoigne, M. *Ann. Inst. Pasteur.* **1927,** 41, 148.

[19] Di Lorenzo, M. L.; Raimo, M.; Cascone, E.; Martuscelli, E. *J. Macromol. Sci., Phys.* **2001,** B40 (5), 639.

[20] Zhun, K. J.; Liu, X.; Yang, S. *J. Appl. Polym. Sci.* **1990,** 39, 1.

[21] Li, S.; Vert, M. *Degradable Polymers-Principles and Applications*; Chapman

and Hall: London, 1995.

[22] Bergsma, J. E.; Bos, R. R. M.; Rozema, F. R.; Jong, W. D.; Boering, G. *J. Mater. Sci.: Mater. Med.* **1996,** 7, 1.

[23] Ray, S. S.; Okamoto, M. *Macromol. Rapid Cmmun.* **2003,** 24(14), 815.

[24] Chandra, R; Rustgi, R. *Prog. Polym. Sci.* **1998,** 23, 1273.

[25] Van Natta, F. I.; Hill, J. W.; Carruthers, W. H. *J. Am. Chem. Soc.* **1934,** 56, 455.

[26] Potts, J. E.; Clendinning, R. A.; Ackart, W. B.; Niegish, W. D. *Polym. Sci. Technol.* **1973,** 3, 61.

[27] Sinha, V. R.; Bansal, K.; Kaushik, R.; Kumria, R.; Trehan, A. *Int. J. Pharm.* **2004,** 278, 1.

[28] Rosa, D. S.; Calil, M. R.; Guedes, C. G. F.; Rodrigues, T. C. *J. Polym. Environ.* **2004,** 12(4), 239.

[29] Rezgui, F.; Swistek, M.; Hiver, J. M.; G'Sell, C.; Sadoun, T. *Polymer*, **2005,** 46, 7370.

[30] Pitt, C. G.; Chasalow, F. I.; Hibionada, Y. M.; Klimas, D. M., Marks, T. A.; Schindler, A.. *J. Appl.Polym. Sci.* **1981,** 26, 3779.

[31] Chang, HI.; Williamson, M. R., Perrie, Y.; Coombes, A. G. A. *J. Controlled Release*, **2005,** 106(3), 263.

[32] Koening, M. F; Huang, S. J. *Polym. Degrad. Stab.* **1994,** 45, 139.

[33] He, B.; Chen-Park, M. B. *Macromolecules* **2005,** 38(20), 8227.

[34] Wang, XL.; Yang, KK.; Wang, YZ. *J. Macromol. Sci .– Polym. Rev.* **2003,** 43(3), 385.

[35] Rosa, D. S.; Lopes, D. R.; Calil, M. R. *Polymer Testing*, **2005,** 24, 756.

[36] Hartmann, M. H. *Biopolymers from Renewable Resources*; Springer-Verlag: Berlin, 1998; pp 367-411.

[37] Carothers, W. H.; Dorough, G. L.; Van Natta, F. J. *J. Am. Chem. Soc.* **1932,** 54, 761.

[38] Lowe, C. E. 1964. US Patent 2, 668, 162.

[39] Garlotta, D. *J. Polym. Environ.* **2001,** 9(2), 63.

[40] Kim, KS.; Chuang, S. Chin, IJ.; Kim, MN.; Yoon, JS. *J. Appl. Polym. Sci.* **1999**, 72, 341.

[41] Miyoshi, R.; Hashimoto, N.; Koyanagi, K.; Shmihiro, Y.; Sakai, T. *Int. Polym. Process.* **1996,** XI, 320.

[42] AL.Raouf, A.; Samudin, R.; Samian, R.; Akool, K.; Abdulla, N. *Annal. Microscopy*, **2003,** 3, 9.

[43] Enomoto, K.; Ajioka, M.; Yamaguchi, A. 1994. US Patent 5, 310, 865

[44] Cargill Dow LLC homepage: http://www.cargilldow.com (accessed Nov., 2004)

[45] Lunt, J. *Polym. Degrad. Stab.* **1998,** 59, 145.

[46] Gerald. S. *Trends Polym. Sci.* **1997,** 5(11), 361.

[47] Eggins H.; Mills. J.; Holt, A.; Scott, G. *Microbial aspects of pollution*; Academic Press: London; 1971, pp 267-277.

[48] Kemnitzer, J. E.; McCarthy, S. P.; Gross, R. A. *Macromolecules*, **1992,** 25, 5927.

[49] Pavlath, A. E.; Robertson, G. H. *Criti. Rev. Anal. Chem.* **1999,** 29(3), 231.

[50] Tsuji, H.; Ikada, Y. *Macromol. Chem. Phys.* **1996,** 197(10), 3483.
[51] De Santis, P. ; Kovacs, A. J. *Biopolymers* **1968,** 6(3), 299.
[52] Cartier, L. ; Okihara, T. ; Ikada, Y. ; Tsuji, H. ; Puiggali J.; Lotz, B. *Polymer* **2000,** 41(25), 8909.
[53] Di Lorenzo, M. L. *Eur. Polym. J.* **2005,** 41, 569.
[54] Hoogsteen, W.; Postema, A. R.; Pennings, A. J.; Ten Brinke, G.; Zugenmaier, P. *Macromolecules* **1990**, (23), 634.
[55] Eling, B.; Gogolewski, S.; Pennings, A. J. *Polymer* **1982,** (23), 1587.
[56] Okihara, T.; Tsuji, M.; Kawagushi, A.; Katayama, KI.; Tsuji, H.; Hyon, SH., Ikada, Y. J. *J.Macromol. Sci., Phys.* **1991,** 30, 119.
[57] Brizzolara, D.; Cantow, HJ.; Diederichs, K.; Keller, E.; Domb, AJ. *Macromolecules* **1996,** 29, 191.
[58] Puiggali, J.; Ikada, Y.; Tsuji, H.; Cartier, L.; Okihara, T.; Lotz, B. *Polymer* **2000,** 41, 8291.
[59] Lemstra, P. J.; Postma, J.; Challa, G. *Polymer* **1974.**15, 757.
[60] Blundell, D. J.; Osborn, B. N. *J. Adv. Mater. (SAMPE Quarterly)* **1985,** 17, 1.
[61] Vilannova, P. C.; Ribas, S. M.; Guzman, G. M. *Polymer* **1985,** 26, 423.
[62] Elyashevich, G. K; Poddubny, V. I. *J. Macromol. Sci., Phys.* **1990,** B29, 249.
[63] Patel, R. M.; Spruiell, J. E. *Polym. Eng. Sci.* **1991,** 31, 730.
[64] Maffezzoli, A.; Kenny, J. M.; Nicolais, L. *J. Mater. Sci.* **1993**, 28, 4994.
[65] Kalb, B.; Pennings, A. J. *Polymer* **1980,** 21, 607.
[66] Vasanthakumari, R.; Pennings, A. J. *Polymer* **1983,** 24, 175.
[67] Kishore, K.; Vasanthakumari, R. *Colloid Polym. Sci.* **1988,** 266, 999.
[68] Tsuji, H; Ikada, Y. *Polymer* **1995,** 36, 2709.
[69] Miyata, T.; Masuko, T. *Polymer* **1997,** 38(16), 4003.
[70] Miyata, T.; Masuko, T. *Polymer* **1998,** 39 (22), 5515.
[71] Di Lorenzo, M. L. *Polymer* **2001,** 42(23), 9441.
[72] Kikkawa, Y., H. Abe, T. Iwata, Y. Inoue, and Y. Doi. 2001. *Biomacromolecules*, 2: 940.
[73] Abe, H.; Kikkawa, Y.; Inoue, Y.; Doi, Y. *Biomacromolecules* **2001,** 2, 1007.
[74] Gazzano, M.; Focarete, M. L.; Riekel, C.; Scandola, M. *Biomacromolecules*, **2004,** 5: 553.
[75] Nakafuku, C. *Polym. J.* **1996,** 28(7), 568.
[76] Sheth, M.; Kumar, R. A.; Dave, V. A.; Gross, R. A.; McCarthy, S. P. *J. Appl. Polym. Sci.* **1997,** 66 (8), 1495.
[77] Yang, J. M.; Chen, H. L.; You, J. W.; Hwang, J. C. *Polym. J.* **1997,** 29(8), 657.
[78] Focarete, M. L.; Ceccorulli, G.; Scandola, M.; Kowalczuk, M. *Macromolecules*, **1998,** 31(24), 8485.
[79] Ohkoshi, I.; Abe, H.; Doi, Y. *Polymer* **2000,** 41(15), 5985.
[80] Keith, H. D.; Padden, F. J. Jr. *J. Polym. Sci.* **1959,** 39, 101.
[81] Keith, H. D.; Padden, F. J. Jr. *J. Polym. Sci.* **1959,** 39, 123.
[82] Price, F. P. *J. Polym. Sci.* **1959,** 39, 139.
[83] Keller, A. *J. Polym. Sci.* **1959,** 39, 151.
[84] Bassett, D. C.; Hodge, A. M. *Polymer* **1978,** 19, 469.

[85] Keith, H. D. *Macromolecules* **1982,** 15, 114.
[86] Keith, H. D.; Padden, F. J. Jr. *Polymer* **1984,** 25, 28.
[87] Bassett, D. C.; Vaughan, A. S. *Polymer* **1985.** 26: 717
[88] Bassett, D. C.; Olley, R. H.; Al Raheil, A. M. *Polymer*, **1988,** 29, 1539.
[89] Keith, H. D.; Padden, F. J. Jr. *Macromolecules* **1996,** 29, 7776.
[90] Keith, H. D. *Polymer* **2001,** 42, 9987.
[91] Patel, D; Bassett, D. C. *Polymer* **2002,** 43, 3795
[92] Schultz, J. M. *Polymer* **2003,** 44, 433.
[93] Kikkawa, Y.; Abe, H.; Fujita, M.; Iwata, T.; Inoue, Y.; Doi, Y. *Macromol. Chem. Phys.* **2003,** 204, 1822.
[94] Marega, C.; Marigo, A.; Di Noto, V.; Zannetti, R. *Makromol. Chem.* **1992,** 193, 1599
[95] Iannace, S; Nicolais, L. *J. Appl. Polym. Sci.* **1997,** 64, 911.
[96] Ohtani, Y. ; Okumura, K.; Kawaguchi, A. *J. Macromol. Sci., Phy.* **2003,** B42 (3&4), 875.
[97] Fujita, M.; Doi, Y. *Biomacromolecules*, **2003,** 4, 1301.
[98] Fischer, E. W.; Sterzel, H. J.; Wegner, G.; Kolloid, Z. Z. *Polymer* **1973,** 251, 980.
[99] Iwata, T; Doi, Y. *Macromolecules* **1998,** 31, 2461.
[100] Iwata, T.; Doi, Y. *SEN'I GAKKAISHI*, **2001,** 57, 172.
[101] Kikkawa, Y.; Abe, H.; Iwata, T.; Inoue, Y.; Doi, Y. *Biomacromolecules*, **2002,** 3, 350.
[102] Abe, H.; Harigaya, M.; Kikkawa, Y.; Tsuge, T.; Doi, Y. *Biomacromolecules*, **2005,** 6, 457.
[103] Geil, P. H. *Polymer Single Crystals*; John Willy and Sons: New York, 1963.
[104] Bassett, D. C. *Principles of polymer morphology*; Cambridge University Press: Cambridge, 1981.
[105] Tsuji, H. *Macromol. Biosci.* **2005,** 5, 569.
[106] Ikada, Y.; Jamshidi, K.; Tsuji, H.; Hyon, S. H. *Macromolecules* **1987,** 20, 904.
[107] Tsuji, H.; Ikada, Y. *Macromolecules* **1993,** 26, 6918.
[108] Brochu, S.; Prud'shomme, R. E.; Barakat, I.; Jerome, R. *Macromolecules* **1995,** 28, 5230.
[109] Urayama, H. ; Kanamori T.; Fukushima, K. ; Kimura, Y. *Polymer* **2003,** 44, 5635.
[110] Tsuji, H.; Tezuka, Y. *Biomacromolecules* **2004,** 5, 1181.
[111] Tsuji, H. ; Ikada, Y. *Polymer* **1999,** 40, 6699.
[112] Tsuji, H. *Polymer* **2000,** 41, 3621.
[113] Tsuji, H.; Fukui, I. *Polymer*, **2003,** 44, 2891.
[114] Tsuji, H. ; *Biomaterials* **2003,** 24, 537.
[115] Reeve, M.; McCarthy, S. P.; Downey, M. J., Gross, R. A. *Macromolecules* **1994,** 27, 825.
[116] Macdonald, R.; McCarthy, S. P.; Gross, R. A. *Macromolecules* **1996,** 29, 7536.
[117] Cai, H.; Dave, V.; Gross, R. A., McCarthy, S. P. *J. Polym. Sci., Polym. Phys.* **1996,** 34, 2701.

[118] Li, S.; McCarthy, S. P. *Macromolecules* **1999,** 32, 4453.
[119] Tabushi, I.; Yamada, H.; Matsuzaki, H.; Furukawa, J. *J. Polym. Sci., Polym. Lett. Ed.* **1975,** 13, 447.
[120] Fukuzaki, H.; Yoshida, M.; Asano, M.; Kumakura, M. *Eur. Polym. J.* **1989,** 25(10), 1019.
[121] Zhang, X.; Wyss, U. P.; Pichora, D.; Goosen, M. F. A. *J. Bioact. Compat. Polym.* **1994,** 9, 80.
[122] Tsuji, H.; Ikada, Y. *J. Polym. Sci., Polym. Chem.* **1998,** 36, 59.
[123] Tsuji, H.; Miyauchi, S. *Polym. Degrad. Stab.* **2001,** 71, 415.
[124] Vert, M.; Li, S. M.; Spenlehauer, G.; Guerin, P. *J. Mater. Sci., Mater. Med.* **1992,** 3, 432.
[125] Tsuji, H; Miyauchi, S. *Polymer* **2001,** 42, 4463.
[126] Tsuji, H.; Miyauchi, S. *Biomacromolecules*, **2001,** 2, 597.
[127] Williams, D. F. *Eng. Med.* **1981,** 10, 5.
[128] Datta, R.; Tsai, S.; Bonsignore, P.; Moon, S.; Frank, J. *FEMS Microbiol. Rev.* **1995,** 16, 221.
[129] Harper, C. A. *Modern Plastics Handbook*; McGraw-Hill: New York, 2000.
[130] Verespej, M. *Winning Technologies: Polylactic Polymers. Ind. Week* **2000,** Dec.11
[131] Rashkov, I.; Manolova, N.; Li, SM.; Espartero, JL.; Vert, M. *Macromolecules* **1996,** 29(1), 50.
[132] Li, SM.; Rashkov, I.; Espartero, JL.; Manolova, N.; Vert, M. *Macromolecules* **1996,** 29(1), 57.
[133] Mohammadi-Ravshandeh, J. ; Farnia, S. M. F. ; Sarbolouki, M. N. *J. Appl. Polym. Sci.* **1998,** 68, 1949.
[134] Zhu, Z. ; Xiong, C.; Zhang, L.; Yuan, M.; Deng, X. *Eur. Polym. J.* **1999,** 35, 1821.
[135] Lee, SY.; Chin, LJ.; Jung, JS. *Eur. Polym. J.* **1999,** 35, 2147.
[136] Bechtold, K.; Hillmyer, M. A.; William, B. T. *Macromolecules* **2001,** 34, 8641.
[137] Choi, Y. ; Kim, SY. ; Moon, MH.; Kim, S. H.; Lee, KS.; Byun, Y. *Biomaterials* **2001,** 22, 995.
[138] Tew, GN.; Sanabria-Delong, N.; Agrawal, SK.; Bhatia, SR. *Soft Matter* **2005,** 1(4), 253.
[139] Grijpma, DW.; Vanhofslot, RDA.; Super, H.; Nijenhuis, AJ.; Pennings, AJ. *Polym. Eng. Sci.* **1994,** 34(22), 1674.
[140] Kim, J. K.; Park, DJ.; Lee, MS.; Ihn, K. J. *Polymer* **2001,** 42, 7429.
[141] Maglio, G.; Migliozzi, A; Palumbo, R. *Polymer*, **2003,** 44, 369.
[142] Schimidt, P.; Keul, H.; Hocher, H. *Macromolecules* **1996,** 29, 3674.
[143] Chen, X.; Gross, R. A. *Macromolecules* **1999,** 32, 308.
[144] Sinclair, RG. J. *Macromol. Sci., Pure Appl. Chem.* **1996,** A33(5), 585.
[145] Martin, O.; Averous, L. *Polymer* **2001,** 42, 6209.
[146] Jacobsen, S.; Fritz, G. *Polym. Engineer. Sci.* **1999,** 39(7), 1303.
[147] Labrecque, L. V.; Kumar, R. A.; Dave, V.; Gross, R. A.; McCarthy, S. P. *J. Appl. Polym. Sci.* **1997,** 66(8), 1507.

[148] Ljungberg, N.; Wesslen, B. *J. Appl. Polym. Sci.* **2002,** 86, 1227.
[149] Lostocco, M. R.; Borzacchiello, A.; Huang, S. J. *Macromol. Symp.* **1998,** 130, 151.
[150] Hiljanen-Vainio, M.; Varpomaa, P.; Seppala, J.; Tormala, P. *Macromol. Chem. Phys.* **1996,** 197, 1503.
[151] Iannace, S.; Ambrosio, L.; Huang, S. J.; Nicolais, L. *J. Appl. Polym. Sci.* **1994,** 54, 1525.
[152] Blumm, E. ; Owen, A. J. *Polymer* **1995,** 36, 4077.
[153] Chen, CC.; Chueh, JY.; Tseng, H.; Huang, HM.; Lee, SY. *Biomaterials*, **2003,** 24, 1167.
[154] Wilson, A. S. *Plasticisers: Principles and Practice;* The Institute of Materials: London, 1995.
[155] Kranz, H.; Ubrich, N.; Maincent, P.; Bodmeier, R. *J. Pharm. Sci.* **2000,** 89(12), 1558.
[156] Wang, Y.; Hillmyer, M. A. *J. Polym. Sci., Polym. Chem.* **2001,** 39(16), 2755.
[157] Sheng, J.; Ma, H.; Yuan, XB.; Yuan, XY.; Shen, NX.; Bian, DC. *J. Appl. Polym. Sci.* **2000,** 76(4), 488.
[158] Nijenhuis, A. J.; Colstee, E.; Grijpma, D. W.; Pennings, A. J. *Polymer* **1996,** 37, 5849.
[159] Liu, X.; Dever, M.; Fair, N.; Benson, RS. *J. Environ. Polym. Degrad.* **1997,** 5(4), 225.
[160] Koyama, Y; Doi, Y. *Polymer* **1997,** 38, 1589.
[161] Zhang, L.; Goh, S. H.; Lee, S. Y. *Polymer* **1998,** 39(20), 1998.
[162] Shuai, X.; He, Y.; Asakawa, N.; Inoue, Y. *J. Appl. Polym. Sci.* **2001,** 81, 762.
[163] Park, J. W.; Im, S. S. *Polymer* **2003,** 44, 4341.

Chapter Two: *Phase Behaviour of PLLA and its Blends with PEO*

2.1 Polymer Phase Behaviour: General

Unlike small molecules (e.g., water) that melt and freeze or, crystallize, at a single temperature, the solid and liquid (i.e., melt) phases of polymers are not actually in equilibrium with each other at the observed crystallization or melting temperature. In order to solidify a polymer by melt crystallization, the melt state needs to be cooled to temperatures notably below its observed melting temperature before crystallization occurs at any discernible rates. This undercooling allows the formation of the primary nuclei, as introduced in Chapter One. As the polymer phase transition is a non-equilibrium process, the resultant polymer structures developed through this kinetically-controlled event form with different degrees of order and at different growth rates at different temperatures. Consequently, polymer solids exhibit different melt behaviour according to their thermal history when they are subsequently heated.

The rates at which polymer spherulites radially grow to impingement depend heavily on temperature. The temperature range that provides optimum conditions for measuring these rates is typically between (T_m – 10 K) and (T_g + 30 K).[1] Figure 2.1 contains a sketch of the typical overall spherulite radial growth rate dependence on crystallization temperature. It has a bell-shaped appearance with a characteristic maximum. There are two major factors governing the overall process, which have opposite temperature dependencies. At increasing crystallization temperatures greater than $T_{G(max)}$, the

segmental motion is so great that nuclei tend to collapse before reaching a critical size for continuous growth. On the contrary, with decreasing crystallization temperatures less than $T_{G(max)}$, the melt is so viscous that molecular motion is extremely slow, and the primary nucleation rate is very high. The factors governing spherulite growth rates in these high and low crystallization temperature regions are thus referred to as nucleation and transport, respectively, in the context of the classic polymer crystallization description of Hoffman and Lauritzen.

The Hoffman-Lauritzen crystallization model (H-L model) was originally used to describe the growth of a polyethylene single crystal from dilute solution,[2] and also has been successfully applied to melt crystallized lamellar aggregate crystals (i.e., spherulites) after being modified.[3] Since then, it has been extensively used to interpret and model crystallization behaviour of lots of different polymers with its various modifications.[4-8]

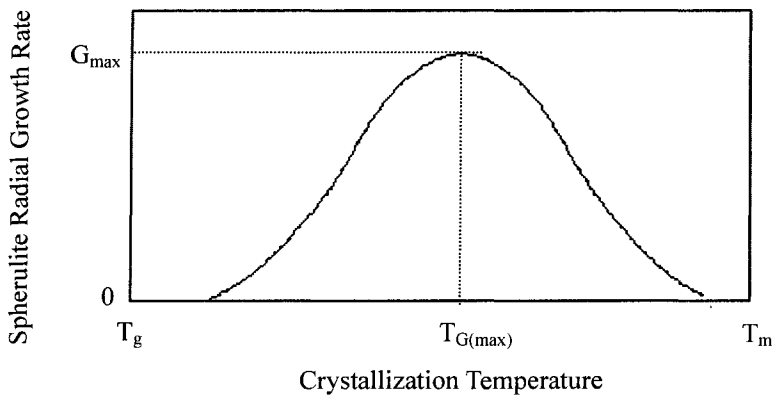

Figure 2.1: Typical dependence of radial growth rates of polymer spherulites on crystallization temperature

According to the H-L model, the governing factors of spherulite radial growth rates are represented in the overall growth rate equation as two exponential terms.

$$G = G_0 \, e^{[-U^*/R(T_c - T_\infty)]} \, e^{[-K_g/(T_c(\Delta T)f)]} \qquad [2.1]$$

In this equation, G (cm/s) is the spherulite radial growth rate; G_0 (cm/s) is a pre-exponential term that contains all of the temperature independent factors; $\triangle T$ (K) is the undercooling, and is defined as the difference between the equilibrium melting temperature (T_m^0) (K) and isothermal crystallization temperature (T_c) (K); U^* (kJ/mol) is the activation energy for transport of polymer chains through the melt; R ($JK^{-1}mol^{-1}$) is the universal gas constant; T_∞ (K) is a hypothetical temperature at which all the molecular motions related to viscous flow are ceased; K_g (K^2) is the nucleation constant; f accounts for the variation of the heat of fusion away from the melting point and is defined as[9]

$$f = \frac{2(T_c)}{(T_m^0 + T_c)} \qquad [2.2]$$

K_g can be further described as

$$K_g = \frac{j\, b_0\, \sigma\, \sigma_e\, T_m^0}{k\, \Delta h_f} \qquad [2.3]$$

where j is the regime coefficient, and has a value of 2 or 4 depending on the *growth regime* of crystallization; b_0 (cm) is known as the crystallizing stem thickness, which is sketched in figure 2.2; σ (erg/cm^2) and σ_e (erg/cm^2) are the lateral and fold surface free energy, respectively; k (erg/K) is the Boltzmann constant; $\triangle h_f$ (erg/cm^3) is defined as the heat of fusion per volume of monomer units.

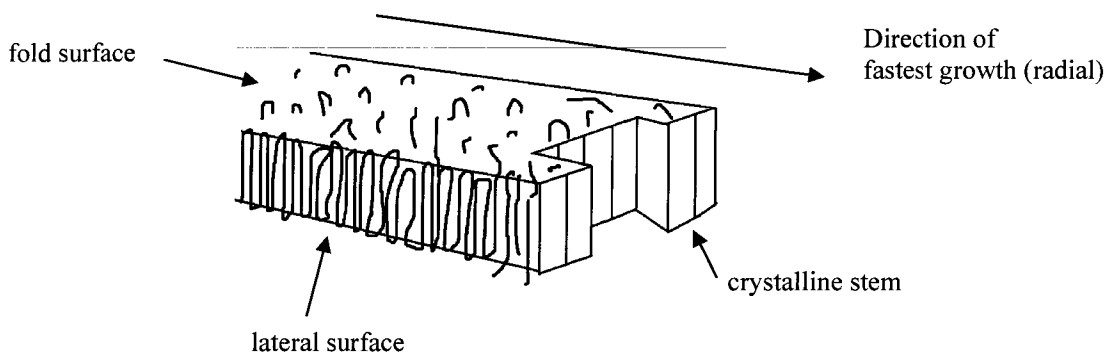

Figure 2.2: Sketch of a spherulite lamellar building block showing its constituent stems and surfaces.

As a further development of the original H-L model, Hoffman nucleation theory[10] addressed an apparent discontinuity in the dependence of spherulite radial growth rate on the crystallization temperature. It was found that the experimental growth rate did not fit a *single* function over the temperature range between $T_{G(max)}$ and T_m. The subtle change in the exponential form can be exaggerated in a logarithmic form, as shown in Figure 2.3. The discontinuity was rationalized as the occurrence of three possible crystallization regimes depending on the relative rates of the attachment of the first segment on the substrate (secondary nucleation) and the completion of the layers (surface spreading). At the smallest undercoolings, i.e., at the relatively high crystallization temperatures, the rate of secondary nucleation is less than that of surface spreading, indicative of growth in regime I. As the undercooling is further increased, the crystallization can occur in growth regime II, where the rate of secondary nucleation approaches the rate of surface spreading. At the largest undercoolings, with the crystallization temperature still greater than $T_{G(max)}$, crystallization may enter regime III. In this growth regime, the rate of secondary nucleation is greater than that of surface spreading.

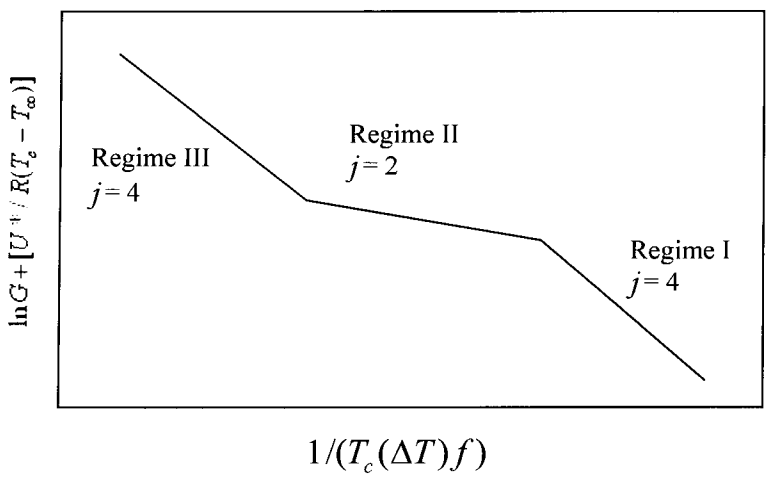

Figure 2.3: The logarithmic form of the growth rate equation plotted as a function of temperature, illustrating the three possible regimes of crystallization.

The completely crystallized polymer spherulites developed from this non-equilibrium condition (in any regime) are metastable, and there can be a thermodynamic drive to lower the chemical potential of these structures. When exposed to temperatures greater than the crystallization temperature of the sample, the thermal energy is converted into kinetic energy. Thus, the chains within the structures gain some mobility, which permits the chains to attain lower energy conformations. Therefore, in a polymer spherulite composed of alternating amorphous and crystalline regions, the less ordered material can partially melt and subsequently be incorporated into more ordered regions upon increasing temperature. This can give rise to lamellar thickening,[11,12] and an increase in the degree of crystallinity of the overall polymer sample. Essentially, a polymer solid can undergo this process of reorganization and restructuring into a more ordered solid with the appropriate applied heat before it finally phase changes to a liquid at the melting temperature. This series of events can only occur with an appropriate heating rate. In addition, while this thermal behaviour is characteristic of crystallizable polymers in general, its manifestation in individual polymer depends heavily on the heating rate and thermal history, as well as its molecular weight and structure.

Differential scanning calorimetry (DSC) is the conventional method used to study thermal behaviour in bulk polymer samples. The changes in heat flow with temperature rely on changes in the physical property of heat capacity in the sample. As polymers exhibit different morphologies in terms of degrees of order in the temperature range between its T_c and T_m, a more unconventional microscopy method can be applied to examine their thermal behaviour, based on changes in morphology. This method relies on changes in the physical property of birefringence of polymer thin film sample. Over this temperature range of interest, the polymer solid structure increases the order before it

finally melts.

Polymer spherulites are birefringent due to their intrinsic anisotropic character. The refractive index along the radial and tangential directions of their chain-folded lamellae building blocks is different. The presence of a birefringent sample rotates the initially plane-polarized light and some light is therefore transmitted in the crossed-polar configuration of the polarized light microscope. The intensity of the depolarized light increases with increasing order in the sample as the chain-folded lamellae are what give rise to the birefringence, before finally being extinguished by the melted sample. The typical configuration of the polarized light microscope used to view these spherulites includes a polarizing lens before and after the sample in a 'crossed-polar' arrangement. In this arrangement, none of the plane-polarized light is transmitted through the second polarizing lens in the absence of a sample, or when the sample does not depolarize the light, as in an amorphous state. Therefore, the measured intensity of the total transmitted depolarized light can be used to monitor the changes in the relative crystallinity of spherulites during heating, melting, annealing, and crystallization.[13-16] When measured at regular intervals during a phase change, this property provides a unique perspective of melt crystallization of polymer spherulites as well as their thermal behaviour during melting.

In this study, it was proposed that depolarized light intensity (DLI) measurements of crystallized PLLA thin films could be used as a qualitative measure of the effects of degradation of the PLLA polymer by enzyme. Specifically, the DLI heating profile would illustrate the effect of degradation on the polymer's natural tendency to undergo anneal-type behaviour during the heating scan. It was believed that the enzyme would attack the relatively disordered fold surfaces of the lamellae in the spherulites and

effectively render that relatively amorphous part of the interlamellar regions, which is therefore unable to be part of an anneal-type of lamellar thickening process. An increase in internal order of the spherulite as a result of any reorganization or annealing of the chains during heating would be reflected in an increase in birefringence which in turn would be manifested in an increase in the intensity of the depolarized light transmitted by the sample. To date, studies on degradation of PLLA had been limited to before-and-after examinations of morphological changes of single-crystal PLLA using electron microscopy. One of the aims of this particular work was to study the effects of degradation on PLLA samples that more represented the actual material of these thermoplastic commodity products, i.e., a bulk sample of polymer thin films of crystallized spherulites. The objective of the work presented in this chapter is to investigate the effect of degradation mainly using DLI, so as to study the phase behaviour of PLLA and its blend with PEO in thin film samples.

2.2 Experimental

2.2.1 Materials

Poly(*l*-lactic acid) (PLLA) was purchased from Polyscience Inc. It has a glass transition temperature (T_g) of 60 °C, an observed melt temperature (T_m) of 178 °C, and an average molecular weight of 50 000 as reported by the supplier. The polymer was stored in a tightly closed container in the fridge at 4 °C. Poly(ethylene oxide) (PEO) was bought from Aldrich Chemical Company, Inc., and has a reported T_g of -67 °C and an observed T_m of 65 °C. The average molecular weight of PEO is 100 000.

Proteinase K (EC 3.4.21.64) with a reported degree of 36 units/mg protein was

purchased from Sigma-Aldrich. It was stored in a dark container in the freezer at -65 °C. Purified tris(hydroxymethyl) aminomethane (TRISMA) was obtained from Fisher Scientific Company. It was stored in a tightly closed dark jar on the bench before use.

Dichloromethane (99.5+ %, Caledon) and ethyl ether (99.0+ %, ACP) were used as received. Water was purified and deionized before use.

2.2.2 Methods

2.2.2.1 Sample Preparation

Polymer blends: Known masses of each of PLLA and PEO were dissolved in appropriate volume of dichloromethane at room temperature and allowed to stir vigorously for 15 minutes. The polymers were shock-precipitated out of solution by the addition of a five-fold volume of freshly-opened, cold ethyl ether. The resultant polymer blend suspension was completely precipitated by centrifuging individual test-tube aliquots using an ADAMS compact II centrifuge. Subsequently, all samples were dried to constant mass, and stored under vacuum at ambient temperature. The resultant polymers and their blends were all white crusty powders in appearance. In this way polymer blends of the following compositions were prepared (in the ratio of weight% PEO/ weight% PLLA): 0/100 (pure PLLA), 10/90, 20/80, 30/70, 40/60, 50/50, 60/40, 70/30, 80/20, 90/10, and 100/0 (pure PEO).

Polymer thin films for microscopy: A surface temperature controlled microscope hotstage (± 1 °C) preheated to 200 °C was used to first melt a crumb of the polymer or polymer blend on a 12-mm diameter microscope glass coverslip. Once the crumb became translucent (this usually takes within 15 s), a second coverslip was quickly put on top of

this polymer sample with downward pressure to form a sandwiched polymer thin film. The sandwiched sample was rapidly removed from the hotstage and placed on the bench to cool and it remained at room temperature until use. For open-face samples, the two cover slips were split apart right after removal from the hotplate, so that the thin film was only on one coverslip. A micrometer was used to measure the thickness of the two glass coverslips without and then with the polymer thin film in between them, to determine the thickness of the film. Only those films that were in the range of 8-15 μm thick were used for further study. All samples were fresh made before use (i.e., same day as study).

Buffered enzyme solution degradation medium: Tris-HCl buffered solution for polymer degradation studies were prepared by first adding 0.6057g of THAM to 90 mL HCl (aq) until pH = 8.5, followed by the addition of purified H_2O to reach a total volume of 100 mL to make a final concentration of 50 mM Tris-HCl buffer. Proteinase K enzyme was added to the buffered solution. Unless otherwise stated in the text, all buffered enzyme solutions for the polymer degradation work are 0.042% wt/vol Proteinase K. Buffered solutions with enzyme were kept in fridge and consumed within two weeks of preparation.

2.2.2.2 Polarized Light Optical Microscopy

Spherulite radial growth rates were measured and spherulite morphology was examined using polarized light optical microscopy (PLOM). A Nikon Coolpix 4500 digital camera was mounted on the trinocular tube of a Nikon Eclipse E400 POL polarized light optical microscope. Polymer thin film samples on or between glass coverslips were loaded into a quartz crucible carrier of a THMS 600 Linkam microscope hotstage. A Linkam TMS 94 temperature controller was used to maintain thermal control

of the sample within ± 0.1 °C by a Linkam LNP cooling system which uses liquid nitrogen as refrigerant. All samples were held at 200 °C for 1 minute to erase the thermal history, and were then cooled at 70 °C/min to the crystallization temperature for a controlled period of time. Details of individual crystallization experiments are included in the text.

An image analysis software program (ScanPro®) was used to process the acquired digital images of the spherulites during crystallization. The software was calibrated by a micrometer slide. Calibrated measurements of the spherulite radius were collected at controlled regular time intervals during crystallization. During a typical isothermal crystallization experiment, five photographs of the spherulites were taken before impingement at known regular time intervals. For each photograph at each interval, four measurements of the spherulite diameter were used to get an average value. The radius of the spherulites was plotted as a function of time and a linear regression analysis performed on the data to get the value of the radial growth rate at that crystallization temperature. The procedure was repeated for the same crystallization temperature using a second freshly made polymer thin film sample. The average of the measured growth rates at the same crystallization temperature was taken as the spherulite radial growth rate (G) at that crystallization temperature.

Growth rate measurements were always performed on thin films grown between two coverslips.

2.2.2.3 Total Depolarized Light Intensity

The crystallization, degradation and melting of polymer thin films were qualitatively examined by measuring the total depolarized light transmitted by the sample.

The depolarized light intensity (DLI) transmitted by the sample was recorded using a Mettler photomonitor in tandem with a Mettler FP80 central processor. One of the oculars of the Nikon Eclipse E400 POL polarized light optical microscope was replaced with this photomonitor. The photomonitor was calibrated for zero DLI by totally dark, and for half of the maximum intensity using a completely crystallized sample. The intensity was displayed on the window of the Mettler FP80 CPU as an analogue voltage system using arbitrary units on a scale from 0 to 2047.

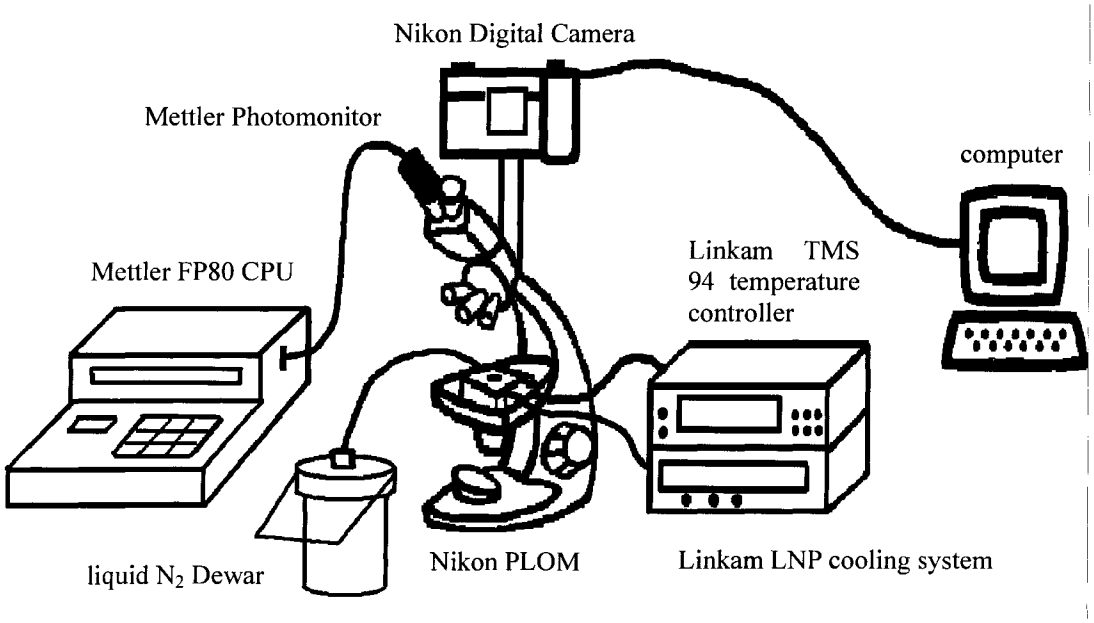

Figure 2.4: Sketch of experimental setup for DLI and PLOM experiments

For non-isothermal heating or cooling DLI experiments, the temperature of the examined thin film sample was controlled by the Linkam temperature controller at a rate of 10 °C/minutes if not otherwise stated in the text. DLI data were manually recorded from the FP80 display screen at the shortest time intervals possible during the experiment. The time and intensity data were then manually entered into an external spreadsheet for processing. The time data were transformed to temperature values using the known

heating or cooling rate.

For each DLI experiment, the intensity values were divided by the maximum intensity value for that experiment to normalize the data, and the resultant relative depolarized light intensity was plotted against temperature for each experiment. The plot is referred to as a DLI heating or cooling profile in the text. Details of the spherulite sample history prior to the DLI experiment are given in the text.

2.2.2.4 Enzymatic Degradation

A buffered aqueous solution of Proteinase K enzyme was used as a degradation medium for polymer and polymer blend thin film samples with unrestrained (open-face) crystallization. The crystallized polymer sample was placed in the crucible. Using an Eppendorf pipette, a volume of 480 μL of the 0.042 wt/vol % Porteinase K solution was added to this crystallized polymer sample by effectively filling the crucible. An 18 mm-diameter microscope glass coverslip was set on top to keep the solution from evaporation. The samples were maintained at 37 °C ± 0.1 °C using the Linkam hotstage for a controlled period of time. After exposure to the degradation medium for the desired amount of time, the liquid on top of the sample was syringed off and the remaining wetness was removed by gentle capillary action using a Kimwipe tissue. The glass-coverslip-supported film was then removed from the crucible holder for further use.

2.2.2.5 Viscosity

The relative viscosity of dichloromethane solutions of the polymer samples after exposure to the degradation conditions was measured using an Ostwald viscometer in a constant temperature water bath. The thin film polymer or polymer blend was weighed

and then subjected to the desired thermal history, including the melting and melt crystallization in the microscope hotstage. The sample was then subjected to degradation by immersing in 1.0 mL enzyme solution at 37 °C in a PTFE sealed microscale reaction vial. The thin film sample was then taken out of the enzyme solution after a desired time period and was dried and subsequently dissolved in 3.0 mL dichloromethane. Efflux time through an Ostwald viscometer was measured at temperature of 23 °C ± 1 °C. For each solution, five flow times were recorded and averaged. To obtain a unitless relative viscosity value, the average efflux time of the degraded sample was reported as flowtime per gram of the undegraded polymer (i.e., original mass) divided by flowtime per gram of the reference polymer sample. The reference sample was subjected to exactly the same pre-degradation thermal history and was subjected to the degradation solution for only 5 seconds.

2.3 Results and Discussion

2.3.1 Crystallization Profile of PLLA

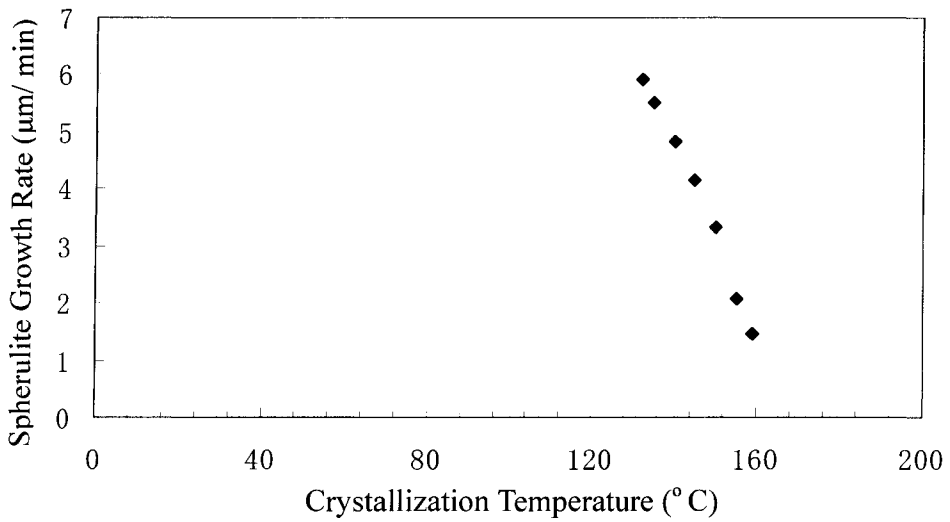

Figure 2.5: Spherulite growth rate of PLLA as a function of crystallization temperature.

The spherulite radial growth rate (G) of PLLA was determined over the crystallization temperature range of 130 °C to 160 °C. Figure 2.5 contains the values of G as a function of the crystallization temperature. The acquired data forms only a portion of the typical, rather symmetric bell-shaped curve that would represent the crystallization profile over a complete range of crystallization temperatures extending from those just above the glass transition temperature (*ca* 56 °C) to those approaching values close to the observed melting temperature (*ca* 178 °C). The data illustrate how the growth rate changes significantly with small changes in crystallization temperature. The data illustrate also how the growth rate increases sharply with increasing undercooling in this range of crystallization temperatures which is to the right of the bell-shaped curve maximum. In this range of temperatures, the growth is predominantly controlled by nucleation. At these relatively high temperatures, the viscosity of the melt is relatively low and the activation energy for transport of a chain through the melt to the crystallizing surface is easily achieved. These same conditions, however, allow for the thermal energy of the melt to be sufficiently high so that nucleation is controlling the overall growth rate. The data presented here are in keeping with expected values of G under these conditions for PLLA of similar molecular weight.[17] The acquisition of an entire growth rate curve is not the main interest of this thesis. The points obtained are over a temperature range in which the growth can be measured with both accuracy and precision. In addition, investigation over this temperature range provides for the growth of spherulites to maturity as the conditions restrict the formation of an unwanted 'bloom of nuclei' that would typically grow to impingement before any useful measurements could take place. This curve provides a reference curve for the later growth rate investigation of the blend

system. This data also provides information that helps to choose the appropriate crystallization temperature for further isothermal experiments for both pure and blend systems.

2.3.2 Melting and Degradation Behaviour of Crystallized PLLA

The measurement of depolarized light intensity (DLI) of degraded and non-degraded polymer thin films was undertaken to investigate the effect of enzymatic degradation on the degree of order within the sample. In order to carry out a systematic investigation, control of the following specific variables was required: T_c, heating rate, and degradation time.

Figure 2.6 contains the DLI heating profiles of PLLA thin film samples with a thermal history of isothermal crystallization at 147 °C for 80 minutes, followed by cooling down to room temperature. The heating rate was varied from 2 °C to 20 °C. It can be seen that the light intensity has an upturn in the temperature range of 90 °C and 110 °C for all the profiles. The upturn in intensity signifies an onset to an ordering process within the sample during heating. The figure also shows that the slower the heating rate, the earlier this anneal type behaviour begins. The effect of heating rate on the profile can be justified by the fact that the polymer chains have more time to reorganize themselves at slower heating rate. The disappearance of polymer spherulites corresponds to the abrupt drop in light intensity at around 180 °C, and signifies the complete melting of crystallized polymers.

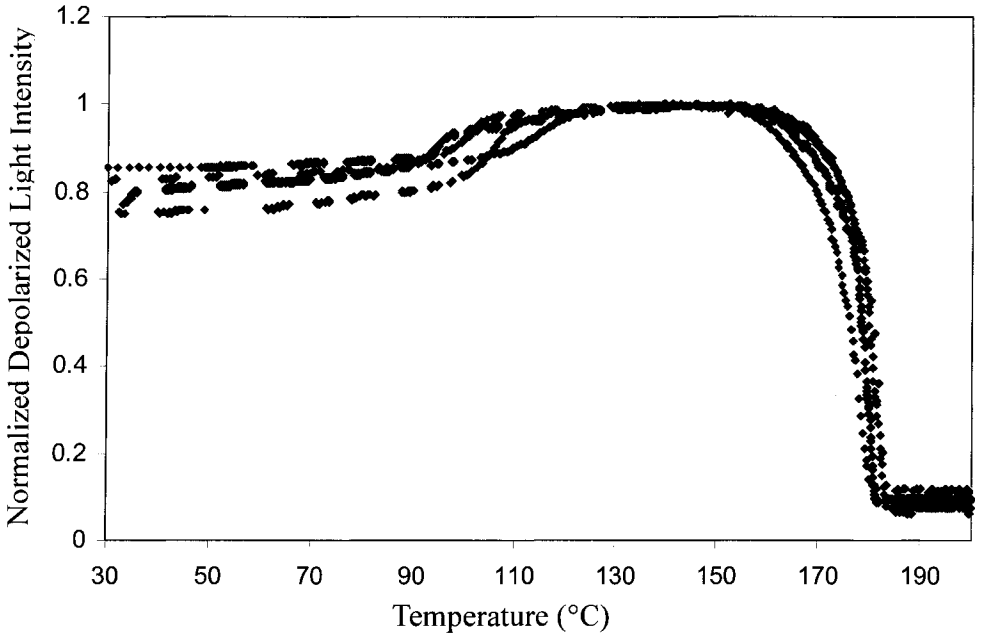

Figure 2.6: DLI heating profiles of PLLA at different rates: 2 °C/min (red); 5 °C/min (pink); 10 °C/min (green); and 20 °C/min (blue). All samples crystallized as open face thin films at 147 °C for 80 min. The error bar is within the size of the data points.

The results in Figure 2.6 confirm the sensitivity of the DLI to internal changes in order. Since profiles obtained at all heating rates were sensitive to these changes, a heating rate of 10 °C/minutes rate was chosen for all of the following measurements.

Different degradation periods were investigated to examine the extent of enzymatic degradation with time. A set of experiments was performed in which only the degradation time period varied from 0 to 8 hours. The subsequent DLI heating profiles from all seven degradation times were compared and are illustrated in Figure 2.7. It can be seen that all of the DLI profiles demonstrate increasing intensity with heating until they finally melt with abrupt drop in intensity. All of the samples exposed to enzyme solution show a slow and steady increase. The sample that was not exposed to enzyme solution has an added feature characteristic as those profiles shown in Figure 2.6. This

sample exhibits an onset to anneal type behaviour at around 100 °C. To make sure the lack of the upturn in the profiles of samples exposed to enzyme solution is an effect of enzymatic degradation, the following test was performed. The 3-hour run in Figure 2.7 was repeated without enzyme (not shown), and again without enzyme or buffer (not shown). No noticeable changes were apparent, when comparing the DLI profiles of these two test experiments. This implies that Tris-HCl buffer alone does not degrade PLLA spherulites during the time period of interest. Therefore, the apparent effects of the degradation are attributed to the enzyme. The absence of the upturn indicates no onset to reorganization, which signifies that no amorphous material is able or available to reorganize.

For the DLI profiles of enzyme-affected films, it can be postulated that a certain amount of amorphous areas had been chopped up by enzyme during the degradation period. These chopped-up amorphous regions could either stay in the places where they were or be removed with the enzyme solution after degradation. In the first case, the chains are not able to reorganize because the enzymatic chain scission has made them too short to fold. No significant differences were observed among the DLI profiles of samples exposed to enzyme from 80 minutes to 8 hours, indicating the 80-minute period of enzymatic degradation is sufficient for discovering the effect of enzymatic degradation on the degree of order within the sample under these experimental conditions.

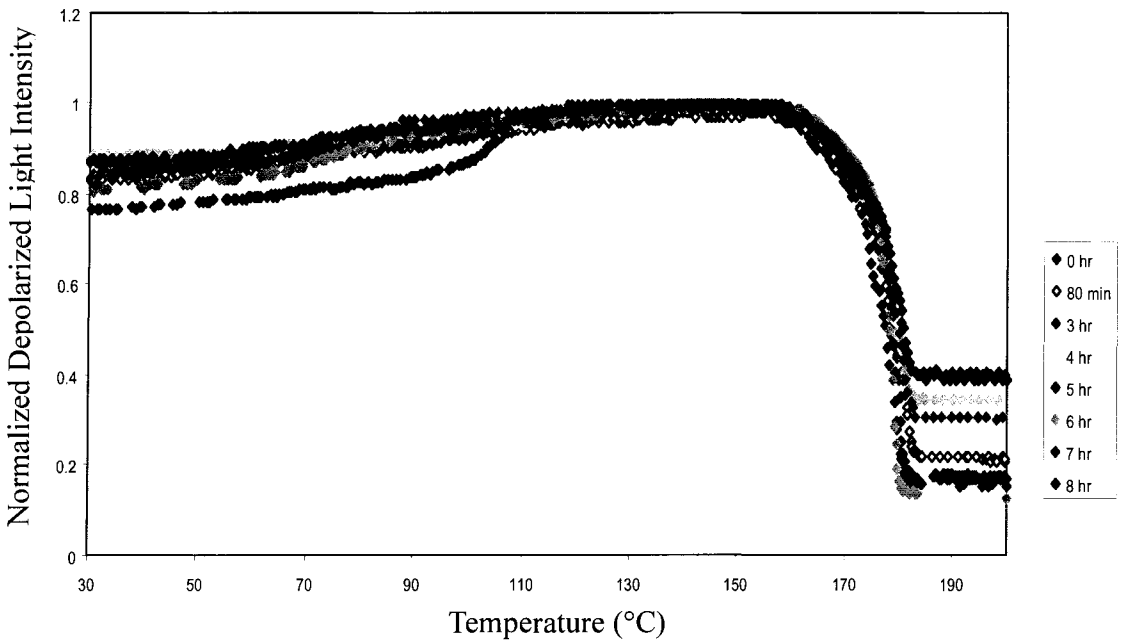

Figure 2.7: DLI heating profiles (10 °C/min) of PLLA following enzymatic degradation for different periods according to legend. All samples crystallized as open face thin films at 147 °C for 80 min prior to degradation. The error bar is within the size of the data points.

To further probe the origin of the apparent upturn in the DLI profiles, another set of experiments was performed in which the thermal history was changed: a crystallization temperature of 130 °C was used. The crystallization time remained for 80 minutes, because it was found by using DLI method during crystallization, that the sample reached its maximum DLI value within this time period (less than 60 minutes). In this set of experiments, the variable of degradation time was changed from 15 minutes to 12 hours. An extreme run was also applied with a more concentrated enzyme solution (0.15 wt/vol %) and for a much longer degradation time (17 hours).

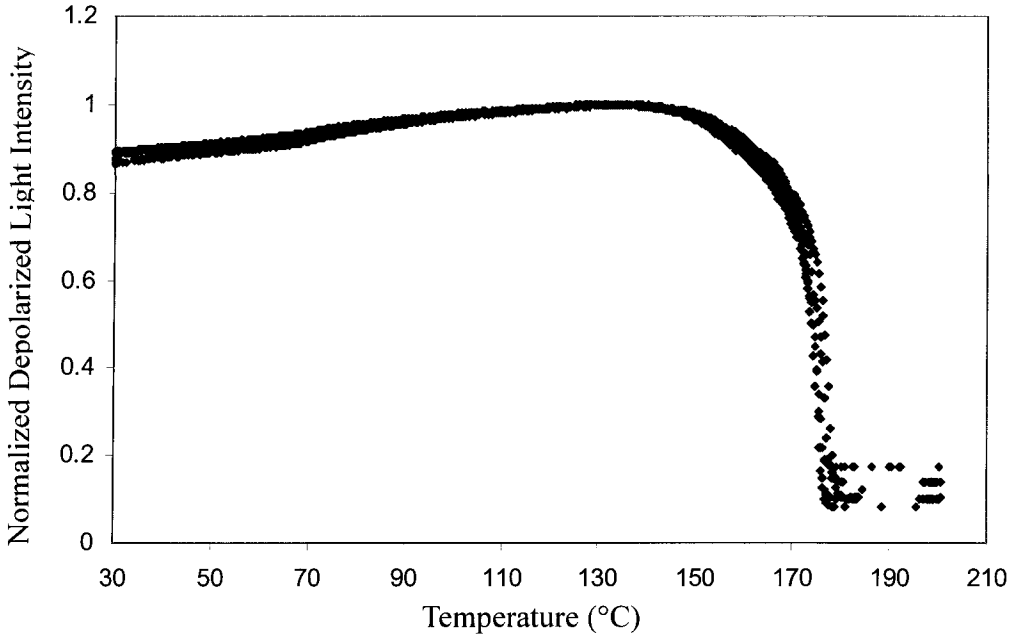

Figure 2.8: DLI heating profiles (10 °C/min) of PLLA following enzymatic degradation for different periods: 0 min (red); 30 min (pink); 2 hours (green); 12 hour (blue); and 17 hours (black). 17-hour run degraded with 15 times more concentrated enzyme solution. All samples crystallized as open face thin film samples at 130 °C for 80 min. The error bar is within the size of the data points.

The results in Figure 2.8 were unexpected: specifically the lack of upturn. It is well known that spherulites crystallized at lower temperature posses a lower degree of crystallinity, and a greater tendency to reorganize (anneal) during subsequent heating. The results in Figures 2.7 and 2.8 can be reconciled upon considering the images presented in Figure 2.9. The images in Figure 2.9 (a) and (b) are representative of what the samples looked like after 80 minutes of isothermal crystallization at 147 °C and 130 °C, respectively. While the sample in (b) shows that the spherulites had grown to the point of impingement, there remained significant amount of non-crystallized polymer melt in (a). It is this non-crystallized material that would crystallize during the cool to room temperature and which would be most susceptible to reorganization during subsequent

heating. The characteristic upturn feature in preceding DLI profiles is attributed to the annealing of this low crystallinity non-isothermally grown spherulites. The slow and steady increase of DLI profiles in Figure 2.7 and Figure 2.8 is due to the anneal type of lamellar thickening of the isothermally crystallized spherulites.

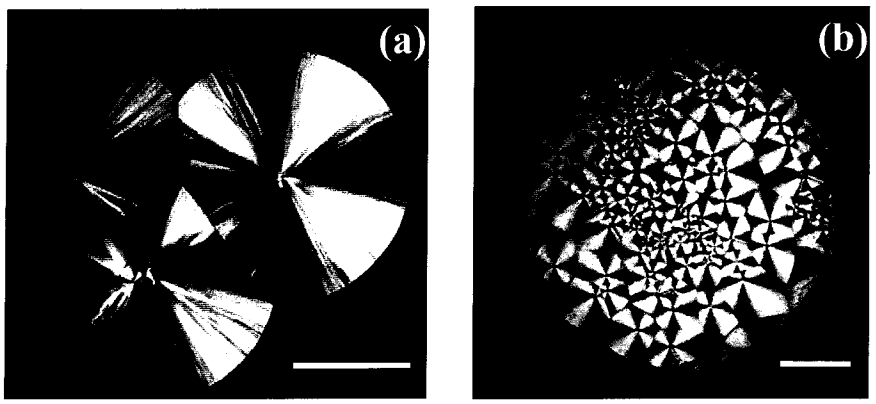

Figure 2.9: Polarized light optical micrographs of PLLA spherulites crystallized at (a) 147 °C and (b) 130 °C both for 80 min. Both images recorded at the crystallization temperature. Scale bar is 300 μm in (a) and 600 μm in (b).

It is concluded that enzyme can degrade the inter-spherulitic amorphous region (free amorphous region) rather than inter-lamellar amorphous region (restricted amorphous region) or any crystalline region under the conditions of the investigation. This conclusion is in general agreement with what Tsuji and Ikada[18] has reported. In that study, degradation took place preferentially in the amorphous region over the crystalline region of films of amorphous, racemic PLA and isotactic, crystalline PLLA. Degradation in that case was non-enzymatic hydrolysis in phosphate buffer, the extent of which was measured using methods of gel permeation chromatography (GPC) and DSC. In a more recent publication by Tsuji and Miyauchi[19] on studies of degradation of PLLA thin films by proteinase K in Tris-HCl buffer, the restricted and free amorphous regions were identified. Using DSC and GPC to measure the effect of degradation, they found that the

free amorphous region is more susceptible to enzymatic hydrolysis. Most recently, another research group[20] had reported that the degradation rate of the free amorphous region is faster than that of the restricted amorphous region, using atomic force microscopy (AFM). In the thesis study, it is proposed that above a certain degree of total crystallinity, enzymatic degradation is hindered. Cai *et al.* [21] and Wang *et al.* [22] have similar results to support this statement.

Degradation investigations are typically qualitatively studied by images collected using PLOM, EM, AFM, or wide-angle x-ray scattering (WAXS),[23,24] depending on the resolution or morphological feature required. Quantitatively, the examination of enzymatic degradation has been carried out by the following methods. GPC [24-26] and size-exclusion chromatography (SEC)[27,28] have been used to measure the molecular weight and the molecular weight distribution before and after the application of enzyme; DSC[24-28] has been employed to characterize changes in crystalline region after degradation; Nuclear magnetic resonance (NMR)[23,24,28] and capillary zone electrophoresis[27] have been performed to analyze the degradation products. In addition, weight loss[24-29] and water absorption[29,30] were also usually evaluated by quite a few research groups, as the latter can facilitate enzymatic attack. The use of physical methods to monitor degradation is therefore common. Chemical methods are less common as the use of buffer can complicate the quantification of these measurements. This study is the first one that uses total depolarized light transmission to evaluate the effects of degradation.

The physical property of viscosity has also been used in the investigations of degradation of polymer chains.[29-35] A polymer solution is more viscous than the solvent itself. Degradation of the polymer chain can lead to chain scission and therefore changes

in molecular weight, which in turn changes the viscosity of the solution. Relative viscosity can be measured by recording the flow times (or, efflux times) of the solution using a capillary viscometer under controlled temperature conditions. The efflux time is essentially related to polymer molecular weight.

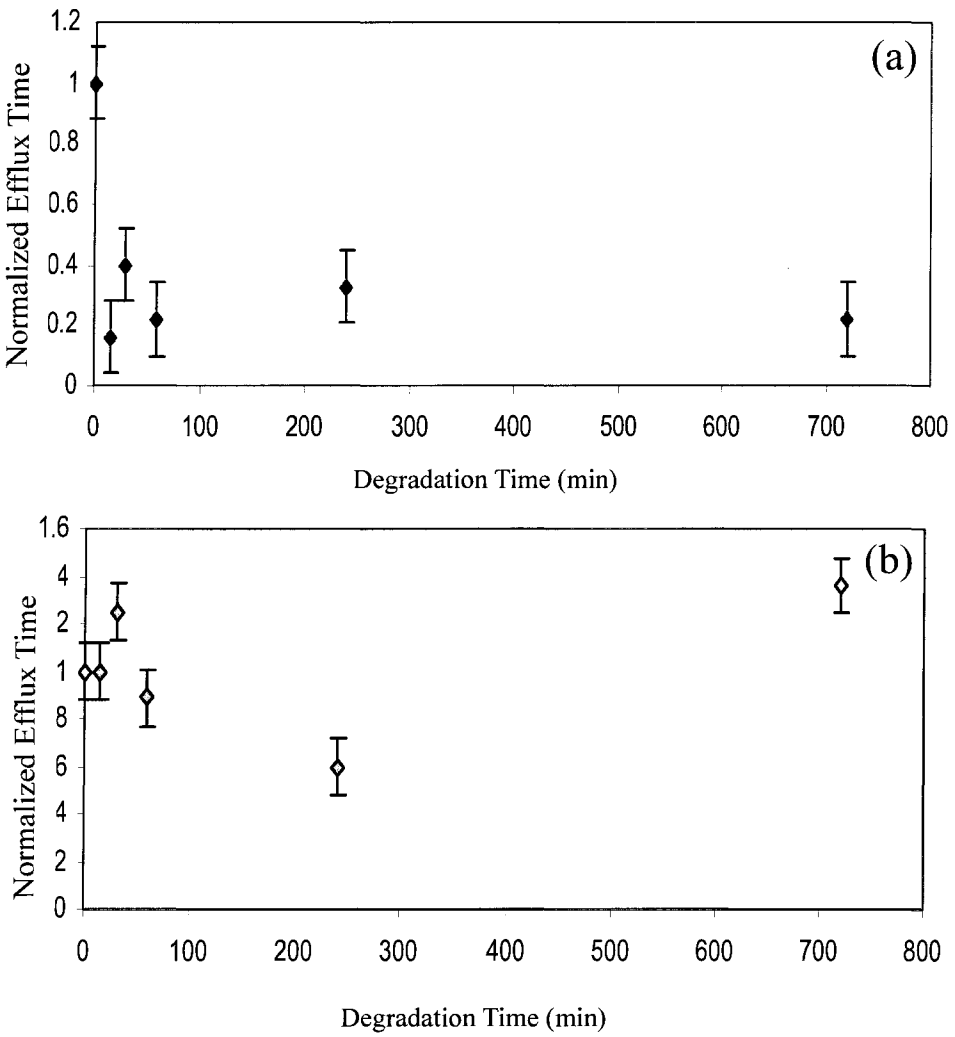

Figure 2.10: Normalized viscometer flow times (efflux) of degraded PLLA in dichloromethane solution as a function of degradation time. PLLA crystallized as open face thin-film at (a) 147 °C and (b) 130 °C for 80 min prior to enzymatic degradation.

Figure 2.10 contains plots of the normalized viscometer efflux times as a function of degradation time for PLLA with the same thermal history as the samples in Figure 2.7

and 2.8. A considerable drop in flow time was seen for the sample degraded for only 15 minutes, indicating that shorter polymer chains had probably been formed by enzyme chain-scission. However, for the sample degraded for a period of 30 minutes, the flow time is greater indicating that its solution is more viscous. This apparent anomaly can be reasoned considering that the short degraded portions had effectively gone into the original enzymatic degradation solution therefore were absent from the viscosity measurement solution. It is important to note that the aqueous enzymatic degradation solution medium was replaced with dichloromethane solvent for the viscosity measurements. The overall response of flow or efflux time indicates the potential continuous degradation and removal of short chain regions. In Tsuji and Miyauchi's paper,[36] they also reported this *removal* of amorphous regions as the reason an apparent rise in crystallinity of the polymer solid upon enzyme hydrolysis. The 130 °C crystallization temperature thermal history polymer sample shows a different viscosity response to degradation time. The difference reflects the absence of the relatively poorly ordered spherulites that appear after the isothermal crystallization period. The sample crystallized at 130 °C had spherulites that grew to the point of impingement, filling the sample.

2.3.3 Melting and Degradation Behaviour of PEO/PLLA Blends

The depolarized light intensity experiments on the pure PLLA samples did not successfully show the effect of degradation on the reorganization ability of the PLLA during heating. They did, however, highlight the high degree of crystallinity in the PLLA solids crystallized under the conditions used. Essentially, the enzyme was not able to penetrate successfully into the internal structure of the PLLA spherulite in which the

layering of the lamellae building blocks present an alternating structure of relatively amorphous and crystalline regions. Without penetrating the spherulite, the enzyme was not able to reach the amorphous inter-lamellar regions.

In an effort to open up the internal structure of the PLLA, and expose the relatively disordered fold surfaces of the lamellae building blocks to the enzyme, and perhaps improve its biodegradability, a second polymer was added to the PLLA. A blend of two crystallizable polymers, PLLA and poly(ethylene oxide), (PEO), was made. PEO is unique in its water solubility and thus might enhance the enzyme penetration ability to allow for those internal areas of the PLLA spherulite to be exposed to the degradation medium. While PEO is crystallizable, it remains amorphous, or, in the melt state, at the crystallization temperatures at which the PLLA crystallizes. Thus, at the T_c of PLLA the blend behaves as a crystalline/amorphous polymer blend. With subsequent cooling to room temperature, however, the PEO passes through its own T_c region while the PLLA passes through its glass transition temperature. Before performing depolarized light intensity experiments on this blend system, the blends were characterized by polarized light optical microscopy and the effect of PEO on the growth rate of PLLA spherulites was investigated.

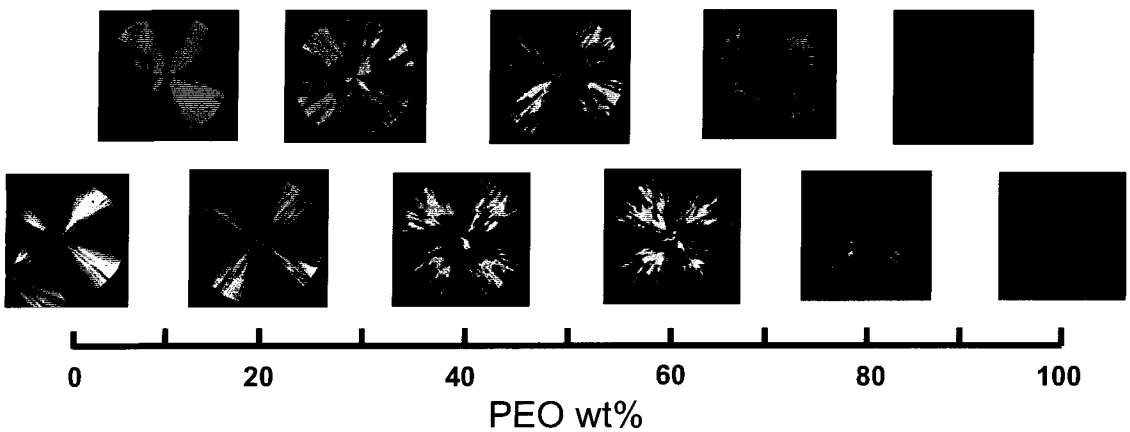

Figure 2.11: Polarized light optical micrographs of PEO/PLLA blends crystallized at 135 °C showing different morphologies. (Mag.) = 200X.

The morphological diversity of the blends with different PEO weight fraction was observed under the polarized light optical microscope (crossed polars configuration) and illustrated in Figure 2.11. All of the samples were isothermally crystallized at 135°C.

With low PEO weight fraction, the PLLA spherulites present smoother surface. With increasing PEO portion, PLLA becomes coarser, and its lamellae tend to be more opened-up by the amorphous PEO component. The last image in Figure 2.11 is totally black, and this is because PEO is above its melt temperature at this temperature. As a first approximation, judging by the above images, it would seem that the effect of increasing PEO on the morphology of the PLLA spherulite is indeed to open-up the texture of the spherulite, in keeping with the expectation stated earlier.

Figure 2.12 shows the growth rates of PLLA spherulites in the PEO/PLLA blends of different PEO composition and includes that of pure PLLA data for comparison. The data is spread over two graphs in an attempt to make a clearer presentation (odd wt% PEO blends in (a) and even in (b)).

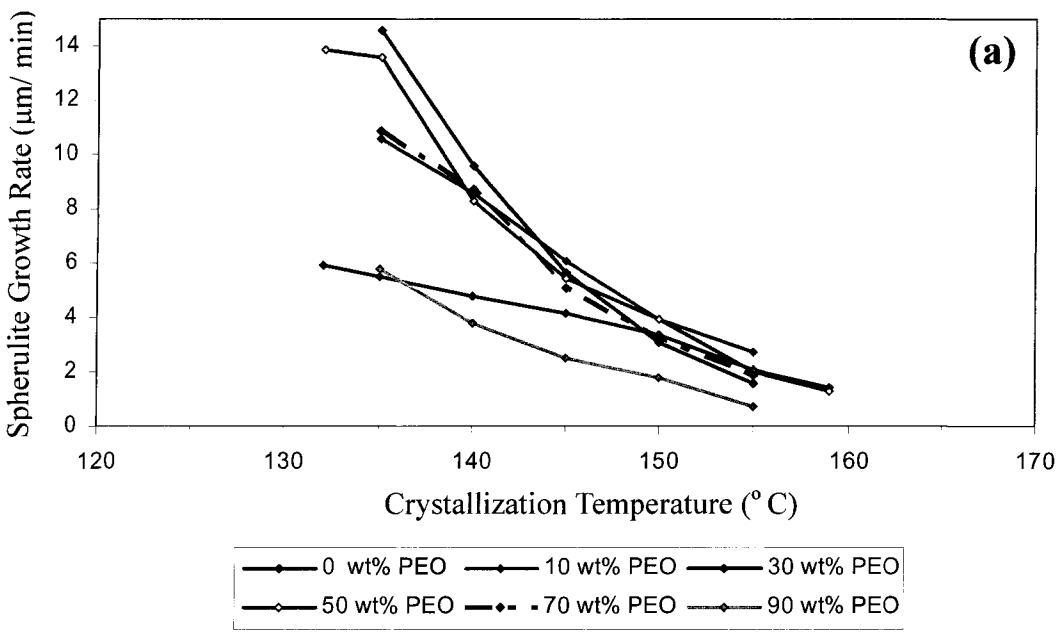

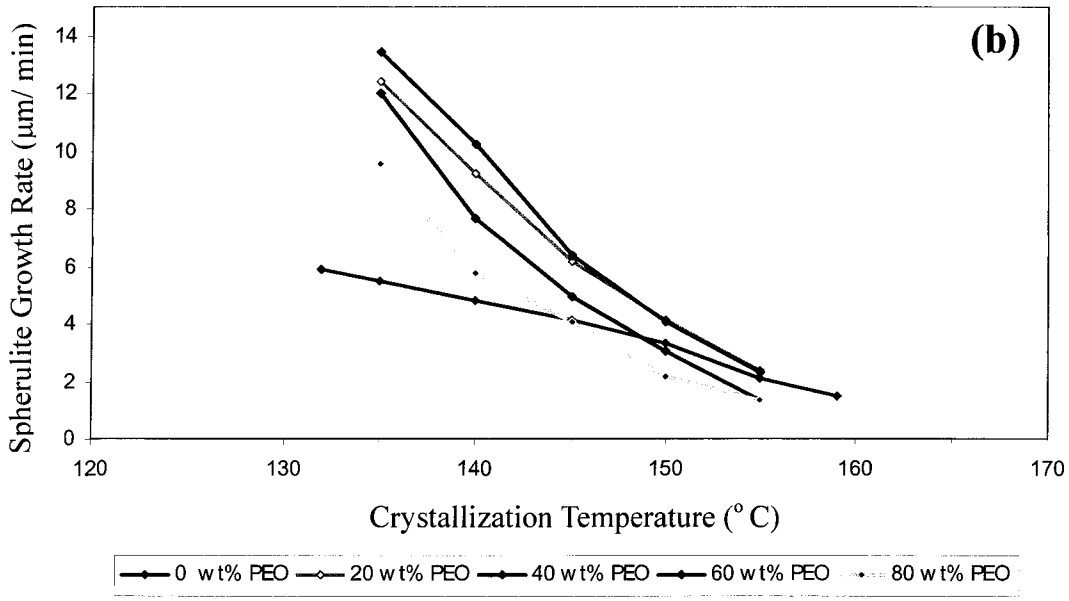

Figure 2.12: Radial growth rates of PLLA spherulites in blends with PEO of different compositions as a function of crystallization temperature. Lines are drawn for the ease of presentation but not denote a fit.

The steeper slope of the blend curves compared to that of the pure sample indicates that PLLA spherulitic growth rates in blends increase with undercooling at a greater rate than that of the pure PLLA. In short, for most blends, PLLA spherulites are growing at a faster rate when PEO is present. The enhanced growth rate can be attributed to the properties of PEO: The low T_g (*ca* -60 °C) of PEO provides increased chain mobility in the blend melts. Consequently, the growth rate of PLLA increases due to the decrease of activation energy of diffusion. As PEO fraction increases, the increasing mobility is counteracted finally by the dilution effect of PEO chains on the crystallizable PLLA. At very large PEO compositions, as in the PEO/PLLA 90/10 blend, the dilution effect is so great that PLLA growth rate is finally retarded relative to the pure PLLA.

On measuring the growth rates of PLLA with various PEO compositions, it was observed in the microscope that, regardless of the amount of PEO present in the blend, the spherulites of PLLA are still able to grow to impingement, given enough time at the

isothermal condition, even when PEO is present in 90 wt%. This observation prompted the question: where is PEO? Entropy does not allow it to be intra-lamellae of PLLA. PLLA spherulites impinged with straight and thin lines of impingement, therefore eliminating the possibility of inter-spherulitic PEO. Thus, PEO has to be either between the fibril of the PLLA, or between the lamellae of the PLLA (i.e., inter-lamellar region). Form a thermodynamic point of view, the crystallization happens so fast at 135 °C that even if complete phase separation is the thermodynamically favoured solid for the blend material, that it is immediately interrupted by the crystallization event and as a result, PEO becomes trapped inside PLLA crystals. However, if given enough time to let them crystallize, PEO and PLLA would totally phase separate ultimately. Thus, the degree of phase-separation is determined by the rate of PLLA growth (i.e., T_c), and the blend composition. With a higher concentration of PEO, perhaps the phase separation is more successful – but still not complete. This leads to the idea that, at a given T_c, the PEO might be 'trapped' at different levels of the structural hierarchy of the PLLA spherulite. It does not necessarily suggest that there will be a linear response to the location of the PEO in PLLA with composition. It might be the case that, for a *range* of blend compositions, the location of the PEO in the PLLA remains constant.

Depolarized light intensity experiments were performed on the PEO/PLLA 50/50 blend and the results are shown in Figure 2.13. The samples were crystallized as open face thin films at 130 °C prior to enzyme solution degradation.

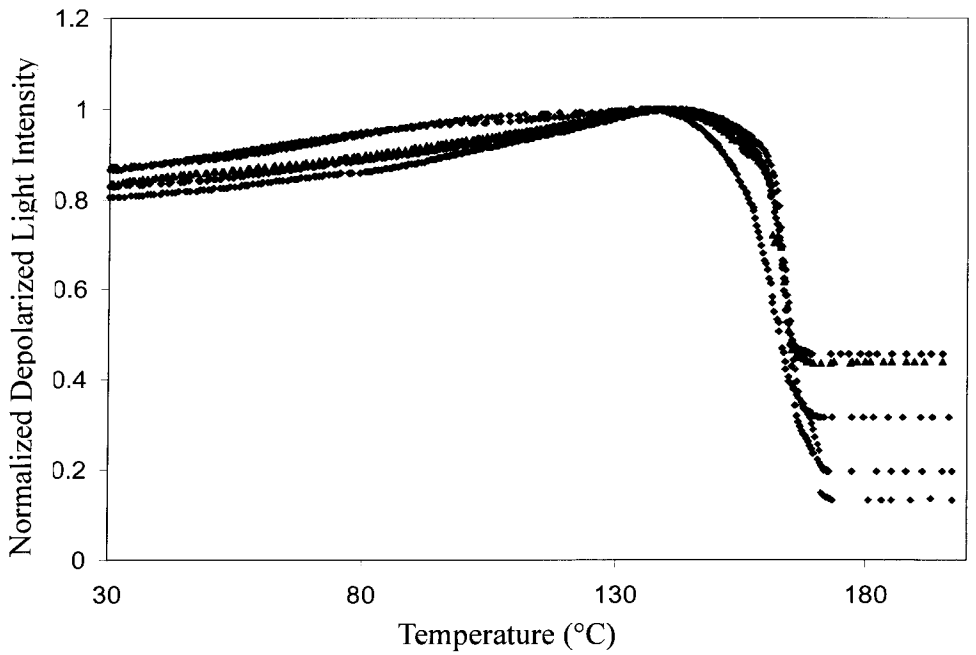

Figure 2.13: DLI heating profiles (10 °C/min) of 50/50 wt% PEO/PLLA blends following enzymatic degradation for different periods: 0 min (no enzyme) (red); 15 min (pink); 60 min (green); 4 hours (blue); and 12 hours (black). All samples crystallized as open face thin-films at 130 °C for 80 min prior to enzymatic degradation. The error bar is within the size of the data points.

Similar to that of the pure PLLA, the light intensity profiles of the blend presented a gradual increase upon heating, suggesting the reorganization of polymer chains. The most outstanding feature in this group of DLI data is the offset difference in the range of 140 °C and 170 °C among the plots. The sample which had not been degraded apparently melts sooner than the rest of the samples. This result might be attributed to two possible actions: (i) enzyme etching; or (ii) PEO diffusion. In the fist case, during the period of enzymatic degradation, the amorphous section has been eaten up and removed, and thus has developed a higher degree of crystallinity. In the second case, the PEO fraction makes the blend more hydrophilic, resulting in faster absorption of a considerate amount of water from the aqueous buffered enzyme solution. Thus, PEO becomes diffused away

from the blend and causes the increase in the degree of crystallinity of the thin film sample. In Figure 2.13, all of the blend samples, as a group, show an onset to melting (indicated by the initial drop in light intensity) at a later temperature than that of the non-degraded sample. The increased crystallinity of the blends as a group (either because of by (i) or (ii) above) accounts for this slightly higher melting temperature.

The results in Figure 2.13 also indicate that the enzyme was effective after or within only 15 minutes degradation. This is indicated by the observation that only the light intensity plot of the 15 minute run differs from the rest of the plots of the blend samples. Pennings *et al.* [37] reported a faster initial degradation in PEO/PLLA blend than in the absence of PEO, from the measurement of mass loss experiment. They reasoned this effect by the increase of hydrophilicity of the blend, and the ester bonds of the PLLA main chain with PEO is more susceptible to hydrolysis than that of the pure PLLA.

Viscosity experiments were also performed on the 50/50 wt% PEO/PLLA blend sample as performed earlier on the pure PLLA samples. Figure 2.14 demonstrates the viscometer flow (efflux) times of the degraded PEO/PLLA 50/50 blend in dichloromethane as a function of degradation time. Similar to that of pure PLLA crystallized at 147 °C for 80 minutes, during the first 15 minutes degradation, a considerable drop in efflux time was noticed, indicating the slicing of longer polymer chains to shorter ones by enzyme chain-scission. The increase in flow time at 30 minutes could be interpreted as the degraded part has been removed away in enzyme solution. Instead of a subsequent fluctuating running time at longer degradation periods, the running time shows a gradual increase. This may be because the effect of dissolution of PEO counteracts the effect of removing PLLA, and therefore shows a steadier signal than that of pure PLLA.

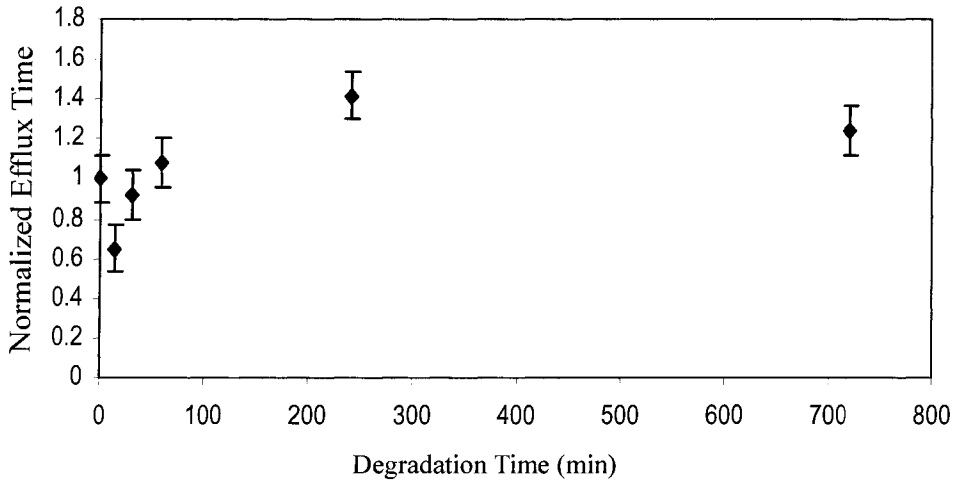

Figure 2.14: Normalized viscometer flow (efflux) times of degraded 50/50 wt% PEO/PLLA in dichloromethane solution as a function of degradation time. All samples crystallized as open face thin films at 130 °C for 80 min prior to enzymatic degradation.

Having seen how PEO in the melt state affected the growth rate of PLLA spherulites, and having suggested that the melt PEO was trapped in the inter-lamellar and/or inter-fibrillar regions of the PLLA spherulites, more experiments were performed to further investigate this idea. Two-step crystallization experiments were done on the blend samples with the second step monitored by DLI. After an isothermal crystallization treatment to crystallize the PLLA component (100 °C), the temperature was then lowered further to crystallize the PEO component. DLI was used to follow the crystallization of the PEO. The results of the cool from 100 to 30 °C are shown in Figure 2.15 for each of the blend samples investigated.

Upon looking at the results in Figure 2.15, it is immediately apparent that the results fall into three groups of DLI profiles. The three different crystallization DLI profiles may be signaling three types of crystallization, specifically, three types of ordering (or not) of the PEO component inside the PEO/PLLA blend.

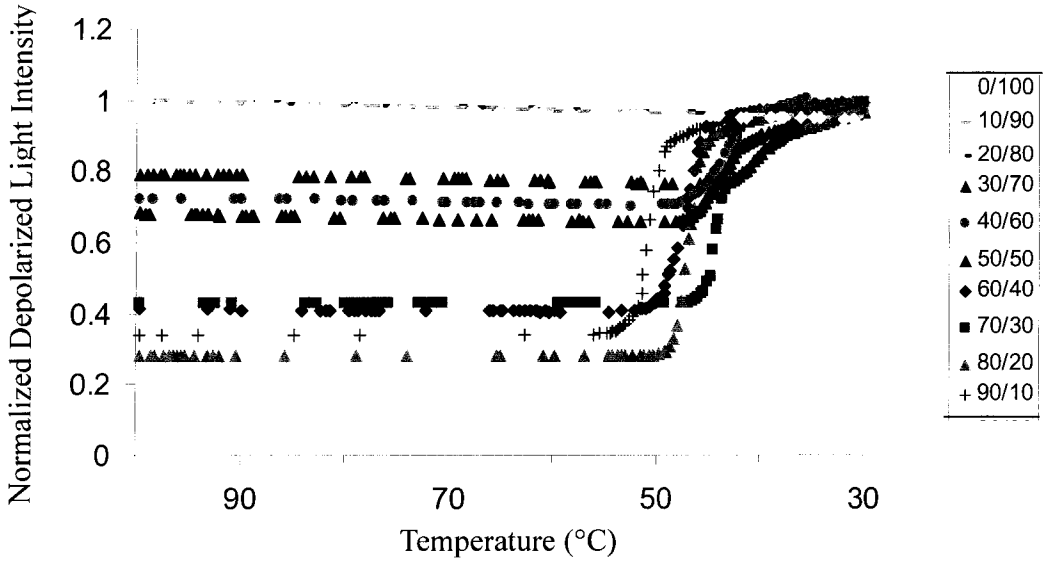

Figure 2.15: DLI cooling profiles (10 °C/ min) of PEO/PLLA blends of different compositions showing PEO crystallization. Compositions listed in legend; first value is for PEO wt%. All samples crystallized as open face thin films at 100 °C for 15 min prior to cooling. The error bar is within the size of the data points.

The crystallization of PEO during the cool to 30°C is apparent by the sudden increase in light intensity in almost all of the plots. Almost no change in signal was detected for the 10 wt% and 20 wt% samples. In this group of two plots it can be postulated that the PEO is not able to crystallize. The apparent inability of PEO to crystallize in these blends can be attributed to its dispersion throughout the inter-lamellar regions of the major component, PLLA spherulites. It is reasonable to suggest that PLLA is able to reject any highly-mobile PEO from entering into the low entropy crystalline lamellae. The relatively small amount PEO can get trapped between two relatively rough fold surfaces of neighbouring PLLA lamellae. This observation at least is in agreement with what Younes and Cohn[38] have reported. They stated that over the whole range of compositions of PEO/PLLA blend, the component is not able to crystallize with a less than 20% weight ratio. Younes and Cohn also indicated that the amorphous phase of

PLLA might accommodate some of PEO molecules, so that the crystallization of PEO is sufficiently hindered by PLLA.

The DLI crystallization profiles of the 30, 40 and 50 wt% PEO/ PLLA blends are similar and standout as a unique second group of blends. Here again, the similar profiles are an indication of a similar internal arrangement of the PEO in the blend. The small but significant increase in intensity for each of these blends in this second group is an indication that the PEO is able to crystallize and do so in a similar fashion. It is proposed that the PEO still finds itself rejected and trapped onto the inter-lamellar regions of the PLLA spherulite. In this group, however, there is more PEO in this region than merely a layer that it accommodated by the fold surface of the PLLA lamellae. In addition to this layer, there is more PEO and it can therefore attain some sort of order upon cooling in this confined space, but not enough to form spherulites of its own.

The greatest increase in intensity upon cooling was found for the third group of blends, those with > 50 wt% PEO. It is suggested that the now major component PEO is able to form its own spherulites among the existing, rather open PLLA spherulites. The PEO might have ultimately been trapped between PLLA fibrils instead of lamellae. It may be able to crystallize in a similarly open spherulitic structure that ultimately forms an inter-digitating network of spherulites with the existing PLLA in the final solid. It is also important to note that the onset to PEO crystallization is earlier in this third group of blends. This indicates that the PEO is present as a more dense component in which nucleation is more likely to occur at a higher temperature, and therefore appear *earlier* during this analysis.

Once each of the blends in the above Figure 2.15 had remained at 30 °C for five minutes, the heater was applied to the sample and the subsequent heating DLI profile was

acquired for each of the blend samples. The results are plotted in Figure 2.16. The results in this figure maintain the distinction of the three blend groups, each showing a unique thermal behaviour upon melting.

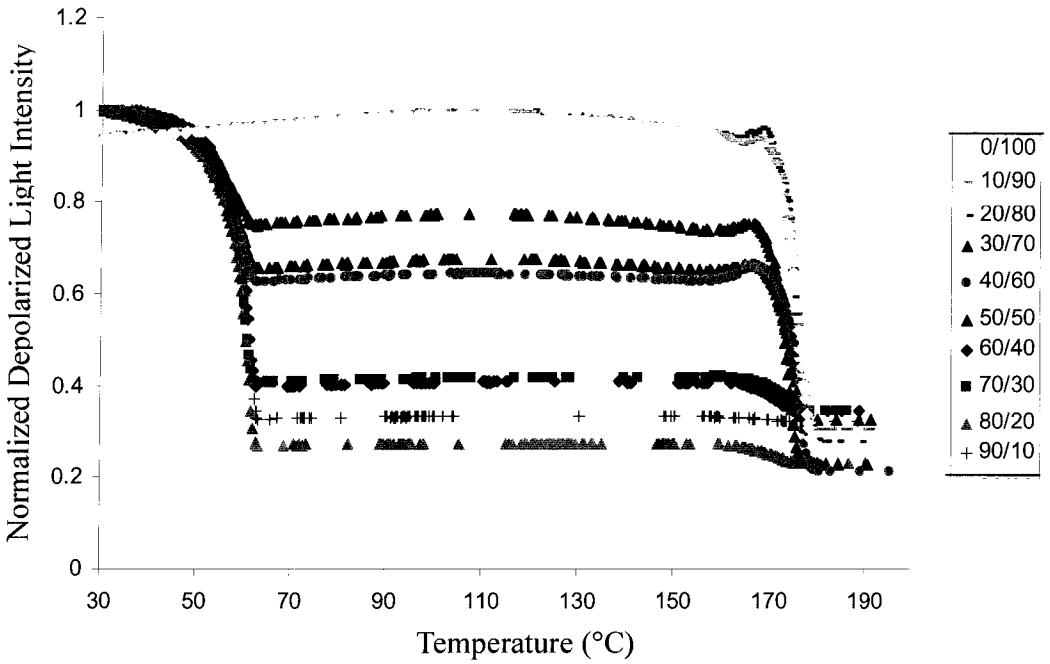

Figure 2.16: DLI heating profiles (10 °C/min) of PEO/PLLA blends of different composition. Legend lists PEO wt% first. All samples crystallized as open face thin films at 100 °C for 15 min; cooled to 30 °C at 10 °C/min for 5 min prior to heating. The error bar is within the size of the data points.

There are two regions of general intensity drop, attributed to the melting of PEO and then PLLA, respectively. In the melting experiment, the 10 and 20 wt% PEO blend samples maintain similar behaviour as group (i) blends. Neither of these samples displayed a melting light intensity loss at about 60 °C for the PEO component, which is in keeping with the lack of any observable crystallization of PEO in this group in Figure 2.15. This also consents to Younes and Cohn's idea in the case of PEO[39] for PEO component less than 60 wt%.

The 30, 40 and 50 wt% PEO blend samples maintained their distinction in this

experiment as group (ii) blends. In this group, the melting of PEO is indeed observed at about 60 °C, as expected and followed by the melting of PLLA in the second drop in intensity. It is interesting to point out that the 50 wt% PEO blend sample intensity profile appears above that of the 40 wt% PEO blend sample, reinforcing the idea that these samples are divided into groups and do not have a linear-type response in their profiles to the change composition.

Finally, the group (iii) blends, in which the PEO is the major component, all possess similar light intensity melting profiles, unique as a group to the other group profiles. This group shows the greatest decrease in intensity upon PEO melting. It is important to mention at this point that the intensity signals have been normalized so that the y-axis can be read as a relative increase in intensity. In this way it is seen that the last group has the greatest crystallinity in the PEO component.

It is interesting to see the feature on the second drop in intensity for each of the samples in Figure 2.16. Just before final melting of the PLLA component above 170 °C, there is a bump in the profile, or, a small increase in intensity just before the final loss. In fact, in the 0 wt% PEO sample, it can be seen that the sample starts to melt, as indicated by a small decrease in intensity, before the subsequent increase in intensity. In this sample therefore, the PLLA is able to partially melt, partially recrystallize, and finally melt. This is a clear manifestation of the metastable nature of the polymer, as described generally earlier in this paper. The small exothermic dip is unique to the 0 wt% blend sample. The anneal-type reordering feature, manifest by the 'bump' before final melting is present on all of the profiles of the group (i) and (ii) blends. There is no apparent reordering of the PLLA in at least the 80 wt% and 90 wt% PEO samples of the group (iii) blend samples in which the PLLA is the minor component.

The two-step crystallization experiments represented by the DLI intensity profiles in Figure 2.15 were also monitored using time-lapse digital photography with a camera on the third ocular of the polarized light optical microscope. The process is illustrated in the images in Figure 2.17 for the PEO crystallization during the cool from 100 °C to 30 °C for the 80 wt% PEO/PLLA blend.

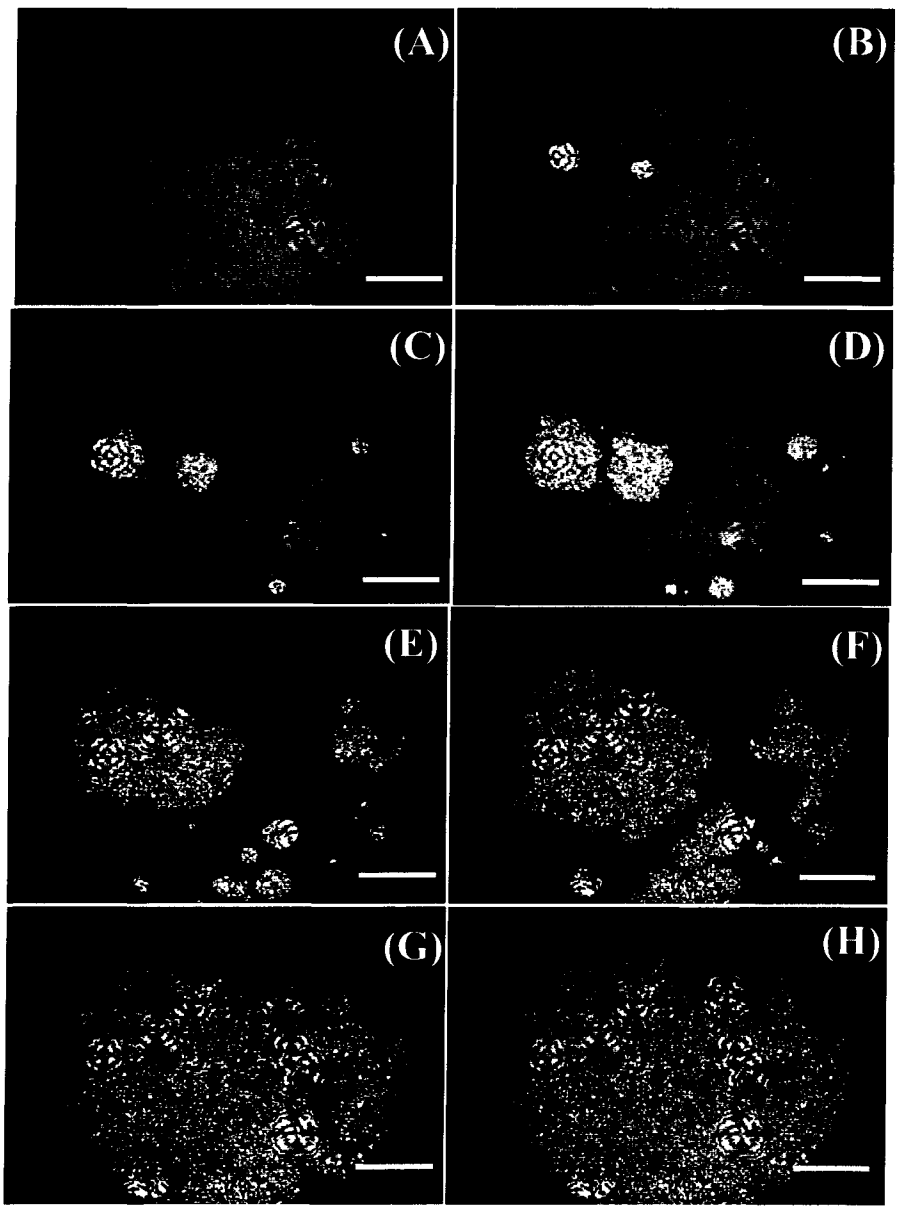

Figure 2.17: PLOM images of PEO/PLLA (80/20 wt%) blend cooling from the melt: (A) 50 °C; (B) 47.7 °C; (C) 46.9 °C; (D) 46.3 °C; (E) 45.8 °C; (F) 45.3 °C; (G) 44.8 °C; and (H) 43.9 °C. All scale bars = 400 μm.

The sample was pre-crystallized at 100 °C to completely crystallize the PLLA component to the point where the whole sample was filled with PLLA spherulites grown to impingement. The sample was then cooled at a controlled rate to 30 °C. The first image was taken before the first sign of crystallization of PEO. It is important to point out that the dimly-lit background in (A) is actually the appearance of the PLLA component completely filling-in the field of view with impinged PLLA spherulites. It is dim because the birefringence is very low on this particular blend sample at this point. The PLLA spherulites have a banded appearance in this blend. The bright spot in the image of (B) is not the direct appearance of a spherulite of PEO. The bright spots in (B) are spherulites of PLLA that were there originally, being illuminated by the new birefringence created by the crystallizing PEO component in the sample. It is not possible to view directly the PEO spherulites, only their birefringence. These bright spots, however, can be seen to enlarge in the same fashion as a spherulite would grow; they appear to be growing radially and taking on the shapes that impinging spherulites would, and also the shapes that clusters of growing nuclei would look like too. And so it that the light intensity of PEO spherulites superpose that of PLLA, until all bright areas take over the entire sample. This observation only applied for PEO wt% greater than 50 wt%, which corresponds to the group (iii) blends.

To summarize, three groups of PEO/PLLA blends have been distinguished: (i) 10-20 wt% PEO; (ii) 30 - 50 wt% PEO; and (iii) 60-90 wt% PEO. With less than 20 wt% of PEO, and without any significant phase separation process, there is not enough PEO in any local area to develop into any sort of folded-chain structure. Rather, it is most likely accommodated by the relatively rough fold surface of the PLLA lamellae. PEO is able to form ordered structures in the two groups, (ii) and (iii), with the PEO assigned to the

intra-spherulitic space (i.e., either inter-lamellar and/or inter-fibrillar). In the work on a similar blend, Nakafuku and Sakoda[39] considered only that PEO crystallized directly from the homogeneous melt of the polymer blend, or that the melt first separated into a PLA-rich phase and a PEO-rich phase and subsequently PEO crystallized from the latter phase. In this thesis work, the acquired results point to supporting the idea that PEO and PLLA are melt-miscible polymers which may ultimately possess a thermodynamic drive to phase separate into two separate solids at the crystallization temperature, but whose final morphology is really kinetically controlled. The crystallization of PLLA, at the temperatures investigated and under the conditions employed, interrupts any such phase separation attempt and takes over the process. In order to consider the second case proposed by the two authors above, the melt would need to be cooled slowly to the crystallization temperature in order for any phase separation in the liquid state to occur to any extent before solidification. In addition, Nakafuku and coworkers only reported that the field of vision turned brighter upon cooling[40] and slightly darker upon heating[39], when they viewed their similar blend sample under the polarized light microscope. There was no further comment regarding specific internal structure of the blend solid.

In an attempt to gather all of the results so far, in a coherent manner, it is proposed that the morphology of the PLLA lamellae may be different in the group (iii) blend samples. It is proposed that in the PLLA spherulites of group (i) and (ii), the lamellar building blocks maintain a tight, crystalline packing of lamellae in a way that might be described as edge-on lamellae. The neighbouring lamellae pack such that their lateral fold surfaces are adjacent. The PEO component finds its way into the inter-lamellae spaces and either remaining amorphous or is able to form slightly ordered structures when the sample is further cooled after passing through the T_c region of PLLA. In contrast, at

higher PEO fraction, i.e., at 60 wt% ~ 90 wt% PEO, PLLA lamellae grow flat-on, as sketched in Figure 2.18. Neighbouring lamellae can thus share a sort-of continuous melt of PEO until it crystallizes, at which time it creates layers of PEO order between layers of flat-on PLLA lamellae. This flat-on growth mechanism offered a spacious room for PEO to grow into spherulites in the interstitial spaces of PLLA spherulites. Thus, these PEO spherulites exhibit larger light intensity step on crystallization and melting, and their effects of their shape were able to be seen directly under PLOM.

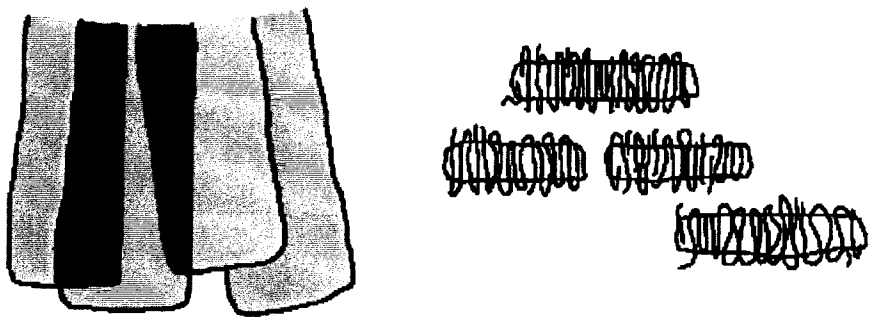

Figure 2.18: Sketch showing the top-down view and end-on view of the proposed flat-on lamellae of PLLA spherulites.

2.4 Conclusion

The degradation of pure PLLA cannot be detected using DLI, but the results are in agreement with what has been reported: (i) the inter-spherulitic amorphous region is easier to be attacked by enzyme than the inter-lamellar amorphous region; (ii) degradation is hindered above a critical degree of crystallinity.

Blending PEO with PLLA increases the growth rate of the PLLA spherulites, depending on two factors of mobility and dilution. For the DLI cooling profiles, three

groups have been identified: i) 10 wt% - 20 wt% PEO cannot form any order in the binary blend; ii) 30 wt% - 50 wt% PEO is able to form some order but not enough to develop spherulitic crystals; iii) 60 wt% - 90 wt% PEO can form spherulites. The DLI melting profiles completely support this proposal. Based on these three groups and visual observation under PLOM, two lamellar growth mechanisms were suggested, and they are edge-on and flat-on of PLLA lamella, respectively.

Combination of DLI and *in situ* observation of polymer morphology under PLOM is a useful way for understanding the phase behaviour of systems of interest; however, it is not sensitive enough for detection of enzymatic degradation. Viscosity can be performed as a complementary tool for this examination but is not a good independent technique for quantifying degradation.

2.5 References

1 Cowie, J. M. G. *Polymers: Chemistry and Physics of Modern Materials*; International Textbook Company Limited: UK. 1973, p186.

2 Hoffman, J. D.; Davis, G. T.; Lauritzen, J.I. Jr. *Treatise on Solid State Chemistry*; Ed. Hannay, N.B., Plenum Press: New York, 1976, Vol. 3, Chapter 7.

3 Hoffman, J. D. *Polymer*, **1983,** 24, 3.

4 Hoffman, J. D.; Miller, R.L. *Macromolecules.* **1988,** 21, 3038.

5 Mansfield, M.L. *J. Phys. Chem.* **1990,** 94, 6144.

6 Hoffman, J. D. *Polymer* **1991,** 32, 2828.

7 Hoffman, J. D.; Miller, R.L.; Marand, H.; Roitman, D.B. *Macromolecules* **1992,** 25, 2221

8 Hoffman, J. D.; Miller, R.L. *Polymer* **1997,** 38, 3151.

9 Ong, C. J.; F. P. Price. *J. Polym. Sci., Polym. Symp.* **1979,** 63, 59.

10 Hoffman, J. D. *Polymer* **1985,** 26, 803.

11 Sanchez, I. C.; Colson, J. P. ; Sanchez, I. C. *J. Appl. Phys.* **1973,** 44(10), 4332.

12 Sanchez, I. C.; Peterlin, A.; Eby, CP. K.; McCrakin, F. L. *J. Appl. Phys.* **1974,** 45(10), 4216.

13 Al-Raheil, I. A.; Qudah, A. A. *Polym. Int.* **1995,** 37, 249.

14 Muchova, M.; Lednicky, F. *J. Macromol. Sci., Phys.* **1995,** B34(1-2), 55.

15 Miyata, T.; Masuko, T. *Polymer* **1998,** 39(22), 5515.

16 Wang, C.; Chen, CC.; Cheng, YW.; Liao, WP.; Wang, ML. *Polymer* **2000,** 43, 5271.

17 Di Lorenzo, M. L. *Polymer* **2001,** 42, 9441.

18 Tsuji, H.; Ikada, Y. *J. Appl. Polym. Sci.* **1997,** 63(7), 855.

19 Tsuji, H.; Miyauchi, S. *Polymer* **2001,** 42, 4463.

20 Kikkawa, Y.; Abe, H.; Iwata, T.; Inoue, Y.; Doi, Y. *Biomacromolecules* **2002,** 3, 350.

21 Cai, H.; Dave, V.; Gross, R. A., McCarthy, S. P. *J. Polym. Sci., Polym. Phys.* **1996,** 34, 2701.

22 Wang, XL.; Yang, KK.; Wang, YZ. *J. Macromol. Sci., Polym. Rev.* **2003,** C43(3), 385.

23 Reeve, M.; McCarthy, S. P.; Downey, M. J.; Gross, R. A. *Macromolecules* **1994,** 27, 825.

24 MacDonald, R.; McCarthy, S. P.; Gross, R. A. *Macromolecules* **1996,** 29, 7536.

25 Tsuji, H.; Miyauchi, S. *Polym. Degrad. Stab.* **2001,** 71, 415.

26 Tsuji, H.; Miyauchi, S. *Biomacromolecules* **2001,** 2, 597.

27 Li, S.; Tenon, M.; Garreau, H.; Braud, C.; Vert, M. *Polym. Degrad. Stab.* **2000,** 67, 85.

28 Li, S.; Girard, A.; Garreau, H.; Vert, M. *Polym. Degrad.Stab.* **2001,** 71, 61.

29 Zhang, X.; Wyss, U. P.; Pichora, D.; Goosen, M. F. A. *J. Bioact. Compat. Polym.* **1994,** 9, 80.

30 Tomita, K.; Kuroki, Y.; Nagai, K. *J. Biosci. Bioeng.* **1999,** 87(6), 752.

31 Breitenbach, A.; Li, Y. X.; Kissel, T. *J. Controlled Release*, **2000,** 64, 167.

32 Cai, Q.; Bei, J.; Wang, S. *Polym. Adv. Technol.* **2002,** 13, 534.

33 Nuutinen, J. P.; Clerc, C.; Tormala, P. *J.Biomater. Sci. Polym. Ed.* **2003,** 14(7), 665.

34 Tomita, K.; Nakajima, T.; Kikuchi, Y. ; Miwa, N. *Polym. Degrad. Stab.* **2004,** 84, 433.

35 Zhou, S.; Deng, X.; Li, X.; Jia, W.; Liu, L. *J. Appl. Polym. Sci.* **2004,** 91, 1848.

36 Tsuji, H.; Miyauchi, S. *Polymer* **2001,** 42, 4463.

37 Nijenhuis, A. J.; Colstee, E.; Grijpma, D. W.; Pennings, A. J. *Polymer* **1996,** 37, 5849.

38 Younes, H.; Cohn, D. *Eur. Polym. J.* **1988,** 24(8), 765.

39 Nakafuku, C.; Sakoda, M. *Polymer Journal* **1993,** 25(9), 909.

40 Nakafuku, C. *Polym. J.* **1996,** 28(7), 568.

Chapter Three: *Microstructure of PLLA and its Blends with PEO*

3.1 Introduction

The phenomena of phase separation and miscibility in polymer blends are very important from a materials industry point of view and they present a very appealing area for further study and understanding from an academic point of view. Understanding the relationship between the physical properties of polymer materials and their internal structure, at all levels, is key to making advances in both theory and application. Environmentally-friendly technologies aimed at the low-cost production of polymer materials with fine-tuned properties are continuously being developed to help satisfy our increasing demand for such commodity items and our growing awareness of our own environmental impact.

Many of the different techniques used to detect and to characterize structures of polymers and polymer blends can be divided into two groups: (i) imaging (real space); and (ii) scattering (reciprocal space). The former group always includes optical microscopy, electron microscopy and atomic force microscopy, whereas the techniques of light scattering, x-ray scattering and electron diffraction are included in the latter group.

Real space techniques output real images that can be seen at the focal point of the light. On the other hand, in techniques which image in reciprocal space, the real lattice is exposed to x-rays or other short-wave radiation and output scattering or diffraction patterns then need to be interpreted based on the scattering of light by regularly-spaced

structural entities in the sample, a process with inherent assumptions. In contrast to real-space structural investigations, the information gained from reciprocal space methods can be confusing and needs expert knowledge to interpret.

3.1.1. Optical Microscopy

Optical microscopy has been used for centuries and is very often applied as a tool of the surface analysis. With a predecessor having only a single lens, the compound microscope with two or more lenses was developed to allow magnification of up to 1000 times.

In practice, if a transparent, polymer thin-film sample is viewed under the ordinary light microscope, only an outline of the sample or perhaps nothing will be seen, because neither the non-crystalline (amorphous) regions nor the crystalline regions absorb a significant amount of light, therefore, providing little to no contrast between them. In the examination of polymer thin-films, contrast is frequently introduced by the use of polarized light. In polarized light microscopy, plane-polarized light is provided by the 'polarizer' lens placed before the sample, and an 'analyzer' polar lens is placed after the sample. In the so-called 'cross-polar' arrangement, (i.e., when the lenses are oriented at right angles to each other) the crystalline birefringent structure of the polymer thin-film sample becomes visible. The polarized light microscope is useful, especially for anisotropic medium.[1]

The optical microscope is widely used in morphological studies of both transparent and opaque materials, as the optical microscope can operate in a transmission or reflectance mode. With the advantage of no further sample preparation once the thin film is made, real-time investigations of the crystallization process of polymers or polymer

blends in thin films is possible.

3.1.2 Electron Microscopy

Electron microscopes use a beam of high-energy electrons to examine objects on a very fine scale. Electron microscopes were developed in response to the resolution and magnification limitations of light microscopes that typically range from 500 to 1000 times magnification and which can provide a maximum resolution of features on the order of 0.5 micrometers. In the early 1930s this theoretical limit had been reached and there was a scientific desire to see the fine details of the interior structures of organic cells. This required greater than 1000 times magnification, which was just not physically possible using conventional method available at the time.

There are two forms of electron microscopy in general use: (i) transmission electron microscopy (TEM) and; (ii) scanning electron microscopy (SEM). The transmission electron microscope was the first type of electron microscope to be developed and is patterned exactly on the light transmission microscope except that a focused beam of electrons is used instead of light to 'see through' the specimen. It was originally developed by Max Knoll and Ernst Ruska in Germany in 1931.[2] SEM debuted in 1942 with the first commercial instruments available around 1965. Its later development was due in principle to the electronic advances needed to produce a 'scanning' beam of electrons across the sample.

3.1.2.1 Basic Operating Principle

Electron microscopes function exactly as their optical counterparts do except that they use a focused beam of electrons instead of light to 'image' the specimen and gain

information as to its structure and composition. Both SEM and TEM methods require the specimen to be conducting and therefore pretreated, or coated appropriately. The basic steps involved in using all EMs, regardless of type, are as summarized here: First, a stream of electrons is formed by an electron source and accelerated toward the specimen using an applied positive electrical potential. Secondly, this stream is confined and focused, using metal apertures and magnetic lenses, into a thin and focused 'monochromatic' beam. This very fine electron beam is then focused onto the surface of the sample using a magnetic lens. The beam is scanned over the specimen in a series of lines and frames called a raster, and the raster movement is accomplished by means of small coils of wire carrying the controlling current. At any given moment, the specimen is bombarded with electrons over a very small area. Several things may happen to these electrons as interactions occur inside the irradiated sample, affecting the electron beam. They may be directly transmitted, or elastically and non-elastically scattered from the specimen (TEM). They may be absorbed by the specimen and give rise to secondary electrons of very low energy, or elastically reflected from the specimen with no loss of energy (SEM). All these effects can be used to finally produce an image on the television-like monitor. By far the most common one is image formation by means of the low-energy secondary electrons because it can be used with almost any specimen, and it gives a three-dimensional image with a large depth of field. The EM does not contain objectives, or intermediate and projector lenses to magnify the image as in the optical microscope. Instead, magnification results from the ratio of the area scanned on the specimen to the area of the television screen. Increasing the magnification in an EM is therefore achieved quite simply by scanning the electron beam over a smaller area of the specimen.

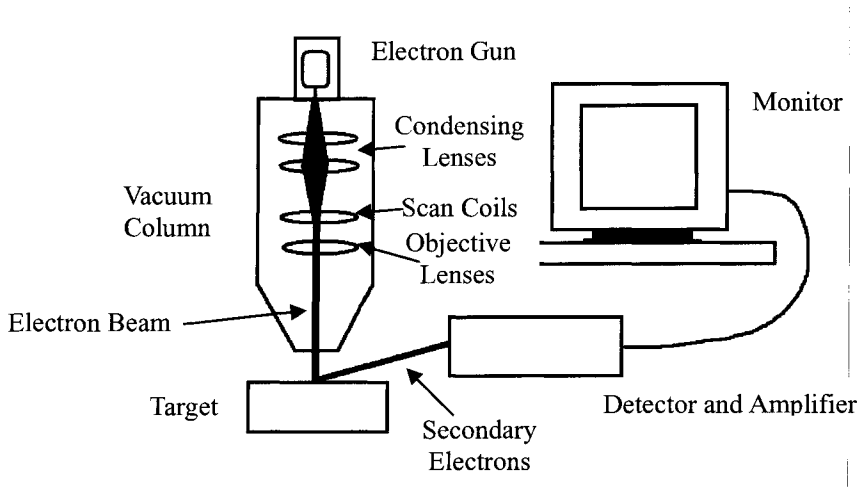

Figure 3.1: Flow chart of basic apparatus of SEM.

The scanning electron microscope (SEM) is the microscope of choice for many materials applications because of its depth of focus and resolving power, and its broad spectrum of application possibilities since the sample is not required to be transparent. As the SEM is a surface-imaging technique, transparent and opaque, thick and thin samples can in principle be investigated.

3.1.3 Digital In-line Holography Microscopy

In 1948 Gabor[3] proposed to overcome the limitations of lenses in the traditional light microscope by proposing a type of holography microscopy. Using a coherent laser light source in the visible range, a fraction of the incident beam would be elastically scattered by an object (sample) and then made to interfere with the unscattered reference beam, producing a two-dimensional interference pattern that contains information on both the amplitude and the phase of the scattered wave. This pattern is referred to as a hologram as it gives rise to an image of the original object. Recent advances in this method have

brought this form of microscopy to its current state which permits the non-destructive examination of a transparent material with resolution of the order of the wavelength of the coherent laser light source.

3.1.3.1 Basic Operating Principle

Figure 3.2 contains an illustration of the basic parts of a DIH microscope (DIHM). A coherent light source (L) is directed at a precision pinhole (P), which acts as a point source for the radiation. The consequently spherical waves which emerge from the point source are then scattered by the sample object (O) in its path. In this *inline* configuration, it is essential that the sample be small enough and sufficiently far from the point source such that a portion of the incident radiation passes (O) without being scattered. The interference at the screen (C) of the scattered waves (– – –) with the reference wave (—) constitutes the hologram.

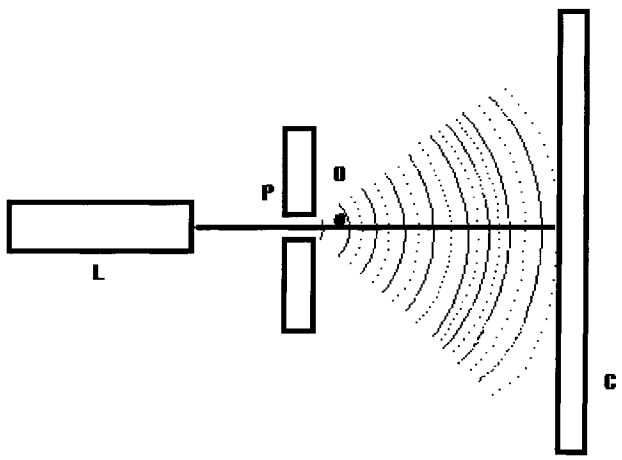

Figure 3.2: An illustration of the basic parts of a DIH microscope.

In this work, the detector at (C) is not a projection screen, but rather a CCD camera which records the hologram directly onto the chip and stores the digital information on an

attached computer for later numerical reconstruction. Numerical reconstruction of the wave front at the sample to convert the hologram to the image at that location involves the application of the Kirchoff-Helmholtz transformation. It is beyond the purpose and scope of this thesis to include the details of the reconstruction process which are available in the literature.[4]

Most of the significant recent advances in this technique have focused on refining the so-called reconstruction step which numerically converts the interference pattern to the real image of the sample at the specified depth. This process is done after acquisition, so that snapshots can be taken of the sample during a phase transition (e.g., crystallization or melting) at a rate dictated by the speed of the detector (CCD camera). There is no need to focus the sample in real time as all of the depth information is captured with the interference snapshot, or hologram. After acquisition, one hologram therefore can give rise to a user-defined number of images at any specified depth. No sample treatment is necessary (e.g., no coating of the sample); no staining is required, and no beam damage is suffered by the sample. This relatively new form of microscopy also has a broad range of applications. The digital in-line holography microscopy technique is being used in such diverse application as study of the erosion process in sediments and biological applications, which include tracing the movement of organisms through salt water media.[5-7]

One of the unique advantages of the DIHM method is that both the surface and the inside of the sample can be examined simultaneously and instantly with lateral and depth resolution. There is a potential for 3-dimensional reconstruction of the sample. A sample can be viewed as a number of two-dimensional slices of user-defined thickness, without physically slicing the sample. This has very exciting implications for spherulite phase

behavior. Moreover, with the appropriate software, the reconstructed sample can then be examined on screen by rotation in three-dimensional space. With the ability to quickly collect digital three-dimensional images it is possible to construct a video of a polymer blend as it begins and continues its phase transition from the melt state to the solid state, simultaneously collecting both kinetic and morphology information, including visual evidence of phase transition.

The advantages of DIHM are compelling: (1) Simplicity of equipment on experimentation: Digital in-line laser holography is a microscopy without objective lenses, and the hardware required is only a laser, a pinhole, and a charge-coupled device (CCD) camera connected to a computer; (2) Simplicity of sample preparation: Neither sectioning nor staining is required; (3) High Speed: The acquisition of the hologram takes seconds or less, so that changes in the specimen can ultimately be followed by the CCD camera, and emerging solid phase and/or phase-separation process can be viewed; (4) Maximum information: All the information can potentially be displayed as a three-dimensional point of view to widen the visual angle; (5) Maximum resolution: Optimal resolution can be obtained easily. The limitation of this new technique is that the resolution is restricted to the wavelength of the light source and therefore to the micron scale when employing visible-light laser.

In this chapter, microscopy is used to investigate the morphology of PLLA and its blends with PEO at different compositions and with different thermal and degradation histories. The aim of these investigations is to add visual conviction to the conclusions put forth in the last chapter. Specifically, SEM images are used to support the existence of the three groups of PEO/PLLA blends, as described in the last chapter; and to add to what is known about the selective enzyme hydrolysis sites on crystallized PLLA.

3.2 Experimental

3.2.1 Scanning Electron Microscopy

A LEO 1450VP scanning electron microscope (SEM) was used to examine the morphology of the spherulites of the PEO/PLLA blends of different compositions, and with different thermal and enzymatic degradation histories.

3.2.1.1 Sample Preparation

Details of both the preparation of the different blends and their subsequent preparation into open-face thin films have been previously reported in Section 2.2.2. The specific thermal history of the thin-film samples for study was achieved by subjecting the sample to the appropriate melting and crystallization conditions provided by the Linkam hotstage on the polarized light microscope. In this way, the samples could be viewed while achieving the desired thermal history. In general, samples were melted at a temperature of 200 °C for 1 minute before cooling the sample in the hotstage at a nominal rate of 80 °C/min to the desired crystallization temperature. Specific crystallization temperatures and isothermal time periods are listed with the SEM micrographs in the text.

For the PEO wash-out experiments, thin-film samples were crystallized open face on a glass cover slip at 140 °C for 15 minutes and then the T_c was lowered to 100 °C for another 15 minutes to complete crystallization in a timely fashion before being cooled to room temperature. Samples were then immersed in distilled/deionized water for approximately 100 hours, dried and examined immediately. During water exposure, the pure water for extraction was exchanged with fresh water every 20 hours.

For the degradation experiments, the thin-film samples were degraded in exactly the

same way as that reported for previous degradation experiments in Section 2.2.2.

SEM specimens were coated with a thin layer of gold to 30-40 nm using a BIO-RAD sputter-coater JBS-PS-3. These coated samples were observed in the secondary electron imaging mode of the LEO 1450VP SEM.

3.2.2 Digital Inline Holography Microscopy

For DIHM study, the preparation of polymer thin-film samples is the same as what has been reported in Section 2.2.2. The thin films were placed in the thermally-controlled Linkam microscope hotstage which in turn was paced on the on the DIHM x-y translation platform stage for the *in-situ* holography study. In this work, a green light laser was used to produce a coherent light source, and a 2-micron diameter aperture served as a point source. The sample was positioned approximately 3 cm from a Retiga 1300 Q-Imaging CCD camera. All components were arranged *in-line* with the pinhole point-source. The CCD camera was controlled by the computer and was programmed to capture images at a specified acquisition frequency (e.g., one image every 10 seconds) rate during the real-time investigation.

Each captured image was subsequently analyzed using LEEPS software package.[5,7,8] The reconstruction procedure was first applied by optimizing the parameters to yield a focused reconstructed image of in-situ growing spherulites. All reconstruction parameters were held constant for study of each thin-film sample once optimized. During the treatment of reconstructed images, various depths could be chosen to analyze the sample at a given time. In addition, the same spherulite sample at different times could be examined at a constant selected depth (e.g., the plane cutting through the center).

3.3 Blend Morphology

It was reported in Chapter Two that there exist three different groups of PEO/PLLA blends with respect to the blend composition: (i) 10 – 20 wt% PEO, (ii) 30 – 50 wt% PEO and (iii) 60 – 90 wt% PEO. It has been claimed that the predominant lamellar structure of the PLLA component is edge-on and flat-on in group (ii) and (iii), respectively. A systematic examination of the morphology of the PLLA spherulites and those of its blends with PEO was thus undertaken with the aim of providing visual support to the claims put forth based upon the results of the PLOM and DLI experiments.

PEO is water soluble, and this unique property was exploited to help define the morphology of the PEO/PLLA blends and to further investigate the proposed three distinct blend groups. A series of experiments was performed in which pre-crystallized samples of different PEO/PLLA blends were immersed in water, effectively washing-out the PEO component. For the pre-crystallization of each sample, the PLLA spherulites were seen to grow to impingement and fill the thin-film sample during the isothermal crystallization, as viewed under the polarized light microscope. At this PLLA crystallization temperature, the PEO is above its melt temperature and it crystallized therefore only when the sample subsequently cooled to room temperature, completing the pre-crystallization thermal history. The washed samples were expected to demonstrate voids left behind by the washed-out PEO and they were examined using SEM. The electron micrographs are included in Figure 3.3 below:

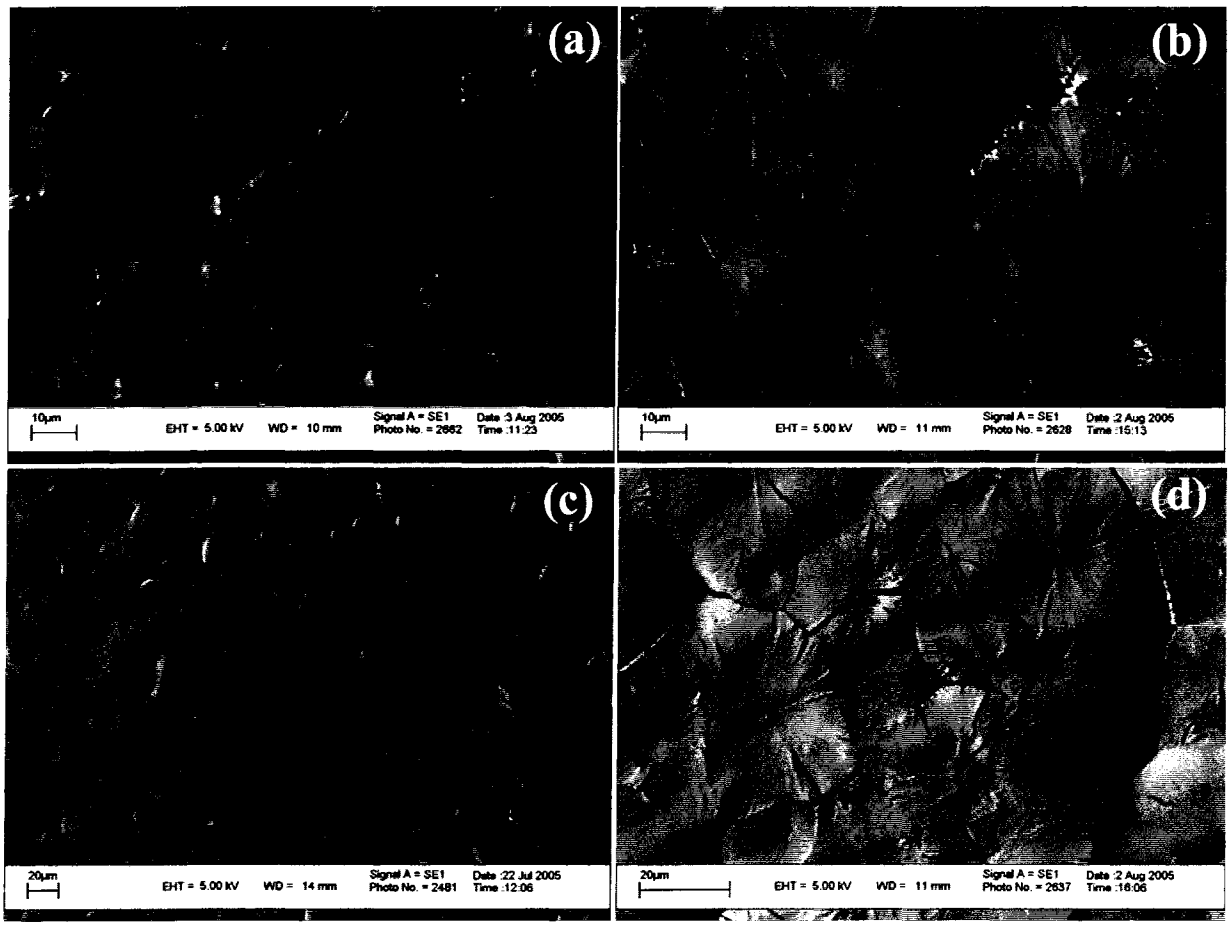

Figure 3.3: Scanning electron micrographs of PEO/PLLA blends after soaking in water for approx. 100 hours. Blend composition (wt%): (a) 70/30; (b) 50/50; (c) 40/60; (d) 30/70. All samples crystallized as open face thin films, seeded at 130 °C for 3 min; crystallized at 140 °C for 15 min, then 100 °C for 15 min (to ensure spherulite impingement), and cooled to room temperature by turning off the heat. Sample (d) not seeded.

The most notable observation upon looking at these four micrographs, is that the 70/30 wt% PEO/PLLA blend in (a) is very different from the other micrographs in the figure. It does not show any cracks. It has a very rough and uneven appearance to the surface of its open-face thin film. It can also be seen that the cracks which are visible in the remaining blend samples in (b) through (d), have propagated mostly in a radial fashion. Cracks are also apparent around the periphery of larger spherulites where they

impinge upon others.

It is very interesting to note that, while at this temperature the spherulite growth rate of PLLA is relatively slow and the mobility of the PEO/PLLA melt is relatively large, there is no sign of PEO build-up at the spherulite impingement lines that would in turn indicate that PEO has diffused away/been rejected from the PLLA spherulite crystallizing growth front. Indeed, the cracks or voids that do exist at the impingement lines are no larger or no more significant in size than those which appear in the radial direction of the blend spherulites in (b), (c), and (d).

The second most notable observation of the micrographs in Figure 3.3 is that there is no linear relationship between the apparent morphology and the blend ratio. Rather, there is a distinction between the sample in (a) and the rest of the samples in (b), (c) and (d). Moreover, there is really no difference in the apparent morphology among the latter three samples. This observation is in keeping with the observations in Chapter Two, regarding the effect of added PEO on the crystallization and melting behaviour of the blends. The sample in (a) belongs to group (iii) (> 50 wt% PEO) for which it is proposed that the PEO and PLLA form an inter-digitated network of spherulites and for which the PLLA lamellae possess a flat-on configuration. The PEO is expected to be crystallized in this group and perhaps is more resistant to dissolution in water in this more ordered state. The samples in (b), (c) and (d) belong to group (ii) (30-50 wt% PEO) for which it is proposed that the lamellae of PLLA spherulites pack in edge-on conformation and for which it is also proposed that the PLLA spherulites accommodate the PEO component in their inter-lamellar regions. In this group the PEO is expected to be only partially crystallized as it is in a confined inter-lamellar region, thus it could be more susceptible to swelling and then dissolving in the aqueous medium.

The cracks can be attributed to the effect of washing out the PEO from the inter-lamellar regions, leaving behind these radial and peripheral voids. These radially shaped cracks in the PLLA support the proposal that the PEO is between the PLLA lamellae in these samples. Thus the proposal made in Chapter Two that the PLLA lamellae are indeed edge-on in these blends where the PLLA is the major component, is supported after reviewing these morphology results. The edge-on orientation is indeed a reasonable growth habit of the PLLA spherulite lamellae when the PLLA is dense with available crystallizable material, whereas in the 70 wt%PEO blend the crystallizable PLLA melt is sufficiently diluted with PEO melt and the flat-on lamellar orientation is more efficient for space-filling under these conditions. The absence of radial cracks in the 70 wt% PEO indicates that whatever is causing the cracks is not a factor in this blend composition. Consequently, the idea that the lamellae are flat-on in the 70 wt% blend is in keeping with the observation of no radial cracking.

The selective removal of PEO from the PEO/PLLA blend has been applied by other reach groups[9,10] to produce a porous PLLA scaffold that can be used in biomedical devices. The pores were effectively the voids left behind by the washed-away PEO spherulites. In the current thesis work, however, there are no pores (e.g., holes) present on these PEO extraction samples, indicating that the PEO did not form large individual spherulites that had phase separated from the PLLA.

It might be reasonable to suggest that the observed cracking in Figure 3.3 is due simply to the unequal thermal expansion coefficients between the two materials and not to the escape of PEO. If this were true, such a material response would be exaggerated upon quenching the samples in liquid nitrogen, following the crystallization pre-treatment. The images presented in the following figure (Figure 3.4) are scanning electron micrographs

of samples following such treatment. The comparison of the samples in both Figures 3.3 and 3.4 immediately demonstrates that no such *radial* cracking is evident in the latter and the explanation put forth above is not challenged.

Except for the pure PEO sample in Figure 3.4 (f), none of the samples in Figure 3.4 crystallized to the point of impingement before being quenched in liquid nitrogen. It is very important to note therefore that in each of the micrographs in Figure 3.4 (a) through (e), both the quenched isothermally-grown spherulite(s) and the quenched surrounding melt are in view. Upon examining the images in Figure 3.4, there are at least two features which make the 40 and 50 wt% PEO samples in (a) and (b), respectively, stand out among the blend samples. The surrounding quenched melt shows a very smooth and even texture. In addition, each of these samples displays a very different type of cracking than that demonstrated in Figure 3.3. These two features are related.

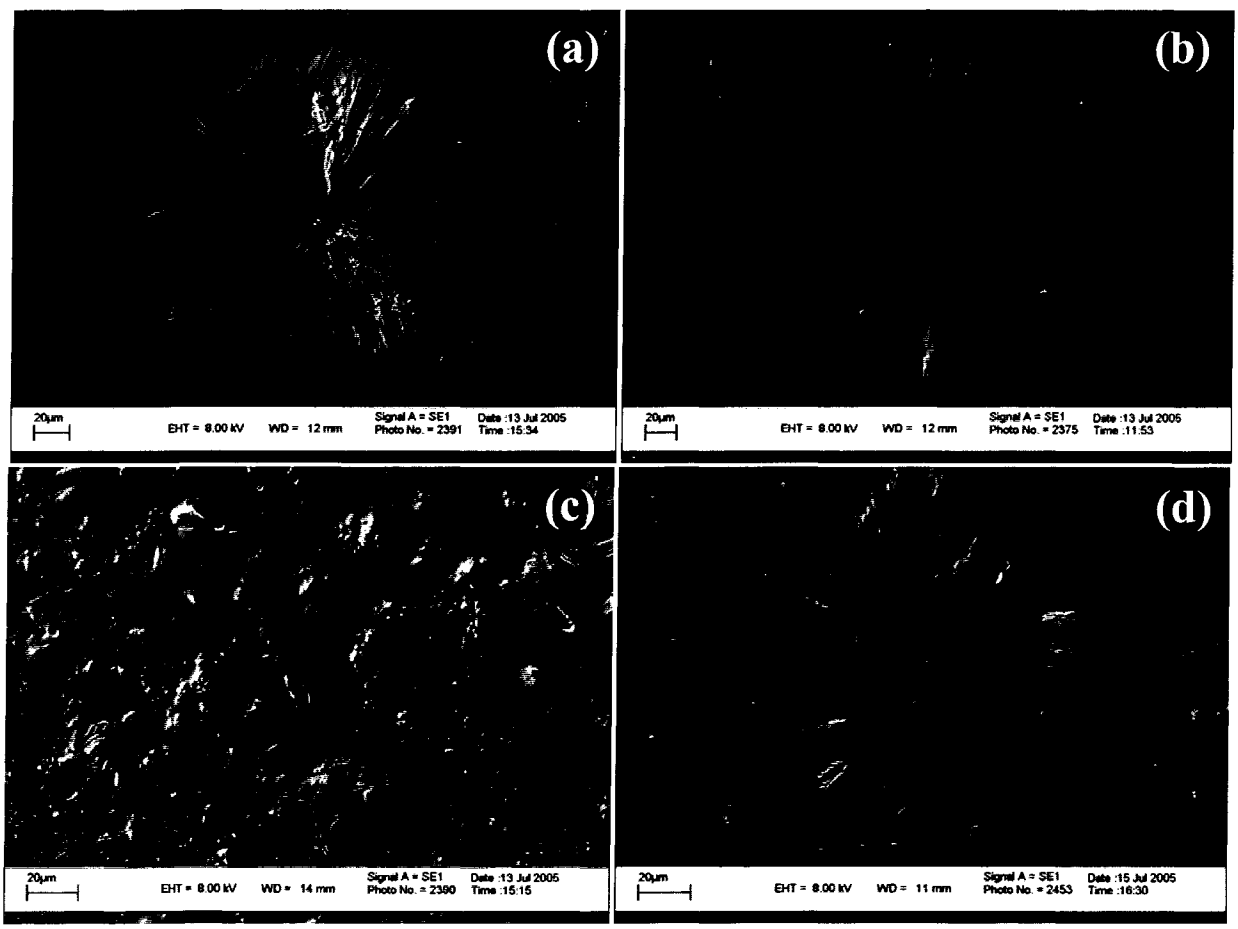

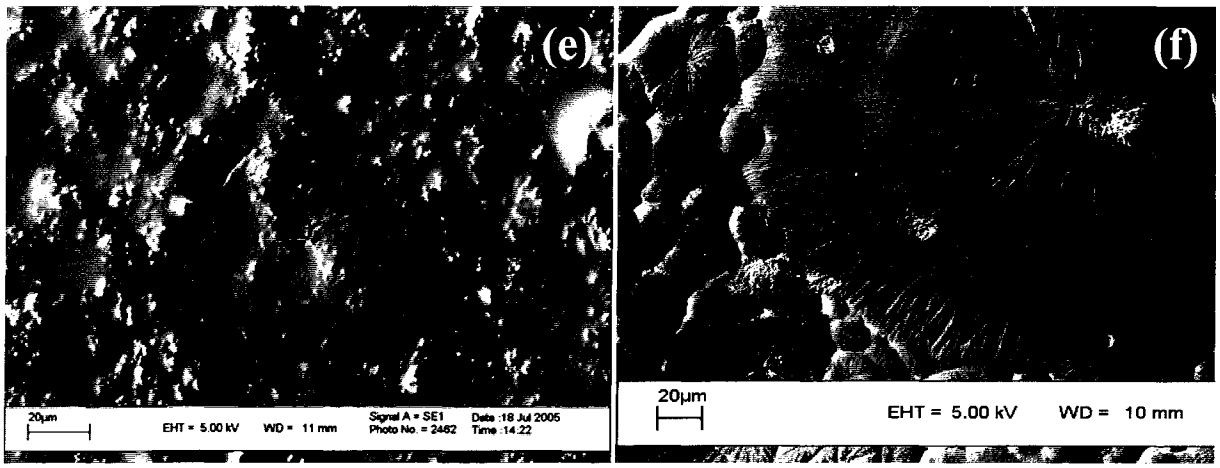

Figure 3.4: SEM micrographs of (a) 40/60; (b) 50/50; (c) 60/40; (d) 70/30; (e) 80/20; and (f) 100/0 wt% PEO/PLLA blend thin-film samples quenched with liquid nitrogen immediately following crystallization: seeded at 130 °C for 2 min (except (e)) and crystallized at 140 °C for 15 min. PEO sample (f) crystallized at 55 °C for 5 min and then cooled to room temperature on the bench.

The cracks extend from the spherulite outwards into the quenched melt, or, glass. These cracks, therefore, are due to the thermal shock of the melt being cooled so quickly to its glassy state. It is noteworthy to point out that the 'shatter' cracks do not propagate right through the spherulite but, rather, are halted upon intersection with the circumferential cracking in the spherulite. The circumferential cracking is addressed later. There is no observed 'shatter-type' cracking in the remaining blend samples (c) through (e). Moreover, the quenched melt in these latter blend samples possesses a very rough texture compared to that in (a) and in (b). This contrast again coincides with the proposed grouping of blend compositions; (a) and (b) are assigned to group (ii) and the remaining blends (c) through (e) are assigned to group (iii) in which the major blend component is the PEO. Unlike PLLA, PEO, with a glass transition temperature of *ca* -67 °C is rather difficult to quench, so that suppression of nucleation upon cooling or quenching is difficult to achieve and indeed, the growth of many tiny nuclei is evident in (c) through

(e). Therefore, the clean and smooth quenched melt area in (a) and in (b) is convincing evidence that those particular systems are relatively easy to quench. This is more evidence, therefore, that the PEO is not in a position to crystallize easily in blends of this composition, in keeping, again, with those conclusions offered in Chapter Two. It is also a clear indication that the two polymers are melt-miscible at least in this composition range. This feature is commented upon further in the context of DIH microscopy results presented later in the text. The image in (f) is of pure PEO. The nucleation rate in PEO is very low and indeed it can be seen that only one large spherulite initially nucleated in the field of view. It grew to a radius of the size indicated by the noticeable circumferential ripple in the spherulite, at which time the sample was removed from the hotstage. The existing large single spherulite proceeded to grow at a faster rate under these cooling conditions and its surroundings became littered with nuclei which grew to small spherulites before impingement. While the nucleation rate in PEO is typically quite low and generally only a few spherulites tend to grow in these thin films under isothermal conditions above the temperature of maximum growth rate, the PEO melt state is typically extremely difficult to quench cool, even with liquid nitrogen immersion (not shown). Efforts to quench the PEO to a glassy state proved unsuccessful as the melt would always 'bloom' upon even such fast cooling rates and produce a field of tiny spherulites instead of a smooth glassy appearance to the quenched sample. Thus it was not possible to quench the melt state of the pure PEO sample. It is not surprising then, that there is a rather rough appearance of the 'quenched melt' in the blend samples in which the PEO is the major component.

As mentioned above, there is no 'shatter-type' cracking evident on the samples shown in (c) through (f). There is, however, in each of the blend samples in (a) through

(e) a different type of cracking visible, that is, circumferential cracking. It is visible both within the spherulite and also around the periphery of some spherulites at the spherulite-quenched melt interface. It is not surprising that cracking has occurred at the melt-crystal interface, or boundary, upon quenching, due to their different thermal properties. Interestingly, this circumferential cracking at both the boundary and within the *spherulite* is not perfectly round – in fact it reflects the hexagonal nature of the growing crystal. Hexagonal crystals have been observed in PLLA grown in ultra-thin films (*ca* < 1 micron thickness),[11] single crystals grown from solution,[12-14] and also in melt-crystallized samples under very small undercooling conditions (i.e., high crystallization temperatures).[15] Under each of these conditions, the crystalline entity is growing under conditions of slow growth and/or conditions of dilute medium. Here, the PLLA is becoming more and more diluted with increasing PEO component and it is reasonable to suggest that the crystal growth habit would reflect that of the conditions just mentioned. If the spherulites in the blend samples are permitted to grow to impingement, however, these hexagonal entities do evolve into the expected spherulite shape. The hexagonal PLLA crystal could therefore be the growth habit of slow or impeded growth either due to ultra-thin film conditions or by solvent dilution, and also be representative of an incipient spherulite for melt-crystallized samples from diluted (i.e., blend) melts. An example of the hexagonal shaped incipient spherulites observed in this work is shown in Figure 3.5. The smaller hexagonal shaped crystal in the top area of the sample is representative of the early-stage growth of the larger, more spherulitic-looking crystals below it. All crystals eventually grow into perfectly round spherulites.

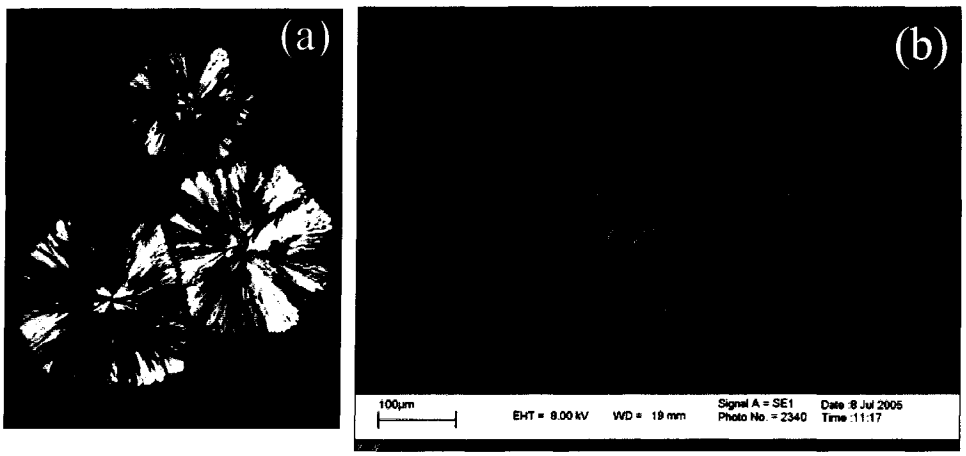

Figure 3.5: PLOM micrograph (a) and SEM micrograph (b) showing hexagonal-shaped PLLA spherulites in the same, single sample of a 30/70 wt% PEO/PLLA blend. Sample crystallized at 140 °C for 15 min and quenched in ice water.

All of the blend morphology features in Figure 3.4 are able to serve as a visual conviction of the suggested groups stated in Chapter Two. It is also meaningful to include the results of the digital inline holography microscopy (DIHM) examination to add support to the melt-miscibility claim put forth earlier for at least the blend samples in which PEO is not the major component. Figure 3.6 illustrates the crystallization of PLLA in a blend of 80 wt% PEO, and pictures were taken immediately on reaching its 140 °C (Figure 3.6(a)) and also after holding isothermally for different periods of time. No visual patterns were apparent in the first image that might indicate any phase separation, which implies that the blend components are melt-miscible. The bold ring patterns appearing in Figure 3.6 (b) and (c) are the PLLA spherulites, and all the less pronounced ring patterns are attributed to dirt as they did not change during this whole procedure.

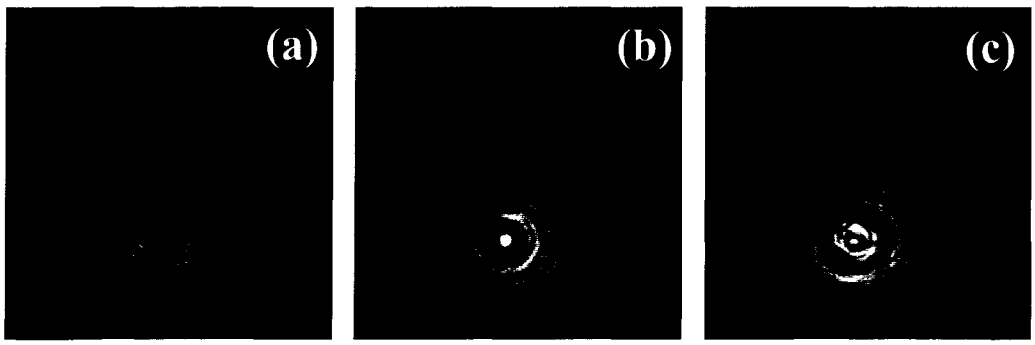

Figure 3.6: Time-lapse reconstructed images of digital inline holograms of a growing PLLA spherulite in an 80/20 wt% PEO/PLLA blend at different times after reaching the isothermal crystallization temperature of 140 °C. Images taken at (a) 0 min; (b) 10 min; (c) 20 min. All images baseline subtracted.

The claim that the PLLA lamellae possess a flat-on mutual orientation with respect to the substrate in the spherulites of the blend group (iii), that is, in blends with greater than 50 wt% PEO, was further investigated. In this particular experiment, the blend composition is chosen as 80 wt% PEO and is held constant while within one single experiment, the crystallization temperature is varied. Figure 3.7 contains the SEM micrographs of the sample.

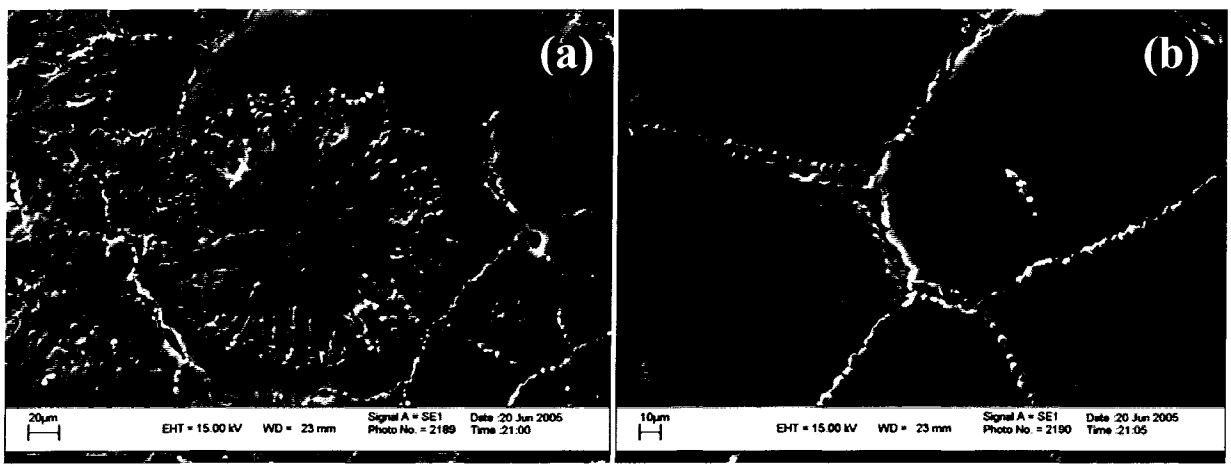

Figure 3.7: Scanning electron micrographs of a 80/20 wt% PEO/PLLA blend sample seeded at 115 °C for 3 min, grown at 120 °C for 5 min, then at 100 °C for 15 min to ensure impingement, and finally quenched in liquid N_2. Images in (a) and (b) are of different regions of the same sample.

The images in Figure 3.7 (a) and (b) were taken from different sites of the same thin-film sample which experienced the following crystallization history: The sample was cooled from the melt to a T_c of 115 °C where it was held isothermally for 3 minutes, followed by a fast heating to a second T_c of 120 °C for 5 minutes and finally to a T_c of 100 °C for 15 minutes before quenching. The central spherulite in (a) exhibits morphological features of each of these thermal history stages. It was nucleated at a temperature of 115 °C and it can be seen that it grew at that temperature to produce the relatively smooth inner region of the spherulite that extends for about 40-50 microns in radius before the texture changes to a more open, branched structure. This change in morphology corresponds to the change in T_c. This region is where the T_c is 120°C and such a change to an open, coarser texture is expected in general, with increasing T_c. Although the time period spent at this temperature is longer than that spent at 115 °C, the radial growth is slower at the higher T_c so that the increase in radius at this temperature is only about 20 microns. Finally, the smoothest part of the spherulite is generated at the lowest T_c, 100 °C. At this temperature, the rate of new spherulite nucleation is great and it can be seen that the rest of the field of view filled-in with spherulites at this temperature.

Figure 3.7 (b) shows a region where the sample did not nucleate until the final T_c of 100 °C was reached. It is very interesting to note that although the PLLA represents only 20% of this blend, the PLLA spherulites fill the entire sample. This observation is supportive of the proposed flat-on PLLA lamellar orientation of the spherulites in this blend composition. Flat-on lamellae would space-fill the sample much more efficiently than edge-on lamellae, since they would cover more surface area faster.

These two electron micrographs were taken after the sample had obviously passed through the crystallization temperature region of the PEO upon quenching; however, the

morphology of the sample would not suggest that PEO is in abundance. The only sign of PEO is the presence of the white nodules that can be seen 'oozing' from in between lamellar layers in the more open structure of the PLLA spherulite in (a), and from the inter-spherulitic regions in (a) and in (b). These white parts apparently do not represent 80% of the material. Clearly, the PEO is within the spherulite of the PLLA for the most part. Hence, these pictures do not present conflicting evidence to the claim put forth in the previous chapter that the PEO major component is situated in between the layers of flat-on PLLA lamellae.

The idea that PEO is inside the PLLA spherulites in the group (iii) blends could be further investigated if the *inside* of the spherulite could actually be viewed. A sample of the 80 wt% PEO/PLLA blend was thus subjected to such analysis via a type of crude surface etching technique. The SEM micrographs in Figure 3.8 demonstrate this etching idea. The same sample appears in each electron micrograph and has the same crystallization history as the pictures in the previous Figure 3.7 with an added detail that they were held at the last T_c of 100 °C for 90 minutes and then cooled down very slowly at a rate of 2 °C /minute until a temperature of -20 °C before finally being allowed to warm up to room temperature on its own before being imaged. The image in (b) is a micrograph of the image in (a) after it was left to sit on the bench under ambient conditions in the lab for three months to degrade.

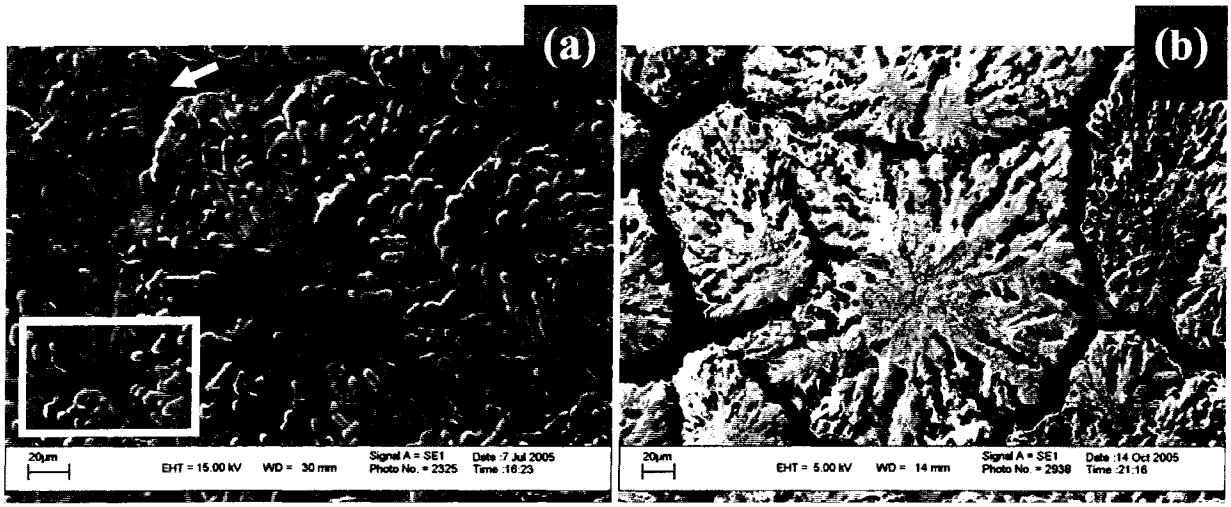

Figure 3.8: Scanning electron micrographs of an 80/20 wt% PEO/PLLA blend crystallized at 115 °C for 3 min, 120 °C for 5 min, 100 °C for 90 min and then cooled slowly to -20 °C at 2 °C/min. Image in (a) was taken immediately following thermal history; and (b) was taken 3 months after sample stored open, on bench at ambient temperature.

Clearly there is some shrinkage of the spherulites in (a) as the extended crystallization history permits some secondary crystallization in the sample. The box and the arrow in (a) point to regions where the orientation of the lamellae are clearly shown as being flat. After 3 months, the effect of degradation of PLLA has been to sweep away the outer layer of the PLLA spherulites, exposing both the internal structure and the internal PEO component, as shown in (b). The residual structure also highlights the branched, open structure of the original PLLA spherulite.

The SEM micrographs in these preceding figures show very good support of the different types of blends morphologies previously claimed in Chapter Two. Thus it is maintained that PEO crystallizes in the interstitial spaces of the host PLLA spherulite when its weight fraction falls in the range of 60 wt% to 90 wt%.

It was reported in Chapter Two that amorphous regions are more susceptible to enzymatic degradation than crystalline regions. Experiments were designed to further investigate this claim in light of the proposal of the flat-on and edge-on lamellae of the

PLLA in the different blends. By varying the blend composition and degradation condition, SEM photographs were used to investigate the effect of degradation step by step. Moreover, it is valuable to add the visual conviction of SEM images to support or question earlier claims surrounding both morphology and degradation. SEM was therefore used to examine the effects of degradation on the morphology of the PLLA and its blends. To maintain a systematic approach experiments were performed on the pure PLLA sample, a representative blend in which PEO is the minor component, and finally on a representative blend in which PEO is the major component. Thus, the first set of images in Figure 3.9 are for the pure PLLA investigation and the following Figures 3.10 and 3.11 contain the results of the investigations on a 30 wt% and 70 wt% PEO component blend samples, respectively.

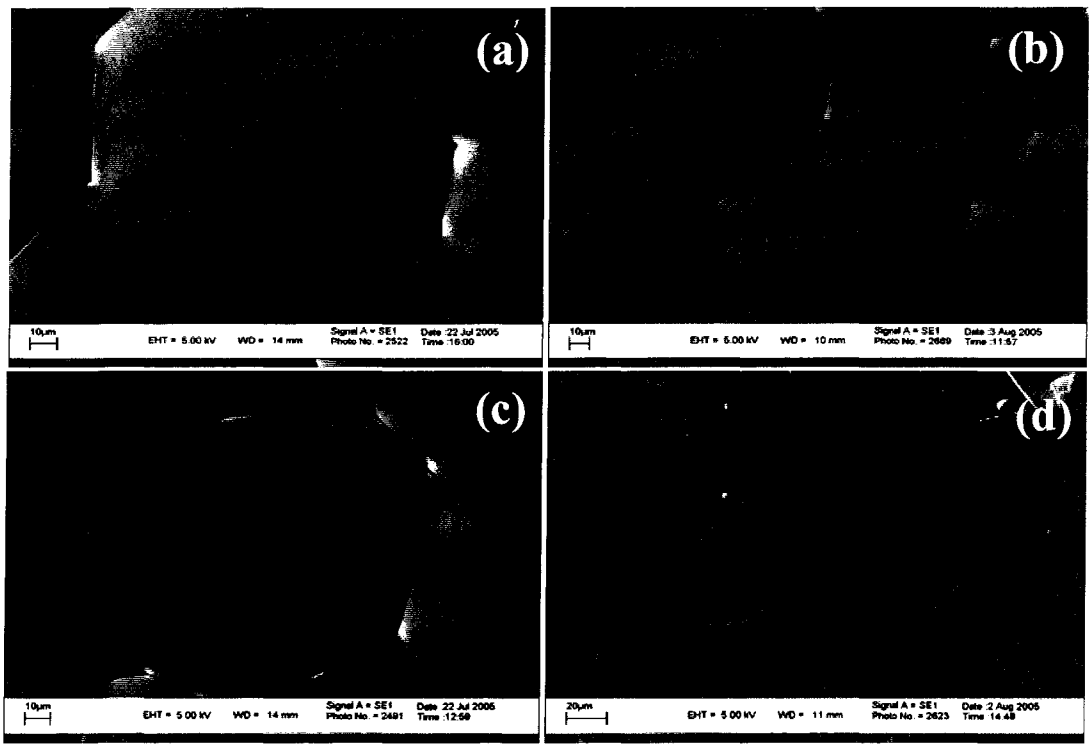

Figure 3.9: Scanning electron micrographs of pure PLLA following (a) no further treatment; (b) 14 hours in degradation medium – no enzyme; (c) 14 hours in enzyme-containing degradation medium; (d) 16 hour in enzyme-containing degradation medium. Samples (a)-(c) crystallized as open face thin films at 130 °C for 80 min; sample (d) crystallized at 140 °C for 4 min, 150 °C for 80 min.

The SEM images in Figure 3.9 can be used to both see the effects of degradation on the pure PLLA sample, and, to distinguish the effects of exposure to the aqueous medium from the effects of exposure to the enzyme specifically. Upon looking at these images the first observation to be made is that there is a clear difference between the images in [(a) and (b)] and the images in [(c) and (d)]. The former group shows smooth surfaces while the latter exhibit dark marks or 'spots' on the surface. Specifically, there is little apparent difference between the surface of the sample imaged immediately following the thermal treatment and that of the sample imaged after being soaked in the aqueous buffer solution (no enzyme) for 14 hours following the same thermal treatment. This result is an important one to any further claims of the effects of enzyme on the morphology. This result clearly shows that on this sample, the visible changes in the surface after exposure to the degradation medium are in fact attributed to the presence of enzyme in the medium. Therefore, it is clear that the formation of those 'dark spots' is due to enzymatic degradation. The degradation is apparent on the cracks and the seams, and both places are therefore evident of initial entry or penetration for the active enzyme. In (d), the sample has developed a circumferential crack in the spherulite that corresponds to the change in crystallization temperature. At this second crystallization temperature, the radial growth rate is slower and it can be said that the continuation of spherulite radial growth is attained through a type of secondary nucleation of a slower growing lamella on the existing one. The changeover presents a weak point that in turn produced a crack in the cooled sample which ultimately proved to be an entry point for the enzyme solution. It is reasonable to state that, had the sample been crystallized isothermally at the higher crystallization temperature, it would have produced a structure with the expected higher degree of crystallinity and which most likely would have been less susceptible, therefore,

to enzyme attack. It is interesting to recall from the earlier experiment in which the DLI heating profile on a similarly-treated PLLA did not lead to any conclusive evidence of degradation in that case. It can be said, therefore, that the DLI method is less sensitive to these changes than the SEM is at visualizing the subtle effects. SEM is therefore an important complimentary technique used in these investigations.

Figure 3.10 shows the SEM micrographs obtained from a similar examination of the effects of degradation on the morphology of a 30/70 wt% PEO/PLLA blend sample.

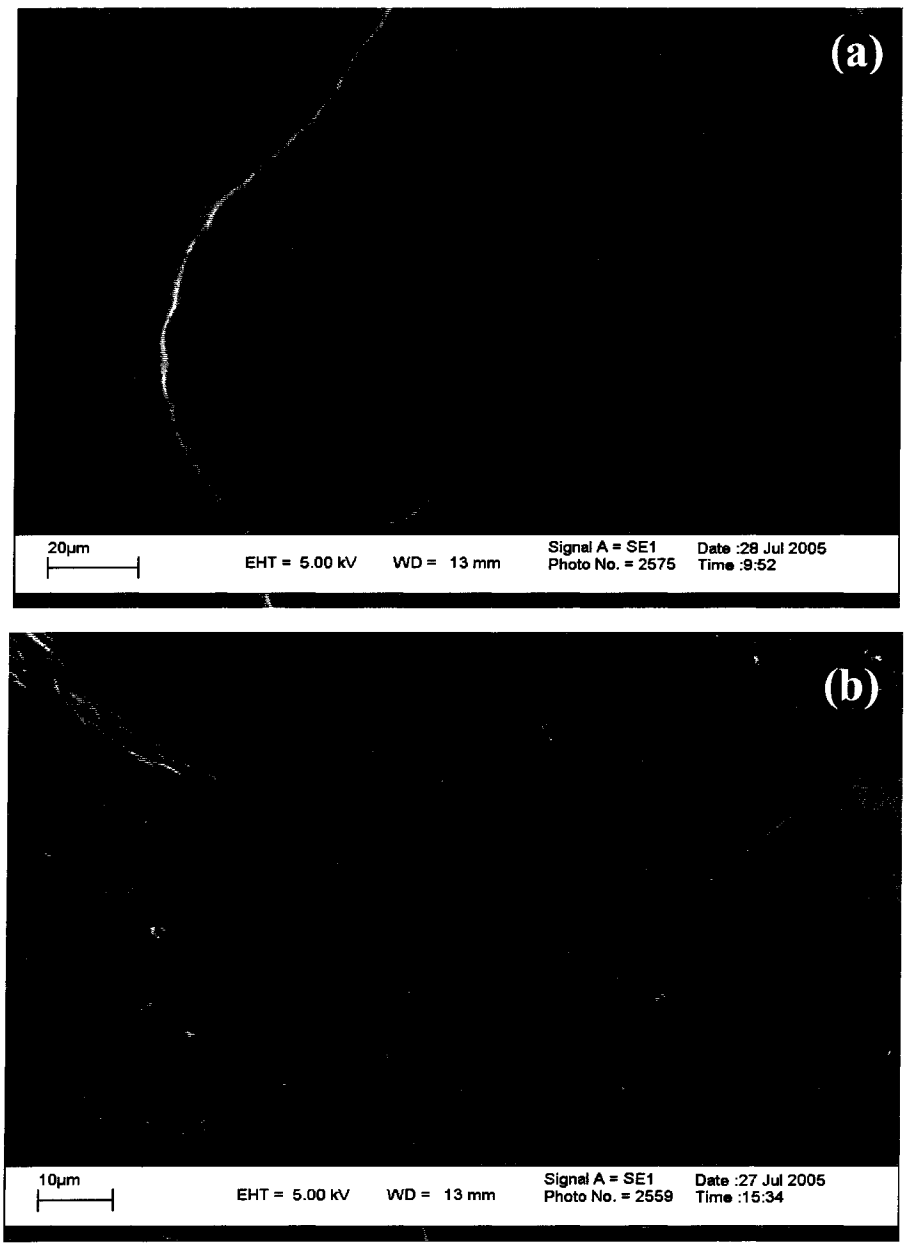

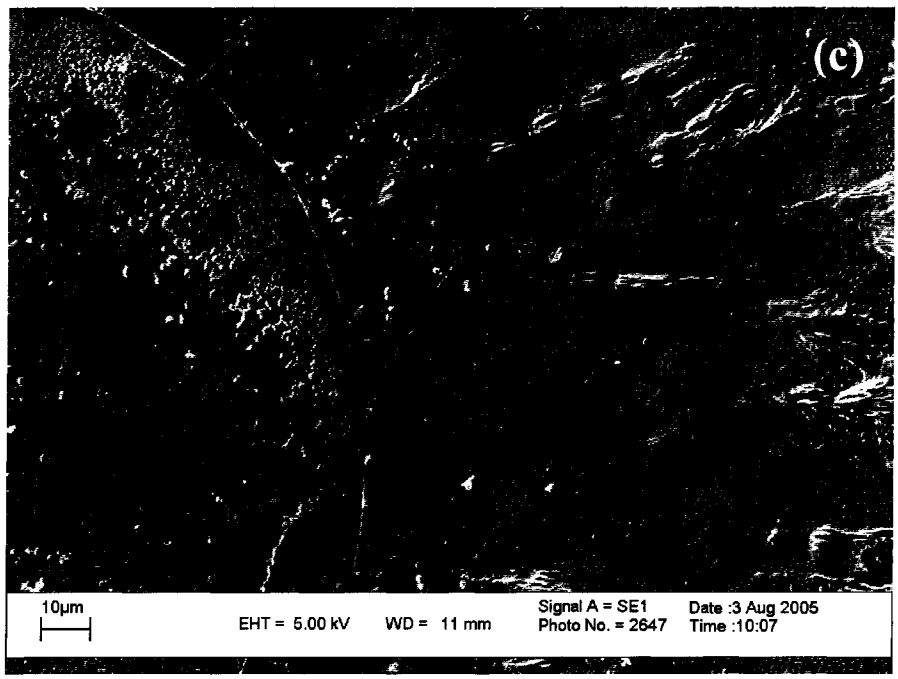

Figure 3.10: Scanning electron micrographs of enzyme degraded 30/70 wt% PEO/PLLA blend samples crystallized at 140 °C for 30 min. Samples degraded for (a) 0 min; (b) 15 min; and (c) 40 min.

These images in Figure 3.10 show the 30 wt% PEO blend sample immediately after the crystallization history (a), and after 15 minutes (b), and 40 minutes (c) of exposure to the aqueous enzymatic degradation medium. The main comparison here is between (a) and (c). While the sample in (a) looks very smooth in texture, the image in (c) shows a rougher surface. This bumpy surface has the appearance of being etched by the enzyme solution, at least in the areas where the PEO may have offered a gateway into the crystal by its affinity for the aqueous medium. On the image in (c), there is evidence of this etching process having started.

For comparison with the above sample in which PEO is the minor component, a sample in which PEO is the major component was treated and examined in a similar fashion. Figure 3.11 shows the SEM micrographs obtained from a similar examination of the effects of degradation on the morphology of a 70/30 wt% PEO/PLLA blend sample.

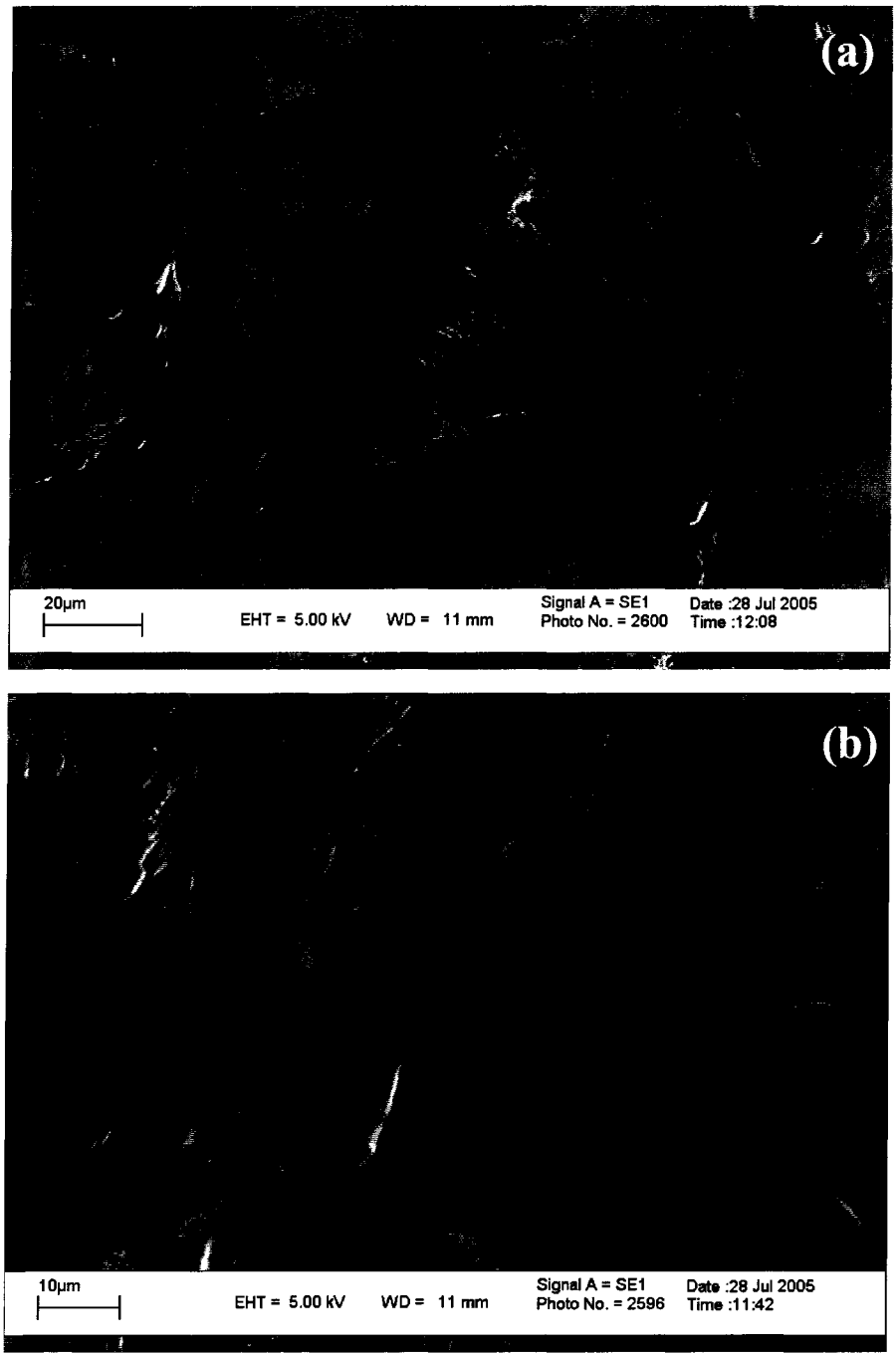

Figure 3.11: Scanning electron micrographs of enzyme degraded 70/30 wt% PEO/PLLA blend samples seeded at 130 °C for 3 min and crystallized at 140 °C for 30 min. Samples degraded for (a) 0 min; and (b) 15 min.

After a close examination of the images in Figure 3.11, it might be argued that the sample with the 15-minute degradation period has evidence of relatively bumpier surface

than that of no degradation, which would indicate the effect of enzyme.

Finally, a sample in which the two blend components are present in equal weight percent composition was subject to a similar examination of the effects of degradation on the blend morphology. Figure 3.12 shows the SEM micrographs obtained from a similar examination of the effects of degradation on the morphology of a 50/50 wt% PEO/PLLA blend sample.

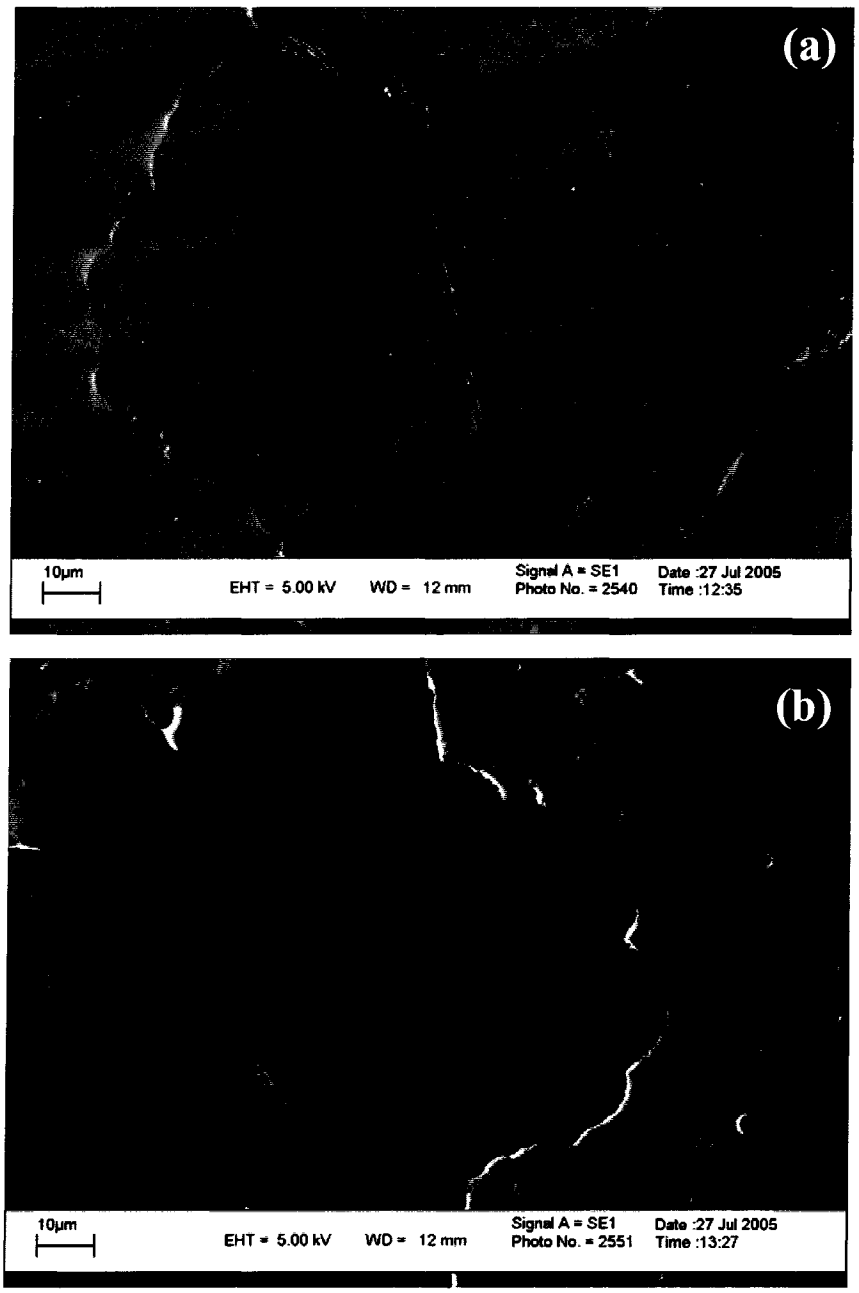

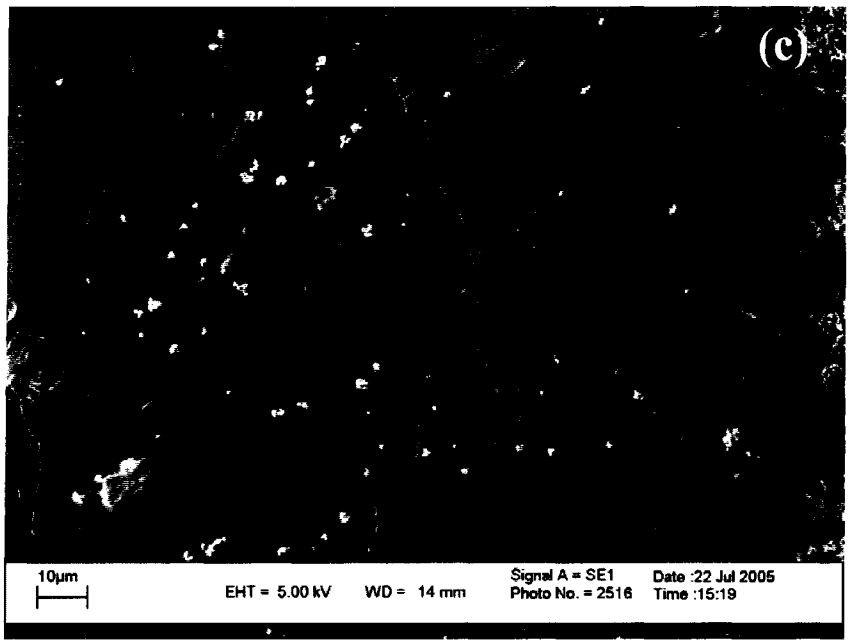

Figure 3.12: Scanning electron micrographs of a 50/50 wt% PEO/PLLA blend seeded at 140 °C for 2 min and crystallized at 150 °C for 60 min. Samples imaged (a) as is; (b) after 15 min in degradation medium without enzyme (i.e., buffer only); (c) after 15 min in enzyme-containing degradation medium.

The images in Figure 3.12 demonstrate that, for this sample composition, there is indeed an effect of degradation after only 15 minutes. It is interesting to compare the images in (a) and (b) first. It is evident that the effect of immersing the sample in simply the aqueous medium without enzyme was sufficient to begin a washing-out process on the water soluble blend component, PEO. It can be seen that the original crystallization treatment was not sufficient to allow the PLLA spherulites to completely fill-in the sample before the PEO subsequently crystallized during cooling to room temperature. This is clear by the appearance of a relatively large spherulite entity (PLLA spherulite with PEO in the interfibrillar spaces) surrounded by a cluster of much smaller crystalline entities (PEO). In addition, the large spherulite had a scalloped edge instead of a smooth circular one. This is evidence that the edge of the existing larger spherulite served as a nucleation surface for many more small spherulites that appeared as the temperature was

cooled to room temperature. These details are important to note because it helps to explain the appearance of the samples in the figure as well as the degradation effects on those samples. In (b) it can be seen that the surrounding small spherulites of mostly PEO component were affected by the degradation medium without enzyme. This is because the PEO is water soluble and began to wash out of the sample. The surrounding area shows little circular holes or voids which were not apparent in (a). These places are indications of where little PEO spherulites used to be in the original material but have been washed out due to its soluble nature. The large spherulite does not show any change in morphology. In (c), the surrounding small spherulites have been completely removed by the effects of exposure to the degradation medium with enzyme. The effects are also evident on the surface of the larger spherulite in (c). It is reasonable to expect that the non-isothermally crystallized melt surrounding the large spherulite would be less crystalline, relatively more amorphous, and therefore much more susceptible to the degradation than the crystalline parts of the spherulite. The spherulite in (c) is quite littered with tiny pock marks all over its surface, which is necessarily interpreted as an effect of degradation. Another striking feature of the image in (c) is the absence of the surrounding quenched melt. It has been removed, leaving only remnants, or, little pieces of the polymer blend behind. Some of them have apparently been deposited on top of the spherulite. Finally, as a general observation, it is interesting that there is no sign of the dark 'spots' of degradation apparent in Figure 3.9 here on the surface of the large spherulite. It might be an indication of a different internal lamellar structure of the blend spherulite versus the pure PLLA spherulite. Also, given the nature of the 50/50 blend sample, the enzyme would prefer to attack the available, more amorphous regions of the sample first.

3.4 Conclusions

The effect of blending PLLA with PEO is to modify the internal lamellar organization inside the spherulite. The distinction of the three proposed blend groups is upheld considering the results of Chapter Three. There are three distinct morphologies in the respective blend samples, as manifest in the SEM examinations. The results of an SEM examination on the degraded samples of the pure PLLA and its blend with PEO do not contradict the claims put forth until that point. While the different edge-on and flat-on orientations of the PLLA lamellae relative to the substrate or free surface might make the material less or more exposed to the enzymatic degradation medium, the PEO which is responsible for that change in morphology is also water soluble. It is therefore difficult to separate the effects of PEO on the degradation of PLLA. The reason why it might be thought that the flat-on lamellae would be more susceptible to degradation is because the relatively rough fold surfaces of the otherwise crystalline lamellae would be more exposed to the degradation medium. It is generally accepted that the enzyme prefers to attack the more amorphous regions first. The group (i) blends which have the PEO in the inter-lamellar region but in which the PEO is not able to crystallize may be a useful material as the glassiness of the PLLA is reduced, making the PLLA less brittle. The increase in crystallization rate for this blend also makes this material good from a processing point of view because the relatively fast rate of crystallization ensures that the PEO indeed gets trapped in the inter-lamellar regions. This relatively small amount of PEO may or may not make the blend more susceptible to enzyme hydrolysis attack but at least does not decrease its biodegradability.

The scanning electron images provided in Chapter Three add visual conviction to

the conclusions put forth in Chapter One.

3.5 References

1 Bower, D. I. *An introduction to Polymer Physics*; University Press: UK, 2002; p 444.

2 Brown, P. D.; Mcmullan, D.; Mulvey. T.; Smith. K. C. *Proc. R. Microsco. Soc.* **1996,** 21(32), 161.

3 Gabor, D. *Nature (London)* **1948,** 161, 777.

4 Kreuzer, H J.; Nakamura, K.; Wierzbicki, A.; Fink, H-W.; Schmid, H. *Ultramicroscopy*, **1992,** 45(3-4), 381.

5 Xu, W.; Jericho, M. H.; Meineitzhagen, I. A.; Kreuzer, H. J. *Cell Biol.* **2001,** 98(20), 11301

6 Owen, R. B.; Zozulya, A. A. *Opt. Eng.* **2000,** 39(8), 2187.

7 Xu, W.; Jericho, M. H.; Meineitzhagen, I. A.; Kreuzer, H. J. *Appl. Opt.* **2002,** 41, 5367.

8 Xu, W.; Jericho, M. H.; Meineitzhagen, I. A.; Kreuzer, H. J. *Opt. Lett.* **2003,** 28, 164.

9 Tsuji, H.; Smith, R.; Bonfield, W.; Ikada, Y. *J. Appl. Polym. Sci.* **2000,** 75, 629.

10 Zoppi, R. A.; Duek, E. A. R.; Coraca, D. C.; Barros, P. P. *Mater. Res.* **2001,** 4(2), 117.

11 Abe, H.; Kikkawa, Y.; Inoue, Y.; Doi, Y. *Biomacromolecules* **2001,** 2, 1007.

12 Iwata, T.; Doi, Y. *Macromolecules* **1998,** 31, 2461.

13 Kikkawa, Y.; Abe, H.; Iwata, T.; Inoue, Y.; Doi, Y. *Biomacromolecules* **2001,** 2, 940.

14 Fujita, M.; Doi, Y. *Biomacromolecules* **2003,** 4, 1301.

15 Singfield, KL. Saint Mary's University, Halifax, NS. Personal Communication, 2006.

Chapter Four: *A Critique of Non-Isothermal Crystallization Method*

4.1 Methods to Measure Spherulite Radial Growth Rate

Spherulite radial growth rate (G) is generally measured under isothermal crystallization conditions. The growth rate is determined at a certain crystallization temperature, T_c, from a plot of the measured radius of the spherulite (r) against the crystallization time (t). The value of G can be determined from the slope of this line.

$$G = \frac{dr}{dt} \qquad [4.1]$$

To obtain a crystallization profile of the polymer in question, the value of G obtained from the data collected from a large number of isothermal crystallization experiments is plotted against T_c. The apparent simplicity of [4.1] and the collective nature of the single crystallization profile of G versus T_c is an understated reflection of the necessary work involved in obtaining this important G vs. T_c crystallization profile. Each data point on a G vs. T_c bell-shaped crystallization profile plot is the result triplicate measurements of a total of at least 50 radial measurements on a single spherulite measured at 5 different times during a single isothermal crystallization; thus each point on a G vs. Tc plot results from at least 150 radial measurements. The G values are typically collected over a wide range of crystallization temperatures (*ca* 50 degrees). The labour-intensive reality of these measurements is one of the shortcomings of this type of study. A second shortcoming of this technique is related

to the limitations of the experiment itself. For many crystallizable polymers, the rate of nucleation increases so quickly with increasing undercooling that, due to the bloom of nuclei that almost instantly become impinged small spherulites, the reproducible measurement of radii and therefore of G at relatively lower crystallization temperatures is rendered difficult, if not impossible. Specifically, then, for many polymers a crystallization profile over the entire crystallization temperature range is not possible to be attained.

Chen and Chung[1,2] first proposed a different way to determine spherulite growth rate, with a view to address the shortcomings of isothermal crystallization measurements outline above. They based their approach on an alternate expression of equation [4.1],

$$G = \frac{dr}{dt} = \frac{dr}{dT}\frac{dT}{dt} \qquad [4.2]$$

where dT/dt is a constant cooling rate of a non-isothermal crystallization condition. The novel experiment involves the measurement of r as the spherulite grows under non-isothermal conditions. In this type of experiment, the sample is melted to remove any thermal history, as usual, but then it is subjected to a range of crystallization temperature using a selected constant cooling rate, instead of subjecting it to an isothermal crystallization temperature. A single experiment on a single sample, therefore, can provide information on the growth of the spherulite at the different crystallization temperatures as it experiences in a non-isothermal fashion. For the fixed cooling rate (dT/dt) crystallization run, the value of G at any temperature can be simply be calculated as long as the value of dr/dT is measured point-by-point

from the plot. Specifically, the raw data of a single experiment generates a plot of radius vs. T_c. This data is best-fit to a polynomial function. The derivative of this function is multiplied by the constant cooling rate and plotted against T_c to generate a plot of G vs. T_c, the familiar crystallization profile curve. The equation [4.2] therefore permits the acquisition of G at different T_c values over a rather broad range of T_c values within one *single*, dynamic experiment.

This new non-isothermal method has been further developed by Di Lorenzo *et al.* to expand the temperature region over which reproducible growth rate data can be measured, by means of a combination of varying cooling rates and self-nucleation techniques.[3-6]

4.2 Published Accounts of the Non-Isothermal Crystallization Method

Since this non-isothermal measurement of G has been suggested, several polymers and polymer blends have been investigated by this novel method. Poly(ether ether ketone) (PEEK) was subject to analysis in this fashion over the temperature range of 266°C – 308°C, which is in the range above the temperature of maximum G on its bell-shaped crystallization profile plot of G vs. T_c. The results are comparable with those obtained by the conventional isothermal way.[2] The spherulite growth rates of isotactic polypropylene/poly(α-pinene) blend have also been reported to have been successfully measured during cooling from the melt state using the non-isothermal method and these results demonstrated great agreement with that measured isothermally.[3] Recently, spherulite growth rates of PLLA were measured

by a combination of both isothermal and non-isothermal procedures and the results fit the expected outline of the whole bell-shape crystallization profile G vs. T_c plot.[4] The non-conventional method provided G data for crystallization temperatures that extended well beyond the lower T_c limit usually reported in the literature. Data was reported for crystallization temperatures as low as 85 °C, corresponding to an undercooling of about 95 °C. The results agree with an extension of the G vs. T_c function obtained at both higher T_c and lower T_c using the conventional and self-nucleation isothermal method, respectively. [4-6]

Other polymer systems which have been studied in this fashion include some polypropylene based poly(vinyl butyral)) blends,[7] a random ethylene-propylene copolymer,[8] polypropylene-based resins,[9-12] nylon12-12,[13] a high density polyethylene,[14] poly(trimethylene terephthalate),[15] and poly(3-hydroxypropionate).[16] In all of these reported studies there was good agreement between the results from both the isothermal and non-isothermal modes of experiment.

4.3 Experimental

Pure PLLA and a blend of 50/50 wt% PEO/PLLA were used for the investigation. The polymers were studied as thin-film samples pressed between glass coverslips, as detailed previous in the experimental section of Chapter Two. The same polarized light microscope assembly was used in these experiments and the same temperature-controlled hotstage was used as detailed in Chapter Two. The sample thickness was maintained at 14-16 μm and the cooling rate was constant at 2 °C

/minute. This slow cooling rate was applied to minimize any possible thermal lags with the non-isothermal method. In addition, all measurements were taken in the crystallization temperature range 160 °C to 130 °C, where measurements are most reproducible and readily measured. A self-nucleation, or self-seeding technique[4] was used in order to form nuclei over a suitable time scale at the chosen crystallization temperature. The samples were melted at 200 °C for 1 minute to remove any thermal history. The sample was then cooled quickly in the same hotstage to the self-seeding temperature and held there until a bright spot in the field of view indicated nucleation (*ca* 2 minutes). The sample was then quickly heated to the start temperature of the non-isothermal crystallization run and then the controlled slow cool ensued. The specific seeding and start temperatures are indicated in the text accompanying the figures containing the results.

An image analysis software program (SigmaPro) was used to analyze the digitized polarized light micrographs taken at regular intervals during the controlled cool. The spherulite radius value was taken as an average of 8-10 measurements on a single spherulite. The spherulite radius (r) was plotted against temperature (T), and the data was fit to a polynomial function. The orders of the polynomial function were varied from 2 to 5 for each sample.

For comparison, isothermal growth rate measurements were also performed at temperatures of 132 °C, 135 °C, 140 °C, 145 °C, 150 °C, 155 °C and 159 °C. In each case, the image of the growing spherulite was recorded at not less than five regular time intervals and an average value of radius was obtained at each interval.

The slope of r against t was used to determine G.

4.4 Results and Discussion

Figure 4.1 contains representative images of the spherulites during the new non-isothermal crystallization for both the pure PLLA and the blend sample.

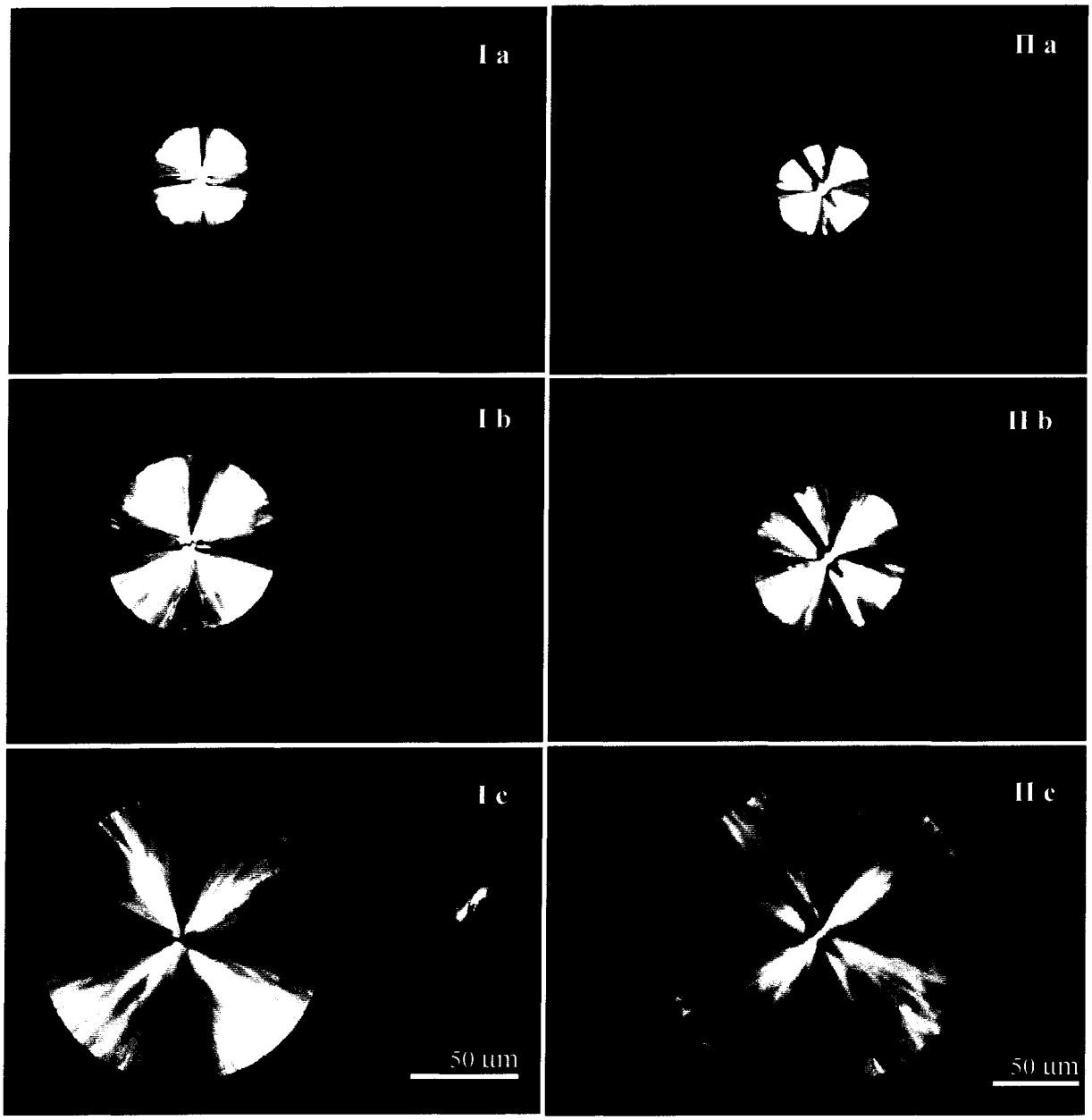

Group I **Group II**

Figure 4.1: Polarized light optical micrographs showing the spherulitic growth of PLLA (Group I) and 50 wt% PEO/PLLA blend (Group II), at (a) 155 °C, (b) 145 °C, and (c) 135 °C from the dynamic crystallization experiment at a cooling rate of 2 °C/min. The scale bar represents 50 μm.

In group I, the pure PLLA spherulite is imaged in (a), (b) and (c) during a single non-isothermal experiment at 155 °C, 145 °C, and 135 °C, respectively. In group II, the corresponding images of the 50/50 PEO/PLLA blend spherulite are shown. During cooling at 2 °C/min from melt, the number of nuclei in the sample field increased over the dynamic crystallization period. Nevertheless, the temperature range over which this experiment was performed was strategically chosen to minimize this problem and allow to the measure of radius before spherulite impingement.

The value of the average spherulite radius of pure PLLA during non-isothermal experiment was plotted as a function of temperature, and the data was curve-fit as shown in Figure 4.2.

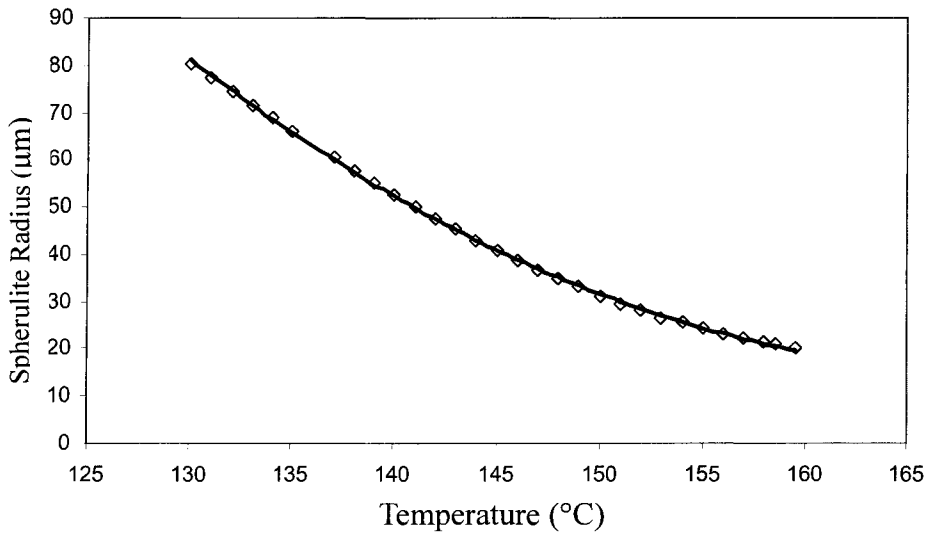

Figure 4.2: PLLA spherulite radius as a function of temperature during a single non-isothermal crystallization experiment, using at a cooling rate of 2 °C/min. Points are raw data and line is fit to a polynomial.

The polynomial function to which the data is fit was selected with order of 2, 3, 4, and 5. There was no significant difference in the values of the correlation coefficients among the fits of different order and all appeared the same as that shown in figure 4.2. The functions manifested their differences however upon taking the

first derivative. The first derivative was calculated accordingly. Taking into account the 2 °C cooling rate, G value was determined according to Equation [4.2]. Polynomial functions with order of 4 and 5 returned negative values for G, and they were manually converted back to be positive. The four plots in Figure 4.3 show the calculated isothermal growth rates by non-isothermal experiments using the original fits of different order. The seven data points (without fit) from isothermal runs are included in each plot for comparison to the blend. The caption for Figure 4.3 is below and the plots are spread over more than one page.

Figure 4.3: Plots of derived spherulite radial growth rate against temperature for the non-isothermal crystallization of PLLA at a cooling rate of 2 °C/min. Order of polynomial function used to fit original data is (a) 2; (b) 3; (c) 4; and (d) 5. Hollow symbols are non-isothermal experimental data fitted in solid lines; solid diamonds are isothermal experiment data for comparison.

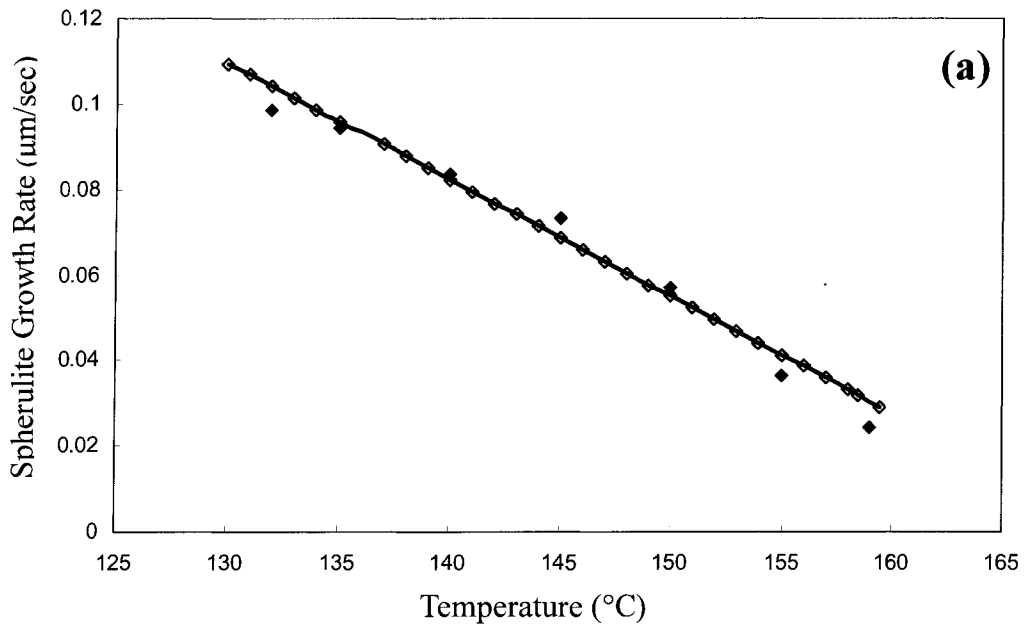

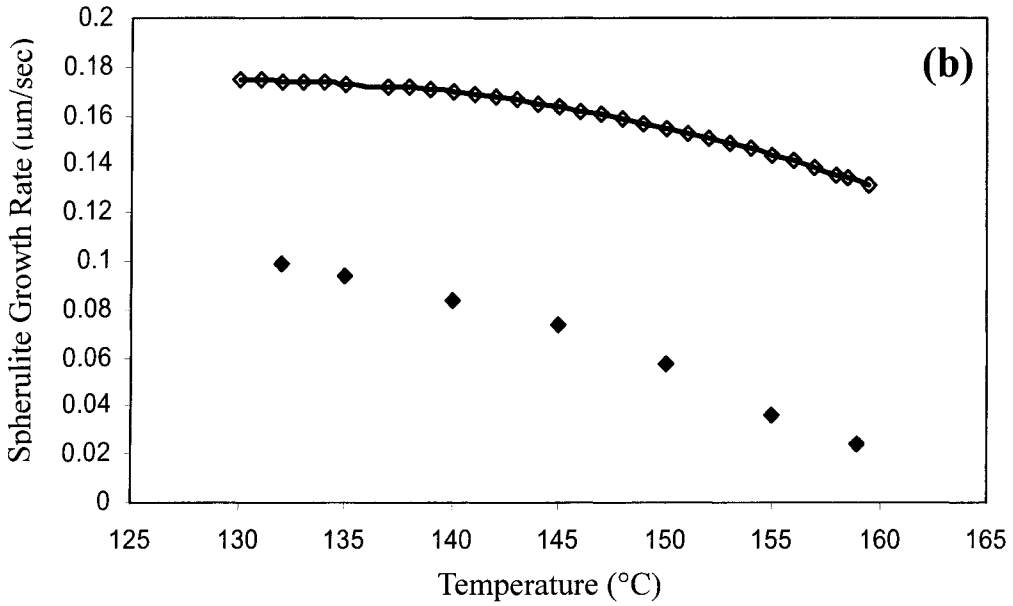

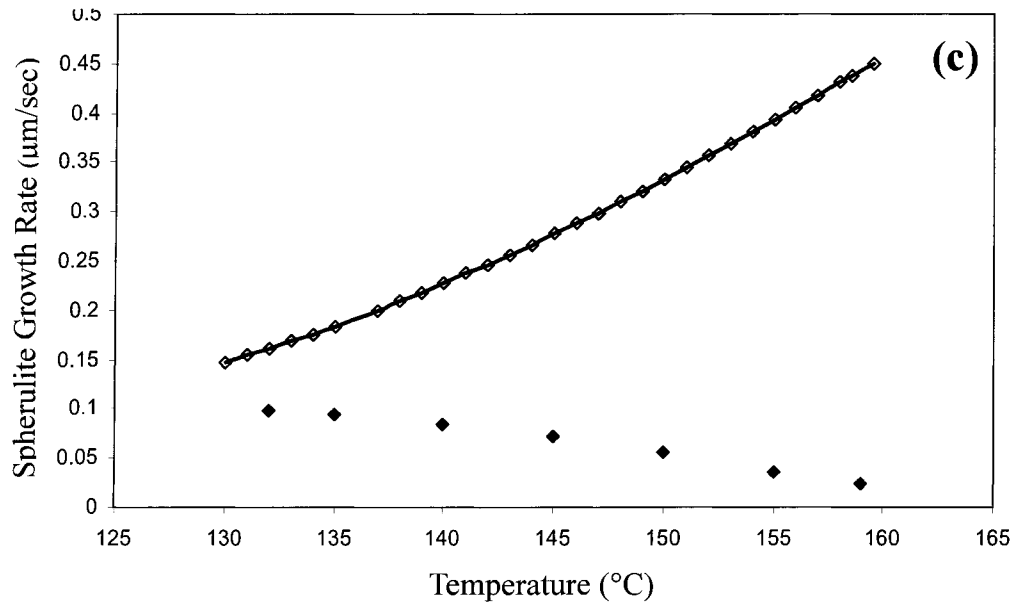

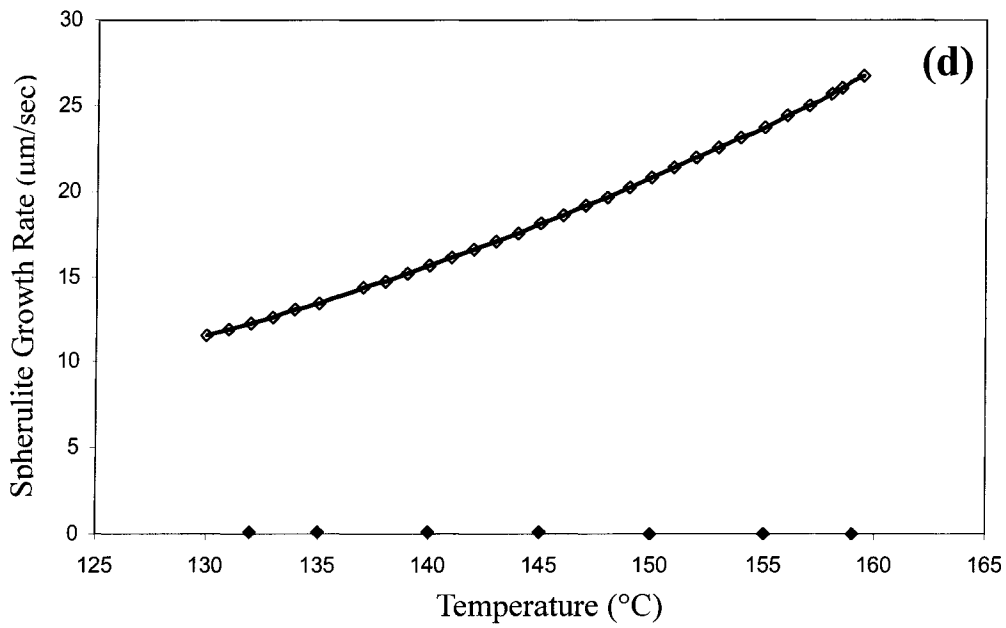

It is obvious that the resultant growth rate from different equation orders are quite different and only the second order dynamic equation curve is comparable with data from isothermal experiments. Similar comparison experiments were carried out for the 50 wt% PEO/PLLA blend, and results were analogously treated and are demonstrated in Figures 4.4 and 4.5.

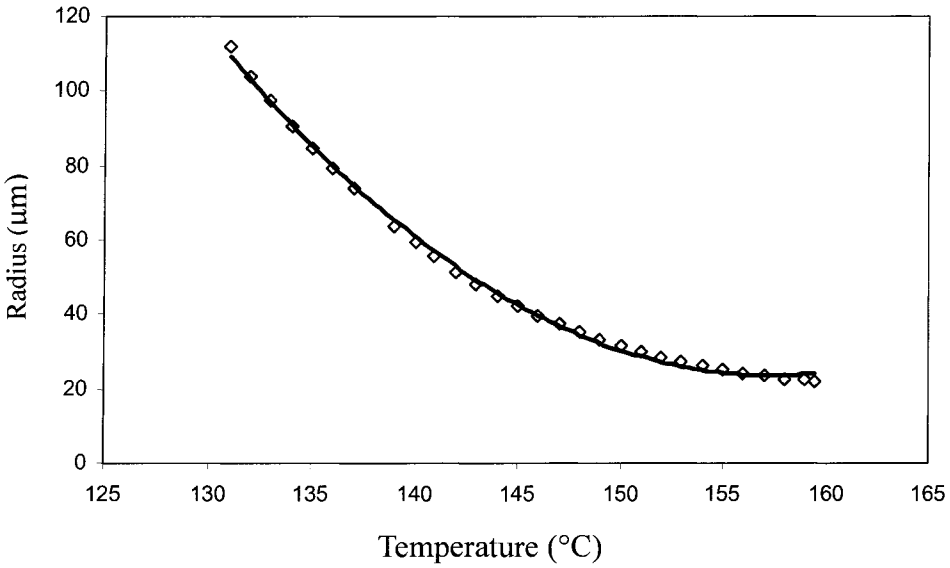

Figure 4.4: 50 wt% PEO/PLLA blend spherulite radius as a function of temperature during a single non-isothermal crystallization experiment, using at a cooling rate of 2 °C/min. Points are raw data and line is fit to a polynomial.

Once again, the caption for the Figure 4.5 is placed before the series of plots A through D which are spread over more than one page.

Figure 4.5: Plots of derived spherulite radial growth rate against temperature for the non-isothermal crystallization of 50 wt% PEO/PLLA blend sample at a cooling rate of 2 °C/min. Order of polynomial function used to fit original data is (a) 2; (b) 3; (c) 4; and (d) 5. Hollow symbols are non-isothermal experimental data fitted in solid lines; solid diamonds are isothermal experiment data for comparison.

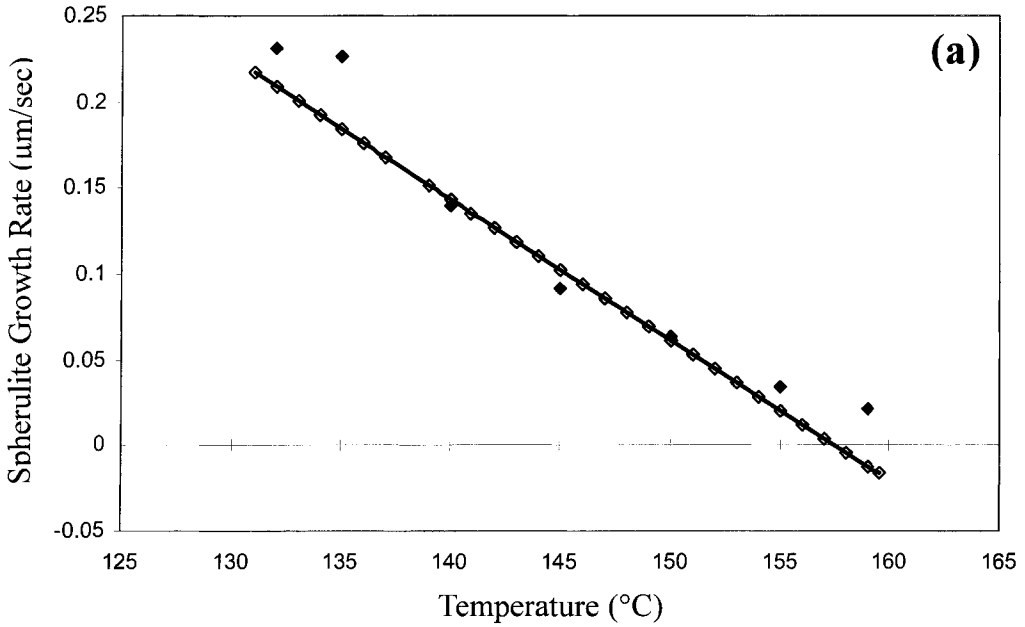

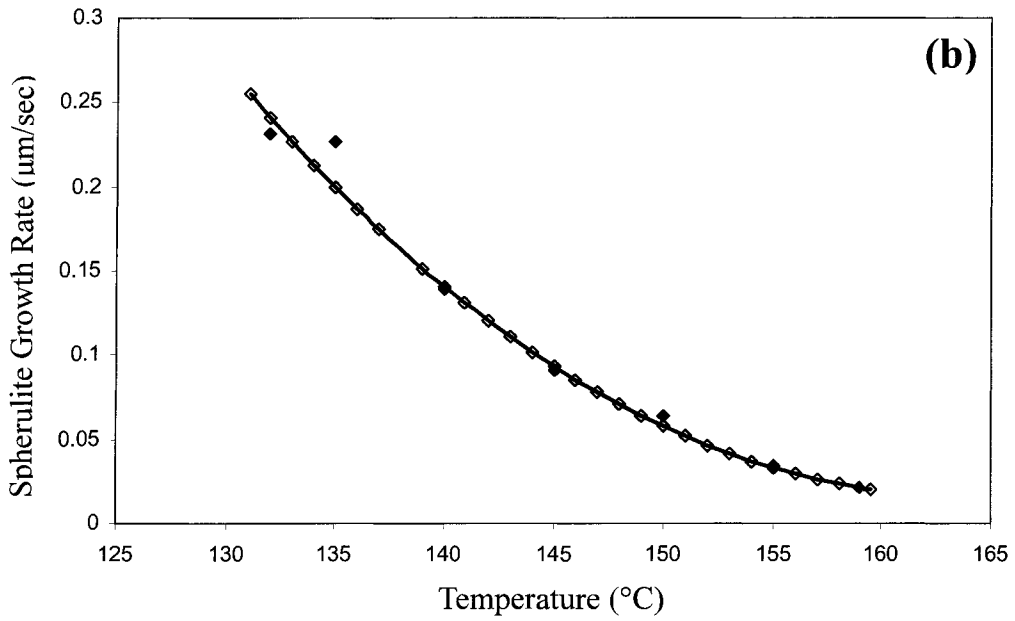

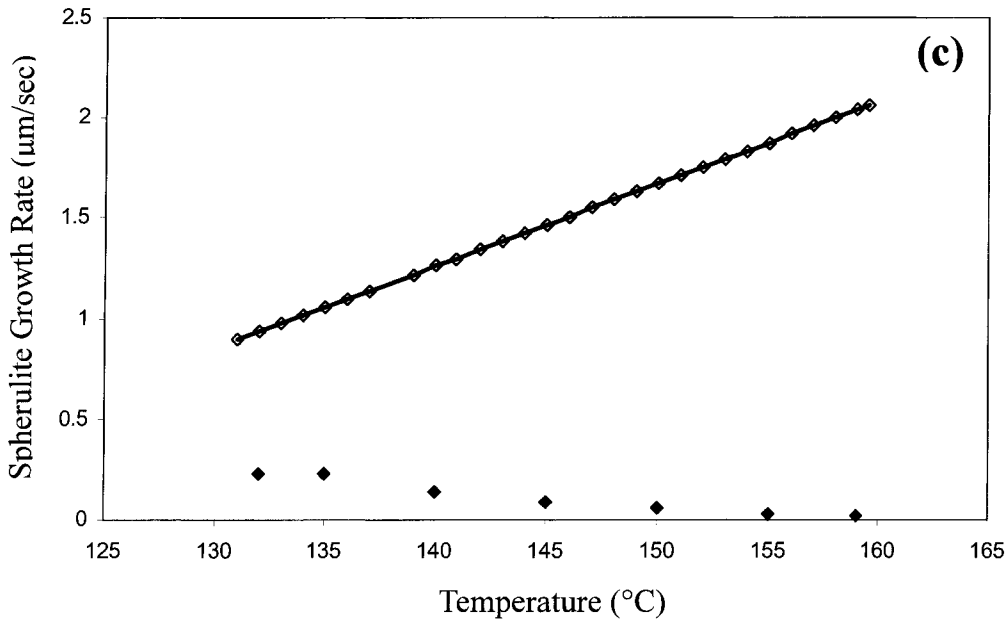

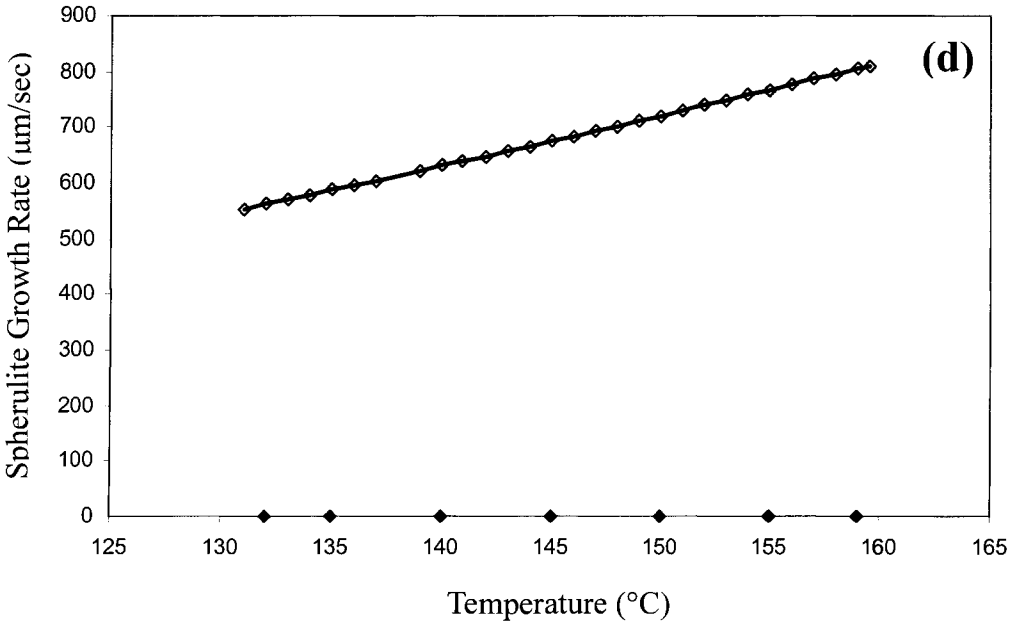

For the growth rate of this blend, the third order dynamic equation curve best fits the data from the isothermal mode.

The relatively new proposed non-isothermal approach is reported to have solved the deficiencies of the isothermal method, such as the excessive time required to do the experiments and the restriction on the range of undercoolings that can be investigated. Specifically, when coupled with a self-seeding technique, it can overcome the limitations of low T_c data gathering. However, it is not a perfect substitute.

While the sample is cooling down, the temperature displayed by the thermal controlling unit is not necessarily in phase with the actual temperature of the sample, and this effect will be exacerbated at higher cooling rates. There can also arise thermal gradients within the polymer thin-film sample itself. In addition, since crystallization is an exothermic process, the generated heat during phase transition may develop local heating and complicate any thermal gradients already present. If an inappropriate cooling rate is chosen, the excess heat evolved from solidification

may even cause a temperature plateau. All of these factors may bring on a thermal lag in the system such that the actual temperature at which transitions occur will not be consistent with that detected by the instrument. This is very significant because it is well known that the value of G varies significantly over one degree of undercooling.

The above citations have been deemed successful applications of the non-isothermal method in part because they compare well to the conventional method results. However, in each case, the conventional results did not present any anomalies in the expected bell-shaped function of G vs. T_c. It is important to note that any subtle yet important features of the growth rate dependence on T_c might be missed upon investigation using the non-isothermal method. An important example of this is the PLLA system. It has been reported that PLLA presents a second maximum in G at a lower T_c than that of the symmetrical maximum of the curve.[17,18] The origin of this anomaly in the crystallization profile of PLLA is not known. Interestingly, the temperature region over which this maximum occurs was omitted from the reported non-isothermal PLLA growth rate study by Di Lorenzo.

In a second criticism of this novel method, the data treatment step of fitting the raw data of r vs. T_c to a polynomial is rather ambiguous. Functions of different order can give suitable fits to the raw data. However, the effect of varying the order of this initial fit is to give distinctly different growth rate curves in the end. The determination of the order of the equation seems to be arbitrary.

4.5 Conclusion

Overall, it has been found that growth rate values from non-isothermal method heavily depend on the chosen order of the equation. In addition to this rather arbitrary assignment of order, there does not seem to be any logical explanation for the negative result for growth rate deduced from this dynamic experiment data treatment. The unit chosen for temperature is crucial, as Kelvin units for T will generate different derivative value from those obtained using temperature units of centigrade. It is important that the experimenter realize that while the application of the non-isothermal crystallization method to determine the growth rate crystallization profile is a quick alternative, there is an apparent trade-off between precision and accuracy and speed of experiment. The method may offer a useful idea of the range and magnitude of the growth rates at different temperatures in general, but the information gained would not be appropriate for the careful deduction of crystallization parameters. When the method is applied it is clear that it needs to be performed with care to avoid possible false results.

4.6 References

[1] Chung, C. T.; Chen, M. *Polym. Prepr. (Am. Chem. Soc. Div. Polym. Chem.)* **1992,** 33, 420.

[2] Chen, M.; Chung, C. T. *J. Polym. Sci., Polym. Phys.* **1998,** 36, 2393.

[3] Di Lorenzo, M. L.; Cimmino, S.; Silvestre, C. *Macromolecules* **2000,** 33, 3828.

[4] Di Lorenzo, M. L. *Polymer* **2001,** 42, 9441.

[5] Di Lorenzo, M. L.; Silvestre, C. *Thermochimi. Acta* **2003,** 36, 67.

[6] Di Lorenzo, M. L. *Prog. Polym. Sci.* **2003,** 28, 663.

[7] Cascone, E. ; David, D. J.; Di Lorenzo, M. L.; Karasz, F. E.; Macknight, W. J. ; Martuscelli, E.; Raimo, M. *J. Appl. Polym. Sci.* **2001,** 82(12), 2934.

[8] Silvestre, C.; Cimmino, S.; Triolo, R. *J. Polym. Sci.,-Polym. Phys.* **2003,** 41(5), 493.
[9] Silvestre C.; Cimmino, S.; Pirozzi, B. *Polymer* **2003,** 44(15), 4273.
[10] Bing, Na.; Wang, Y.; Zhang, Q.; Fu, Q. *Polymer* **2004,** 45(18), 6245.
[11] Zheng, Q.; Shangguan, Y.; Yan, S.; Song, Y.; Peng, M.; Zhang, Q. *Polymer* **2005,** 46(9), 3163.
[12] Silvestre, C.; Cimmino, S.; Lin, J. S. *J. Polym. Sci., Polym. Phys.* **2004,** 42 (18), 3368.
[13] Ren, MQ. ; Mo, ZS. ; Chen, QY. ; Song, JB. ; Wang, SY. ; Zhang, HF. ; Zhao, QX. *Polymer* **2004,** 45(10), 3511.
[14] Tjong, S. C.; Bao, S. P. *J. Polym. Sci., Polym. Phys.* **2004,** 43(3), 253.
[15] Chen, K.; Tang, X. Z.; Shen, J.; Zhou, Y.; Zhang, B. *Macromol. Mater. Eng.* **2004,** 289, 539.
[16] Zhu, B.; He, Y.; Asakawa, N.; Yoshie, N.; Nishida, H.; Inoue, Y. *Macromolecules,* **2005,** 38(15), 6455.
[17] Di Lorenzo, M. L. *Eur. Polym. J.* **2005,** 41, 569.
[18] Hoogsteen, W.; Postema, A. R.; Pennings, A. J.; Ten Brinke, G.; Zugenmaier, P. *Macromolecules* **1990**, 23, 634.

Chapter Five: *General Conclusions & Future Directions*

5.1 General Conclusions

The relatively amorphous portions of PLLA are preferentially attacked when subjected to enzymatic degradation medium. Spherulites grown under non-isothermal cooling conditions following incomplete isothermal crystallization present such preferred, relatively amorphous material. While the fold surfaces of PLLA lamellae represent relatively amorphous regions in the internal structure of the spherulite, the enzyme does not easily penetrate the spherulite under the conditions studied. However, physical cracks in the spherulites allow entry of the enzyme into the spherulites at these locations. While it is widely accepted that polymer spherulites undergo a process of partial melting and recrystallization when exposed to the anneal-type conditions of a slow heating process, there is no conclusive effect of enzyme exposure on the ability of the polymer to incorporate the loops and chain ends of the fold surface into its lamellae in this reorganization process. The lack of any observable effect is either due to the lack of sensitivity of the DLI method for this purpose, or, that the enzyme has not reached this level of the spherulite to render these loops and chain ends unable to reorganize. Nevertheless, the acquired results support what has been reported: (i) the amorphous region of inter-spherulitic is easier to be attacked by enzyme than that of inter-lamellar; (ii) Degradation is hindered above a

critical degree of crystallinity.

The effect of increasing weight ratio of PEO on the spherulite radial growth rate of the PLLA is to significantly increase the growth rate. This is due to the increased chain mobility in the miscible blend melt. The extra chain mobility comes about from the combination of the PLLA with the very flexible (low T_g) polymer, PEO. However, this effect is counteracted by a dilution of crystallizable material at the PLLA crystallization temperature when PEO is present in *ca* 90 wt%. At this level of blending, the growth rate of PLA is finally lower than that in the pure state, at the crystallization temperatures investigated.

The effect of PEO component in the blend material with PLLA was to modify the internal lamellar organization of the PLLA in the blend system. The blending of PEO in PLLA technically 'opens up' the PLLA spherulite, the degree to which depends on the amount of PEO. The monitoring of the depolarized light intensity of the thin-film samples during the phase transitions (i.e., crystallization and melting) of the PEO/PLLA blend systems demonstrated different phase behaviour among three distinct blend groups: Group (i) with PEO between 10 and 20 wt%; Group (ii) with PEO between 30-50 wt%; and Group (iii) with > 50 wt% PEO component. From the DLI cooling and the subsequently melting profiles, the three groups can be further described: (i) 10 wt% - 20 wt% PEO cannot form any order in the binary blend; (ii) 30 wt% - 50 wt% PEO is able to form some order but not enough to develop spherulitic crystals; (iii) 60 wt% - 90 wt% PEO can form spherulites. Based on these three groups and visual observation under PLOM, two lamellar growth mechanisms were

suggested, and they are edge-on and flat-on of PLLA lamella in group (ii) and group (iii), respectively.

SEM photographs confirmed the formation of different degree of order PEO in those three groups with respect to blend composition. Both the *ex situ* SEM and *in situ* PLOM observations add visual conviction to the proposed lamellar orientations.

The use of the physical property of viscosity as a means to measure the effects of degradation may be a useful one. However, the application is complicated in this particular blend case as the PEO is water soluble and the effects of swelling are difficult to distinguish from the effects of viscosity due to chain length. It can be useful as a complementary tool for purpose of this thesis study but not a good independent technique for quantitative degradation work.

The application of the non-isothermal crystallization method to determine the growth rate crystallization profile is a quick alternative of the traditional isothermal method. However, there is an apparent trade-off between precision and accuracy and speed of experiment. It therefore needs caution to perform so as to avoid possible false results.

This work is unique in suggesting and collectively providing convincing evidence for the three groups of PEO/PLLA blends as distinguished by their composition, crystallization behaviour, melting behaviour, degradation behaviour, and morphology. The extension of this idea to the level internal lamellar organization is also a new idea that is presented first in this work. These two suggestions are a useful contribution to the understanding of both the fundamental phase behaviour of crystallizable polymers

and their blends, and to the specific phase behaviour of PLLA and PEO/PLLA industrially important blend.

5.2 Future Directions

5.2.1 Cracks, Bands and Rings

During the course of this thesis, including time spent reading the relevant literature emerging in the last year, it is reasonable to report that PLLA manifests different types of radial and circumferential morphological features often referred to as cracks, or bands, and sometimes, rings. It is important to first differentiate between those observed *physical breaks* in the spherulite and other ring or banding patterns which are due to a periodic birefringence extinction *optical pattern.* The latter is commonly referred to as birefringence banding and is a common observation in spherulites of many different polymers. Only in the last year has there been a report in the literature on the observation of so-called banded spherulites in PLLA.[1] This feature was not observed on PLLA spherulites in this study and further discussion on this matter is beyond the intended scope of this thesis work.

The related morphological features that were in fact observed during the course of this thesis work on PLLA include *radial cracking* in the PEO/PLLA blend spherulites that was explained in terms of the release of inter-lamellar PEO during a washout procedure. Some release of PEO from the inter-spherulitic spaces most likely also contributed to the appearance of some peripheral cracking in these systems. It is concluded that this type of cracking is a function of the presence of PEO in the sample

and is unique to the blend system. Another such feature includes the *random shatter cracking* of the glassy-state pure PLLA and PEO/PLLA blend groups (i) and (ii) spherulites which occurred after quenching the samples in liquid nitrogen. The melt and miscible blend melts, respectively, could be successfully quenched to the glassy state this way. Many commodity thermoplastics possess a T_g lower than room temperature. The T_g of PLLA is around 60 °C and therefore significantly above room temperature. It may simply be the case that many polymers shatter when quenched-cooled to below their T_g but this is a significant feature in the case of PLLA since it is at this 'low' temperature that it needs to be a functional material with desired properties. Finally, the most intriguing type of cracking occurred as periodic, almost perfectly concentric, *rings* on the surface of the pure PLLA spherulites, with a very regular spacing. Also less than one year ago, a paper on this very subject was published, reporting that these rings are indeed deep physical cracks where the lamellae are severed, but which can actually heal in a thermoreversible way across the T_g of the polymer.[2] They reported that they are not likely to be related to the regular birefringence extinction bands but are more likely to be attributed to the general internal stresses generated upon cooling. This paper is commented on in a more detailed fashion in the context of the observations made in this thesis work in a following paragraph.

In this thesis work it was discovered that some concentric rings appeared on the spherulites upon cooling the thin-film samples down to room temperature after being crystallized isothermally at moderately high crystallization temperatures until the

spherulites grew to a significant diameter. The spherulites shown in Figure 5.1 are examples of the observed phenomenon and each have a thermal history of being crystallized at 147 °C for 80 minutes.

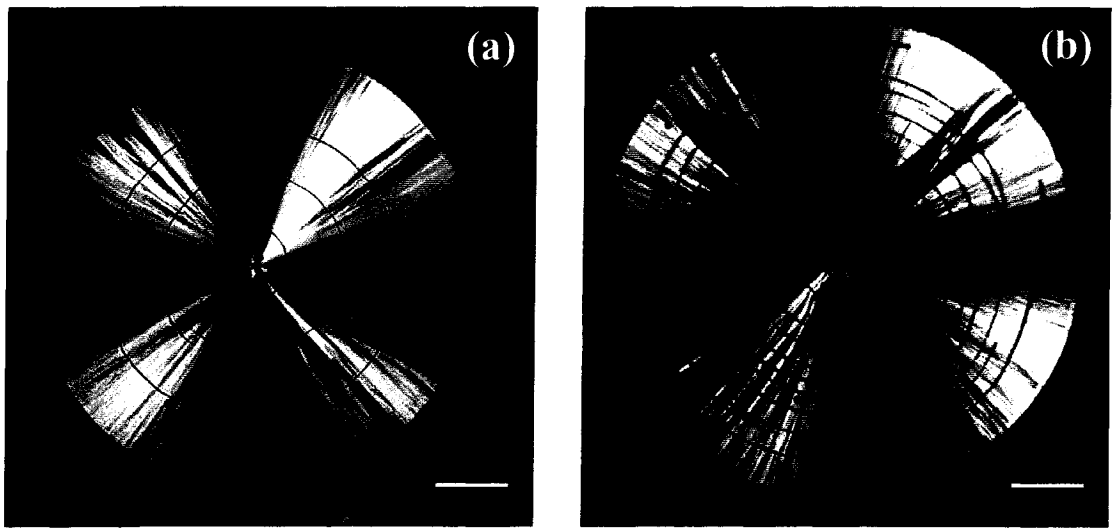

Figure 5.1: Polarized light optical micrographs of PLLA showing the appearance of physical cracks in the spherulites. Both samples crystallized at 147 °C for 80 min. Image taken at (a) room temperature following crystallization; and (b) after 3 hours enzymatic degradation at 37 °C. Scale bar =100 μm.

The image in (a) was recorded after the sample had cooled down to room temperature; and the image in (b) was recorded after the sample had been exposed to enzymatic degradation solution for three hours. These rings are regularly distributed and seem superimposed on the surface of the spherulites, running tangentially to the spherulite radius. Interestingly, many more cracks appeared after an 80-minute degradation period, as shown in Figure 5.1(b). In other words, the 80-minute enzyme immersion created more centric ring cracks. This phenomenon can be interpreted by degradation. It is easier for enzyme to approach and chop up areas that have already been cracked.

In the paper referred to earlier on the same subject,[2] the authors made a thorough study on this phenomenon, and reported the rings as physical cracks, and that they arise due to the differences in thermal expansion coefficient between the PLA polymer and its substrate. They reported that this phenomenon was only witnessed for PLA samples grown restrained between two glass cover slips. In that study, AFM was used to demonstrate that the cracks observed were indeed physical breaks about 300 nm in width. They were found to first appear upon cooling the thin-film sample to around its T_g and to continue to appear if the sample was cooled to even lower temperatures. The onset and number of cracks, along with the crack spacing were all correlated with crystallization temperature. No cracks were observed to form in samples that had been crystallized below 110 °C and the absence of the phenomenon was attributed to the small size of the spherulites attained at that temperature due to the high rate of nucleation.

In this study, the same type of spherulite cracks were also observed in PLLA thin-film samples that were grown unrestrained, that is, without a top coverslip. This is in contrast to the above reported findings in which they report that cracks were not seen in open-face samples. Also, the reported temperature range over which cracks were reported to be observed in the earlier study (*ca* 110 – 140 °C) is different than the temperature range over which cracks were observed in the samples in this thesis (*ca* 130 – 147 °C). It is suggested that this phenomenon be subject to further study.

If these are indeed physical cracks that appear in both unrestrained and restrained growth then they must be occurring at the weak points of the lamellae. It is

reasonable to consider that the cracks are weak points where the lamellae succumbed to the internal stresses in the local, nonisotropic lamella (as opposed to the whole spherulite) upon cooling below the glass transition temperature. It now becomes pertinent to query why there might be regular weak points in the lamellae. It is reasonable to further state that any periodic weak points in the lamellae are a reflection of how the lamellae originally grew, perhaps via a type of periodic or rhythmic growth mechanism. For these reasons, it would be most interesting therefore to investigate the source of these regularly-spaced weak points along the lamellae. Perhaps the results of such a systematic investigation could shed light on the refinement of the classical nucleation and growth model of lamellar growth which needs to be challenged as our methods of investigation become more sophisticated. Perhaps the answers would be related to the other issue which has currently experienced its resurgence in debate in the literature: the cause of the regularly-changing orientation in the lamellae leading to the appearance of a similar birefringence extinction ring pattern among spherulites in other types of polymers. It would be very important to control the thin-film sample thickness in any study of this kind, as well as to keep the molecular weight of the polymer constant. Both sample thickness and molecular weight may contribute to the main differences found between the findings of the recent study on PLLA and the observations made in this thesis: The thin film samples in the Fraschini *et al.* study were 100 microns thick while those of this study were maintained at 8-15 μm in this study; the molecular weights were 16 800 in the other study but 50 000 in this thesis work. This latter difference in

material might be related to the different conditions under which cracks formed in the spherulites of the different systems.

Not only is it important to consider sample thickness among different thin-film samples as a controlled variable in these morphology and kinetics studies, but also to consider the possible variance in thickness within a single thin-film sample. It is quite possible, given the significant relative viscosity of some polymer melts, that there is a variation of sample thickness in a single sample and that the variance is significant because it is of the order of the dimension of the growing three-dimensional crystal. It is wise of the experimenter to avoid using observations of edge effects as representative of the whole sample. The images selected for Figure 5.2 illustrate this point. Figure 5.2 shows two PLOM micrographs in the same sample, with the spherulite in (b) formed at the edge of thin-film sample.

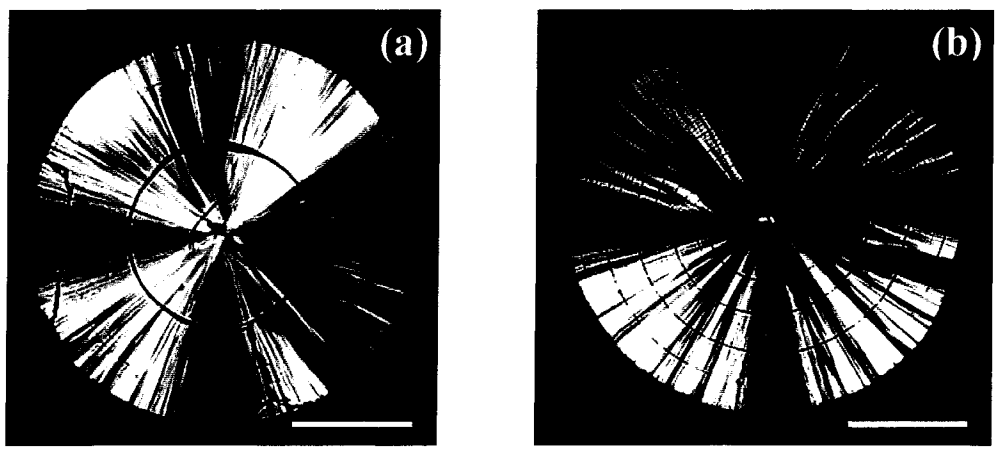

Figure 5.2: Polarized light optical micrographs of 10/90 wt% PEO/PLLA sample crystallized at 140 °C for 15 min, and then quenched in liquid N_2. Images recorded of the same sample at room temperature (a) in the center of the sample and (b) at edge of the sample. Scale bar = 100 μm.

5.2.2 Further Investigation of the Morphology of PLA and its Blends

The 50 wt% PEO blend sample from Figure 3.12(c) was left on the bench for three months and subsequently examined by SEM. The resultant scanning electron micrograph is shown in Figure 5.3. The sample is evidently not in the best condition with crystalline fragments throughout. However, it can easily be seen that there are small spherical entities in the sample and that two distinct morphologies of them are observed.

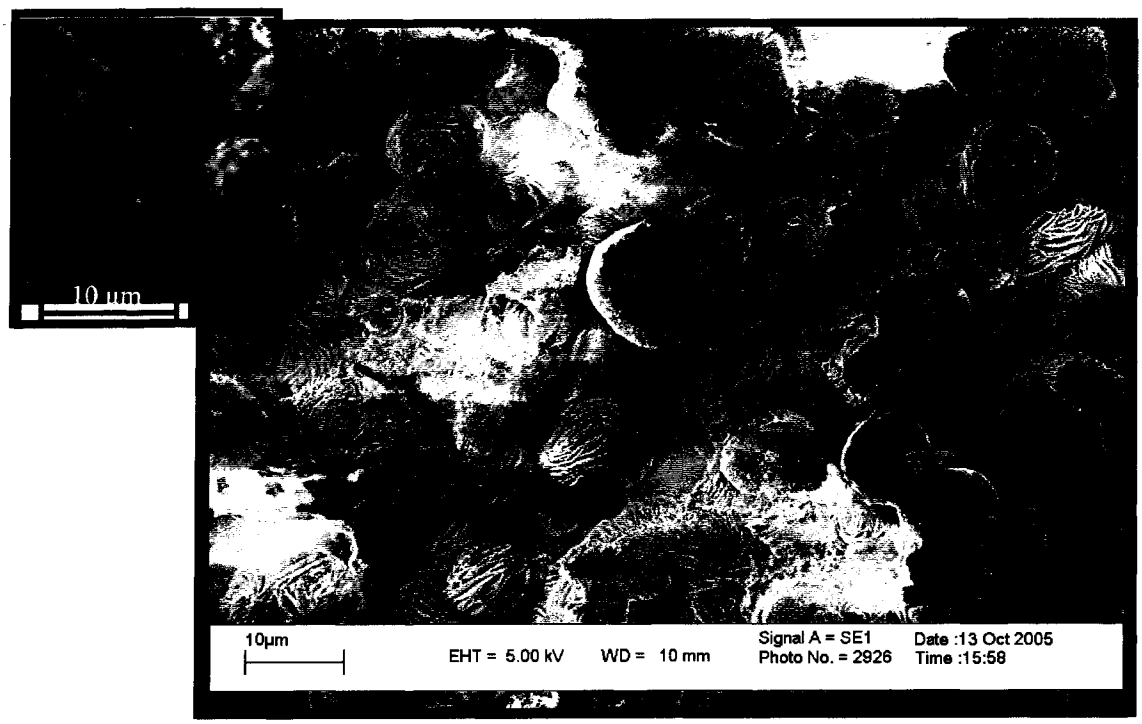

Figure 5.3: SEM micrographs of 50 wt% PEO/PLLA blend crystallized at 150 °C for 60 min with a previous 2-minute seeding at 140 °C, and then cooled very fast to room temperature. This thin film sample was subsequently immersed in enzyme buffer solution for 15 minutes and then dried. Insert is taken immediately after drying; large image taken after a further 3-month standing on bench.

One type shows a flattened top that is generally smooth but upon closer inspection possesses tiny pock marks on its surface. A second type has a multilayer structure.

The former type with little pock marks has been attributed to the effect of degradation of PLLA spherulite, as discussed previously in Chapter Three. The multilayer structure was actually evident before the 3-month period. One of this type of spherulite can be seen in the inset image taken from previously shown Figure 3.12(c). It is seen near the edge of a large spherulite and it has apparently only just nucleated and begun to grow.

It is interesting to see two rather different morphologies of PLLA spherulites in the blend have been developed under the same conditions with the presence of enzyme. The layered-looking small spherulites are very similar to some presented in the SEM micrographs of a recent publication by Tsuji et al.[3] In that study, it was reported that the spherulites were composed of a racemic mixture of PDLA and PLLA chains. The racemic mixture was at the level of the unit cell (i.e., stereocomplexation). Therefore, two possibilities are proposed to account for the sighting of this type of crystal in the present thesis work. First, the effect of enzyme transforms some spherulites of the flat type morphology to that of the multilayer morphology, that is, enzyme made some PDLA from PLLA to get stereocomplex polymer spherulites. The conditions upon which this transformation could happen must be critical and therefore need to be investigated.

The second possibility is related to the observation that the layered type of spherulite is the same as that layered type of spherulite in the inset image and that it has obviously only nucleated near the end of the crystallization process. It is proposed that perhaps there was a trace of PDLA in the commercial PLLA to start

with. If this was true, it may have been rejected from the growth front of the optically-pure spherulite until its concentration would build-up near the periphery and after a time would finally nucleate and grow, producing small spherulites near the edge of pure PLLA spherulites. If this is the case, then the unusual observation of the second maximum in the growth rate curve of PLLA might also be reconciled by this 'impurity' in the sample. As stated in 1.4.1.2, the plotting of crystallization rates (G) with respect to crystallization temperatures (T_c) does not have a common bell-shape curve as for most of other polymers. Instead, a second, even higher peak was evident at T_c lower than that of where the reported maximum G occurs. This second bump might be a separate, superimposed growth rate curve of the stereocomplex spherulite, which has been reported in the literature to nucleate later. A systematic investigation of the effect of PDLA on an otherwise pure PLLA sample is warranted.

5.2.3 Characterization of T_g by Total Depolarized Light Intensity

In this work, total depolarized light intensity had been used to investigate the bulk thermal and crystallization behaviour of quenched PLLA thin-film samples. A pure PLLA thin-film sample was prepared as described previously between two glass cover slips and was melted at 200 °C for 1 min to erase its thermal history, followed by quenching in liquid nitrogen to obtain the polymer glass. Light intensity was recorded subsequently upon heating different quenched samples at different rates until the sample had totally melted. The thickness of polymer thin film was in a range of 8-15 μm and heating rates were chosen of 20 °C/min, 10 °C/min, 5 °C/min, 2 °C/min

and 1 °C/min, respectively.

During the heating run of a melt-quenched thin-film PLLA sample, the light intensity profile shown in Figure 5.4 was attained. Surprisingly, there was a significant change step in the baseline light transmittance at a temperature of about 47 °C. It would appear that the light intensity shift is indicating the glass transition temperature of the sample, which has not been reported in the literature.

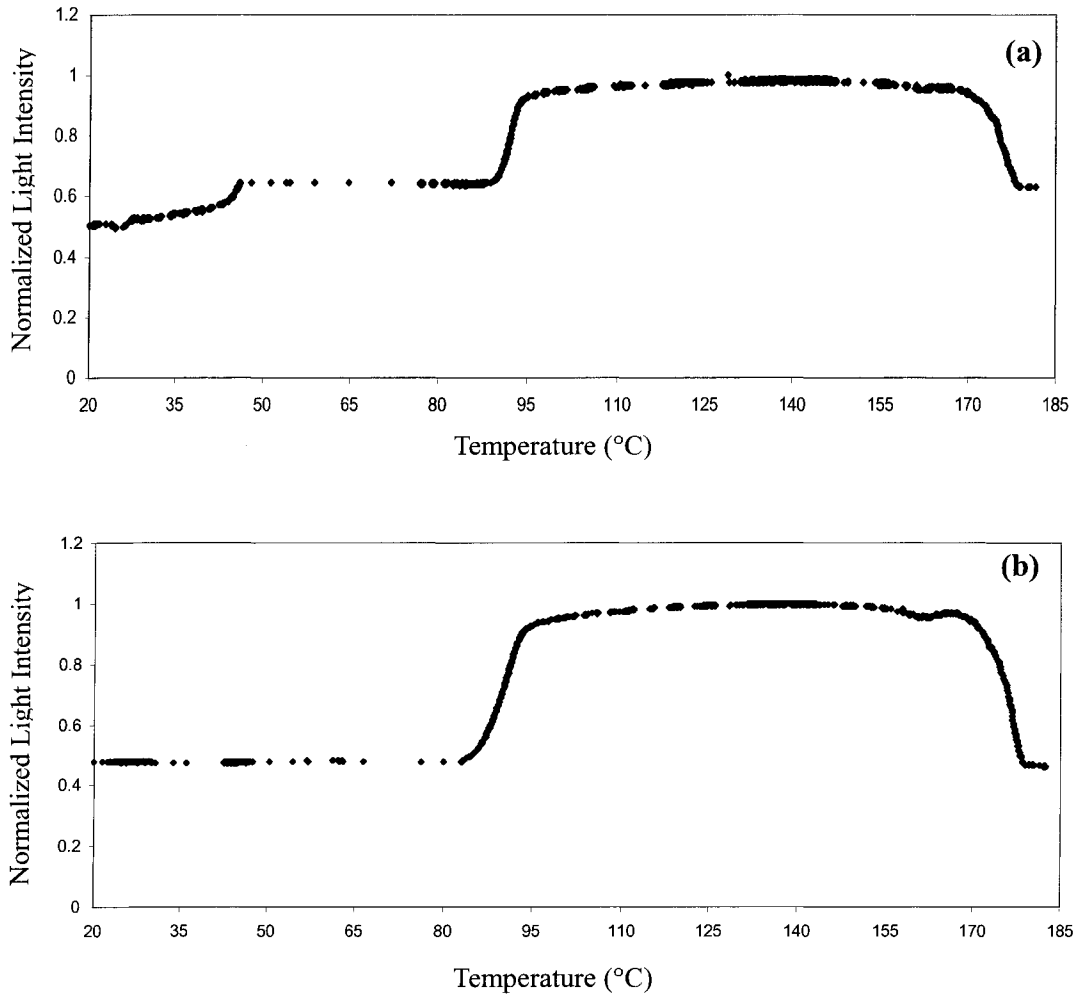

Figure 5.4: Total depolarized light intensity heating profiles of (a) sandwiched and (b) open face PLLA thin-film sample quench-cooled from the melt and heated at a rate of 2 °C/min.

Figure 5.4(a) shows an onset to this baseline step at about 47 °C, which is

comparable to that of the T_g of PLLA. No T_g was detected at other heating rates, or with open face thin film samples, and this response was not able to be successfully reproduced, suggesting that this observable fact at least partially resulted from the stress generated between the two glass slips and only happens for very particular sample thickness. It would therefore not be suggested as a new reliable method of detecting the T_g. However, it would be interesting to pursue a systematic study of the previously described cracking phenomenon in different samples at different temperatures using depolarized light intensity measurements, as the cracks are black lines and would affect the total amount of depolarized light being transmitted by the sample.

5.3 References

1. Xu, J. ; Gao, B-H. ; Zhou, J-J. ; Li, L. ; Wu, J. ; Kowalczuk, M. *Polymer* **2005,** 46, 9176.
2. Fraschini, C. ; Plesu, R. ; Sarasua, J. ; Prud'Homme, R. E. *J. Polym. Sci.,Polym. Phys.* **2005,** 43, 3308.
3. Tsuji, H. *Macromol. Biosci.* **2005,** 5, 569.